1.	2. REPORT DATE	3. REPORT TYPE AND DATES COVERED
	11-5-93	

4. TITLE AND SUBTITLE

On the Dynamic Mechanical Behavior of 3-D Integrated Fabric Reinforced Composites

5. FUNDING NUMBERS

DAAL03-86-G-0069

6. AUTHOR(S)

Frank K. Ko and Harry C. Rogers

7. PERFORMING ORGANIZATION NAME(S) AND ADDRESS(ES)

Department of Materials Engineering
Drexel University
32nd and Chestnut Sts
Philadelphia, PA 19104-2884

8. PERFORMING ORGANIZATION REPORT NUMBER

9. SPONSORING/MONITORING AGENCY NAME(S) AND ADDRESS(ES)

U. S. Army Research Office
P. O. Box 12211
Research Triangle Park, NC 27709-2211

10. SPONSORING/MONITORING AGENCY REPORT NUMBER

ARO 23798.2-MS-F

11. SUPPLEMENTARY NOTES

The view, opinions and/or findings contained in this report are those of the author(s) and should not be construed as an official Department of the Army position, policy, or decision, unless so designated by other documentation.

12a. DISTRIBUTION/AVAILABILITY STATEMENT

Approved for public release; distribution unlimited.

12b. DISTRIBUTION CODE

13. ABSTRACT (Maximum 200 words)

In order to elucidate the role of fiber architecture and test geometry on the impact behavior of 3-D braided composites, 3-D braided preforms having thicknesses varying form 0.3 in. to 1.0 in. were prepared for resin transfer molding with a vinylester resin system. Angle ply composites were fabricated for comparison with the 3-D composites to investigate the role of yarn interlacing in their dynamic impact response. The yarn interlacing was found to play an important role in raising the composites' ability to absorb impact energy, increasing its damage threshold and improving its damage containment. The 3-D network of fibrous reinforcement adds through-thickness strength and creates a complex path for crack growth. The superiority of the 3-D yarn interlacing was most obvious in the thicker structures where the degree of interlacing is more pronounced. During the course of this study, two non-destructive evaluation techniques (x-ray transmission and light transmission) were developed and utilized. X-ray transmission techniques were useful in detecting voids, improper wetting and fiber alignment in the as-molded composite plates. Light transmission was effective in characterizing the extent of damage by showing areas of delamination, debonding and cracking.

14. SUBJECT TERMS	15. NUMBER OF PAGES
3-D braid, textile composites, dynamic mechanical behavior, impact	109
	16. PRICE CODE

17. SECURITY CLASSIFICATION OF REPORT	18. SECURITY CLASSIFICATION OF THIS PAGE	19. SECURITY CLASSIFICATION OF ABSTRACT	20. LIMITATION OF ABSTR
UNCLASSIFIED	UNCLASSIFIED	UNCLASSIFIED	UL

DISCLAIMER NOTICE

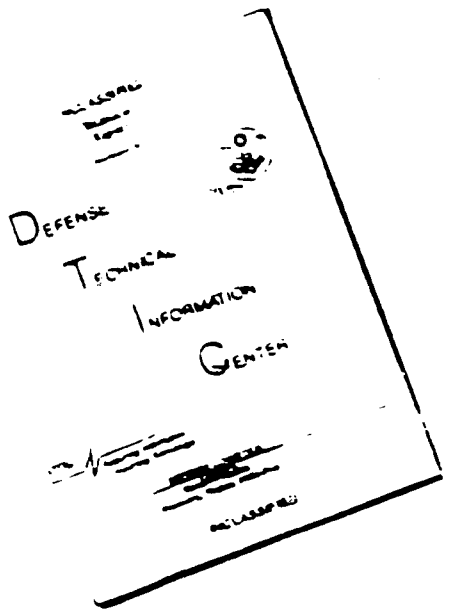

THIS DOCUMENT IS BEST QUALITY AVAILABLE. THE COPY FURNISHED TO DTIC CONTAINED A SIGNIFICANT NUMBER OF PAGES WHICH DO NOT REPRODUCE LEGIBLY.

ON THE DYNAMIC MECHANICAL BEHAVIOR OF 3-D INTEGRATED FABRIC REINFORCED COMPOSITES

FINAL REPORT, PROJECT NO. IG-402

FRANK K. KO AND HARRY C. ROGERS

SEPTEMBER, 1991

U.S. ARMY RESEARCH OFFICE

GRANT NUMBER: DAAL03-86-G-0069

DEPARTMENT OF MATERIALS ENGINEERING
DREXEL UNIVERSITY
32ND AND CHESTNUT STS.
PHILADELPHIA, PA 19104-2884

APPROVED FOR PUBLIC RELEASE; DISTRIBUTION UNLIMITED.

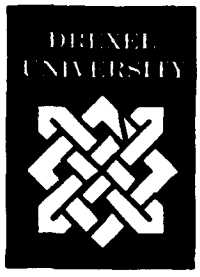

On The Dynamic Mechanical Behavior Of 3-D Integrated Fabric Reinforced Composites

ABSTRACT

In order to elucidate the role of fiber architecture and test geometry on the impact behavior of 3-D braided composites, 3-D braided preforms having thicknesses varying from 0.3" to 1.0" were prepared for resin transfer molding with a vinylester resin system. Angle ply composites were fabricated for comparison with the 3-D composites to investigate the role of yarn interlacing in their dynamic impact response.

The yarn interlacing was found to play an important role in raising the composites' ability to absorb impact energy, increasing its damage threshold and improving its damage containment. The 3-D network of fibrous reinforcement adds through-thickness strength and creates a complex path for crack growth. The superiority of the 3-D yarn interlacing was most obvious in the thicker structures where the degree of interlacing is more pronounced.

During the course of this study, two non-destructive evaluation techniques (x-ray transmission and light transmission) were developed and utilized. X-ray transmission techniques were useful in detecting voids, improper wetting and fiber alignment in the as-molded composite plates. Light transmission was effective in characterizing the extent of damage by showing areas of delamination, debonding and cracking.

TABLE OF CONTENTS

Page

Page

LIST OF TABLES

LIST OF FIGURES

Page

Page

CHAPTER 1

INTRODUCTION

1.1 Motivation

Fiber reinforced composite materials have been shown to be vulnerable to internal damage caused by low velocity impact loading. The resultant damage can have detrimental effects on the physical properties of composite structures [1-3]. This frequently prohibits the design of structures from taking full advantage of the high stiffness or strength to weight ratios that composites provide. Consequently, understanding the impact response of composite materials is of great academic and practical interest.

Conventional laminate structures are known to possess low strength in the through-thickness direction, as well as limited damage tolerance and delamination resistance [4-7]. Although unidirectional lay-up of fibers is the most efficient means of orienting the fibers in the direction of the applied stress, they can not provide

damage tolerance equivalent to textile based structures [8]. In many practical situations, out of plane stresses occur within the composite structures. These stresses can exceed the relatively low through-thickness strength, causing failure. Progress in the development of composite structures is being made in an effort to increase the damage tolerance to a level above that of traditional laminated composites.

Over the past few years many approaches have been pursued in an attempt to improve the impact tolerance of composite materials. These include: control of fiber-matrix interfacial adhesion, use of tough resin systems, changes in lamination design (i.e., laminate stacking sequence), introduction of through the thickness reinforcements, insertion of interlaminar layers, fiber hybridization and utilization of high strain fibers [4,6,7,9-15]. Work continues in many of these areas; however, our grasp of the impact response of composites is still limited, possibly because this complex phenomenon involves many different interactions and parameters.

In addition to developing new techniques to improve the damage tolerance of composites, investigators are studying the failure mechanisms including their interactions with material properties

and conditions of impact. In general, when a solid is impacted, it can absorb energy by two basic mechanisms: (1) creation of new surfaces and (2) material deformation. Examples of more specific mechanisms include fiber strain and breakage, matrix deformation and cracking, fiber debonding, fiber pull-out, and delamination cracks [16-20].

The introduction of instrumented impact testing has made it possible to quantify some of the dynamic impact responses of composite materials. Several physical phenomena have been found to correspond to distinct regions of the impact response curves. Although the instrumented impact test has been proven to be an effective tool in examining the impact behavior of composites, it has one major disadvantage in that there is no single standard test method [21-25]. Each company or institution is using a different test technique with varying specimen size and geometry, support fixtures, indenter shape, impact velocity, etc. This makes comparison of impact data only marginally useful.

1.2 Statement of the Problem

There is a need to establish the role of the fiber architecture in resistance to impact damage. The two fiber systems that were studied in response to this need are: (1) 1x1x1 braided structure with a ±20 degree surface angle on the x-y plane and (2) +20/-20 angle-ply laminate. The preforms were manufactured with fiberglass reinforcement, Owens Corning Type 30 E-Glass. They were consolidated by resin transfer molding with Dow Chemical's Derakane 411 vinylester resin catalyzed with methyl ethyl ketone peroxide. The contribution of the through-thickness reinforcement in the 3-D braided structures to impact damage tolerance was examined over a range of specimen thickness on both a local and a global level.

1.3 Scope and Objectives

Two fiber architectures, braids and unidirectional laminates, were evaluated in terms of their dynamic response during impact. The composites were evaluated in the form of 6 inch by 6 inch E-glass/vinyl ester plates, with thicknesses that varied from 0.3 inch to 1.0 inch. They were impact tested with a Dynatup model 8140

instrumented drop weight tester under similar conditions to compare their behavior.

One output from the instrumented impact tester is the load on the specimen as a function of time or displacement. An integral curve giving the energy absorbed by the specimen is also obtained. The shape and magnitude of the impact response curves for each material will be compared.

X-ray transmission was used as a non-destructive evaluation technique for each sample prior to impact testing to confirm the quality of the composite. In order to relate the features on the impact response curves to physical attributes, the specimen were examined by light transmission after impact to quantify the extent of damage on a global level. Microscopic examination of the impacted area was also employed to reveal the damage and failure mechanics on a local level.

The objective of this study is to improve the understanding of the role of the reinforcing fiber architecture of composite materials in their dynamic response to impact loading. In particular, two different preform types were evaluated to isolate the contribution

of the integrated structure of the braid because it introduces an interlacing through the thickness or "z" component in the reinforcing fibers. The influence of the two different fiber architectures were evaluated over a range of sample thickness.

Another objective of this study is to understand the influence of the fiber architecture on the types of failure modes present after impact. The failure mechanisms and extent of the damaged area can be related to the dynamic response curves. With a better understanding of the failure mechanisms, it is possible to tailor fiber orientations in textile based composite structures to optimize their physical properties while increasing their damage tolerance.

CHAPTER 2

BACKGROUND AND LITERATURE SURVEY

2.1 Fiber Architecture

In many practical applications, composites are often used for plate members that are susceptible to impact loads perpendicular to the surface which can cause severe out of plane loading [26-27]. These interlaminar stresses, both tensile and shear, can lead to delamination in conventional laminate composites, greatly reducing their intrinsic properties. In these laminate composites the interlaminar strength is totally a function of the strength of the matrix which is typically an order of magnitude lower than the composite's in-plane properties.

One method of increasing the interlaminar strength of composites is to introduce a fraction of the reinforcing fibers in the through-thickness or "z" direction. This can be accomplished by a variety of techniques such as: stitching laminate structures together, 2.5-D fabric or "hairy laminates", multi-directional weaving, and 3-D

braiding [6]. This study focuses on the introduction of reinforcement in the z-direction by braiding.

Braiding is a textile process in which the yarns are introduced along a common axis by means of an intertwining or bias interlacing construction to achieve a fully integrated structure of near net shape for a variety of complex geometries [28]. In 3-D braiding, a textile structure of the necessary thickness is created, thus easing the problems associated with delamination because there are no laminae to separate.

There are two general classes of 3-D braiding, differing by the number of distinct motions in each repetition (two step or four step). The two step braiding process has two distinct movements per cycle; these are repeated to produce the prescribed preform. The 2-step braiding process uses two sets of yarns: axial and braiders. The axial yarns are placed parallel to the forming direction in the general geometric shape of the structure. The braider yarns are laced through the stationary axial yarns to lock and stabilize the cross sectional shape of the fabric. Figure 1 shows the path of the braider yarn.

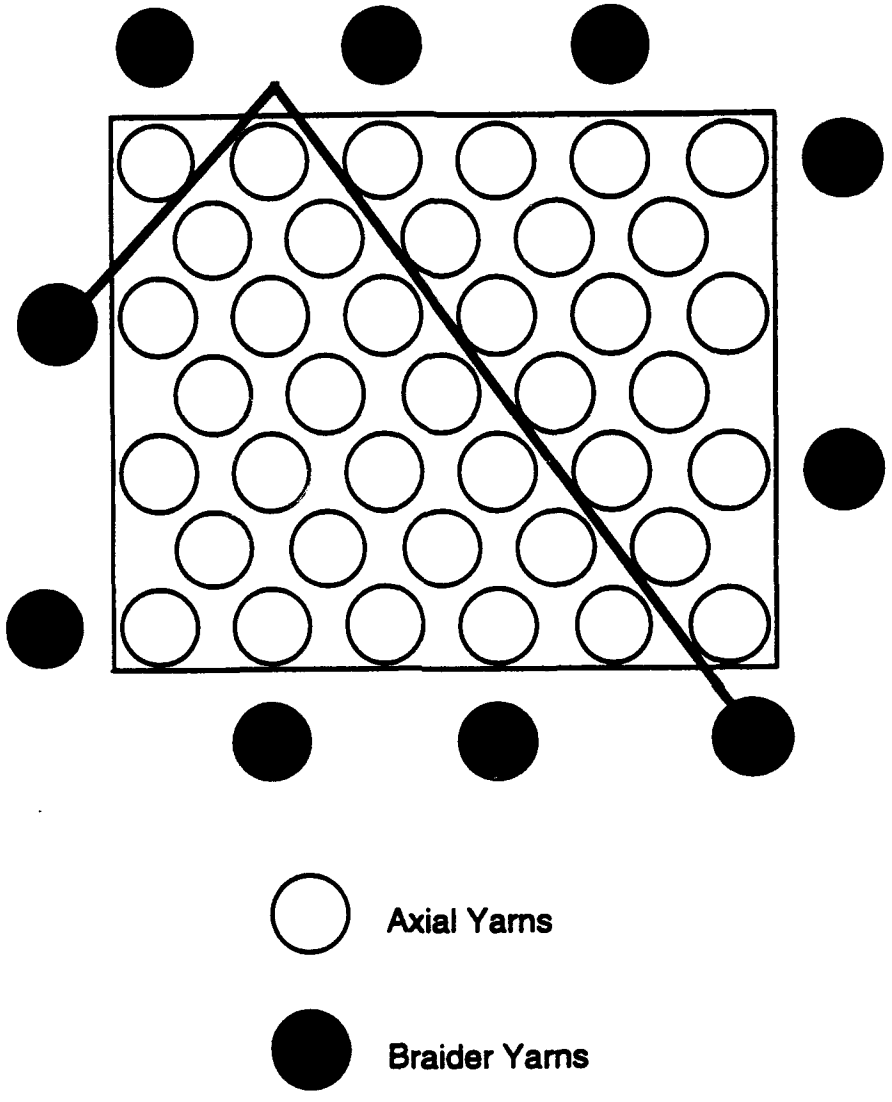

Figure 1: 2-Step Braiding Loom Design

This study however, concentrates solely on the structure produced by the four step braiding process. Figure 2 shows the 4-step braiding machine arrangement along with the path followed by a single yarn for a rectangular loom. The 4-step braiding process, also known as Euclidian, Omniweave, Magnaweave or Cartesian braiding, requires at least four distinct machine operations per cycle as shown in Figure 3. At the conclusion of each cycle the loom is identical to the initial arrangement. A four step braid can consist of either all braiding yarns or a combination of braider and axial yarns.

In addition to altering the ratio of braider to axial yarns, the four step process can produce a variety of fiber structures by varying the ratio of track movement to column movement. This will effect the degree of interlacing and the orientation of the reinforcing fibers, which in turn will alter the basic unit cell geometry. A three dimensional unit cell of a 1x1x1 (the ratio of track movement to column movement per cycle) 4-step braid is shown in Figure 4.

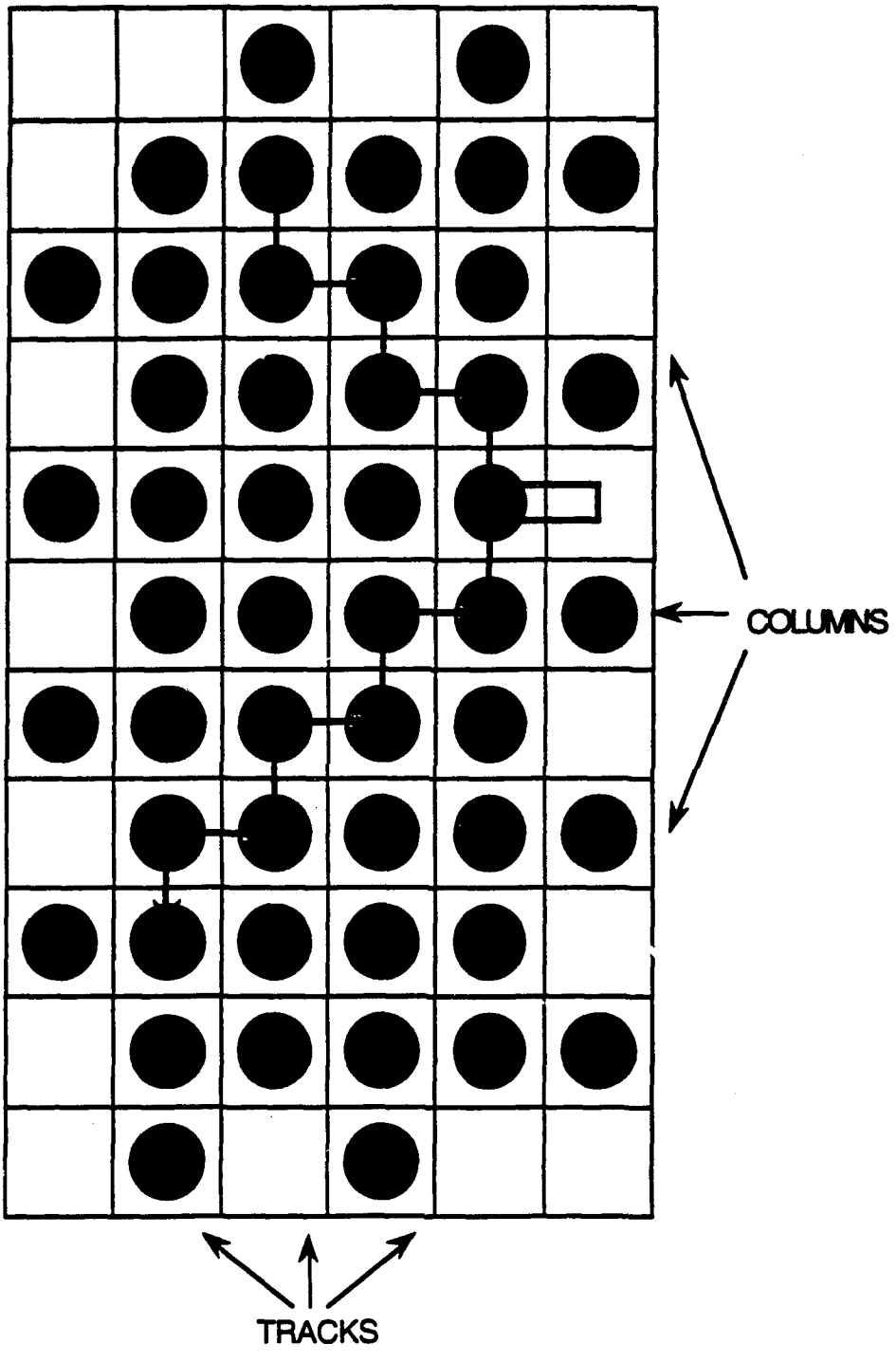

Figure 2: 4-Step Braiding Loom Design

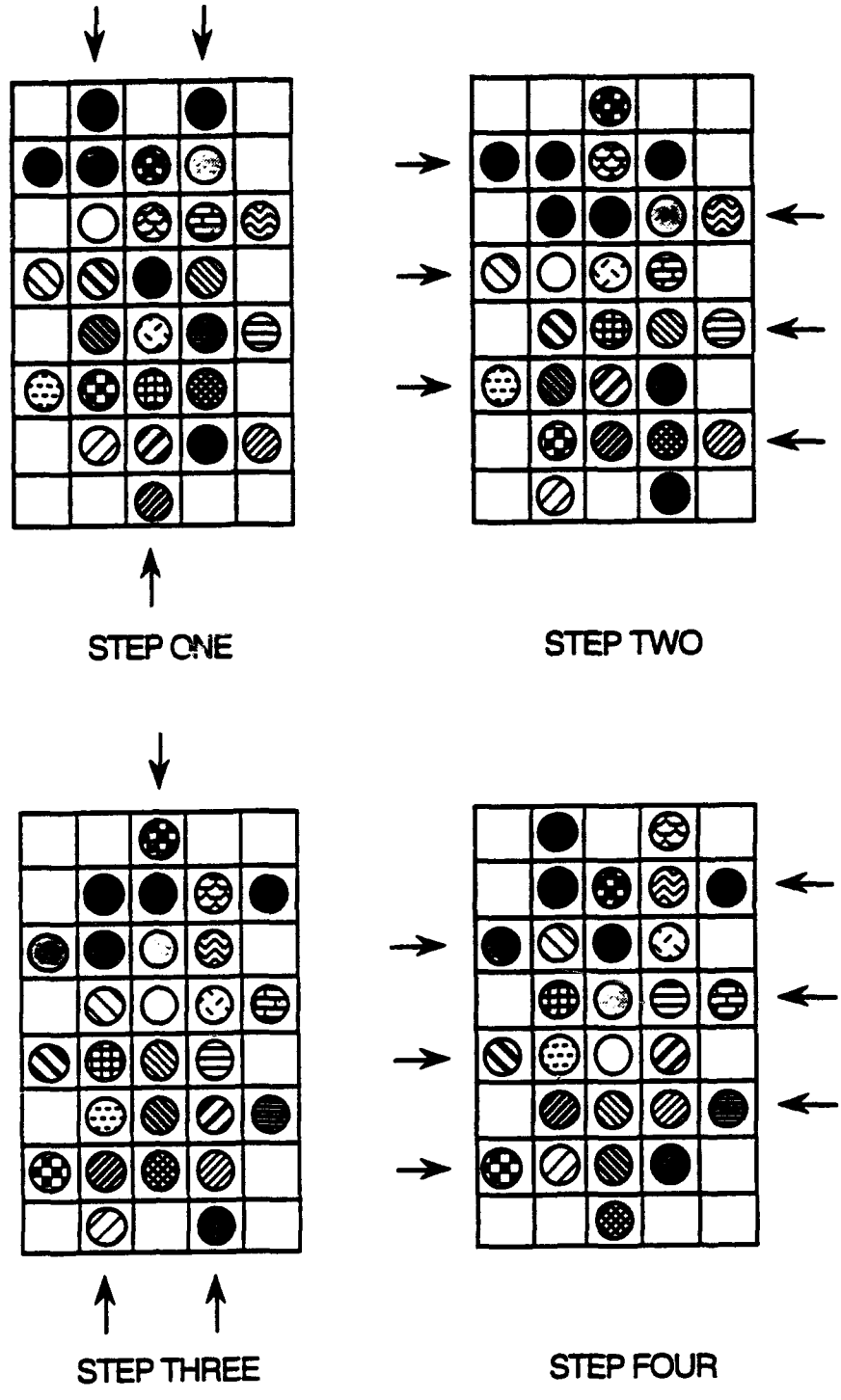

Figure 3: 4-Step Braiding Loom Machine Operations

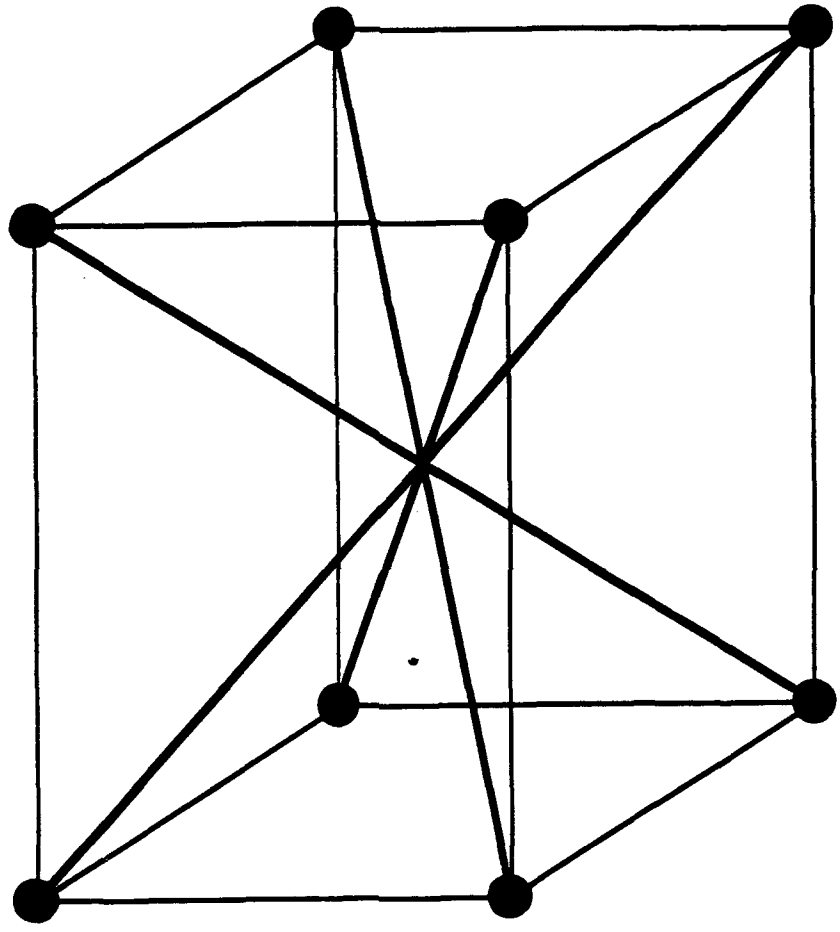

Figure 4: Simple Unit Cell for a 1x1x1 4-Step Braid

2.2 Instrumented Impact Testing

In the past a great deal of effort was spent using Charpy and Izod tests to gain a better understanding of the impact response of composite materials. It has been recognized that these test geometries rarely represent the end-use application of the composite. The drop weight impact testing equipment permits the use of a variety of test geometries which can more closely represent the plate configuration typical of a variety of composite material applications [29-32].

The instrumented impact testing equipment currently available enables the researcher to record valuable information during the impact event. Such instruments typically consist of an apparatus designed to apply a dynamic load (either a drop tower or pendulum) using an indenter, equipped with a force transducer, to contact the surface of the specimen. The indenters may have a wide variety of shapes and sizes. The combined assembly of force transducer and indenter is called the tup. The signal generated by the transducer is a function of the load on the sample and is sent to a data acquisition system for analysis. The load on the sample as a function of time or

displacement is used to create an integrated curve of the energy absorbed as seen in Figure 5.

Figure 5: TYPICAL IMPACT RESPONSE CURVES

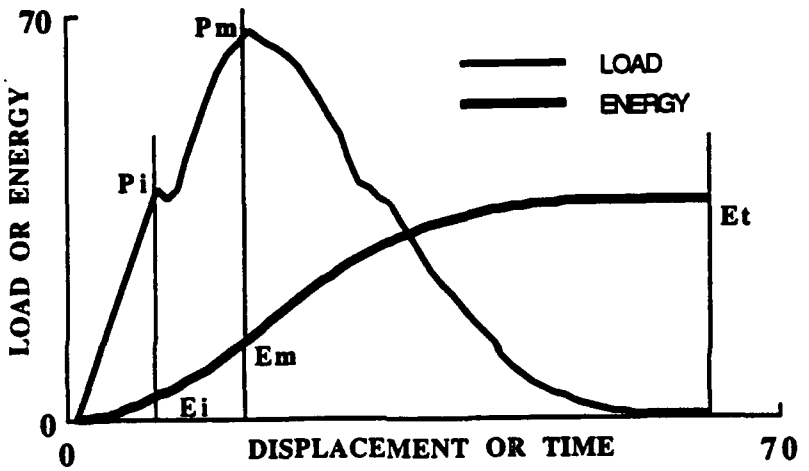

CHAPTER 3

SAMPLE PREPARATION

3.1 Preform Geometry and Manufacture

The object of this study is to evaluate the effect of differences in fiber architecture between a 3-D braided textile structure and a ±20 angle-ply laminate on their impact damage tolerance. In order to accomplish this objective, an effort was made to design fiber preforms that isolate the effect of the fiber interlacing and through-the-thickness reinforcement of the integrated 3-D braided structure.

A 3-D braided structure was manufactured by the 4-step or Euclidian braiding process using a movement of 1x1x1. This was accomplished using the loom shown in Figure 6, whereby the yarns are manipulated by a series of tracks and columns comprising a Cartesian grid at the base of the loom. The yarns are placed parallel to the braiding direction and are connected to bobbins that are moved within the grid at the base.

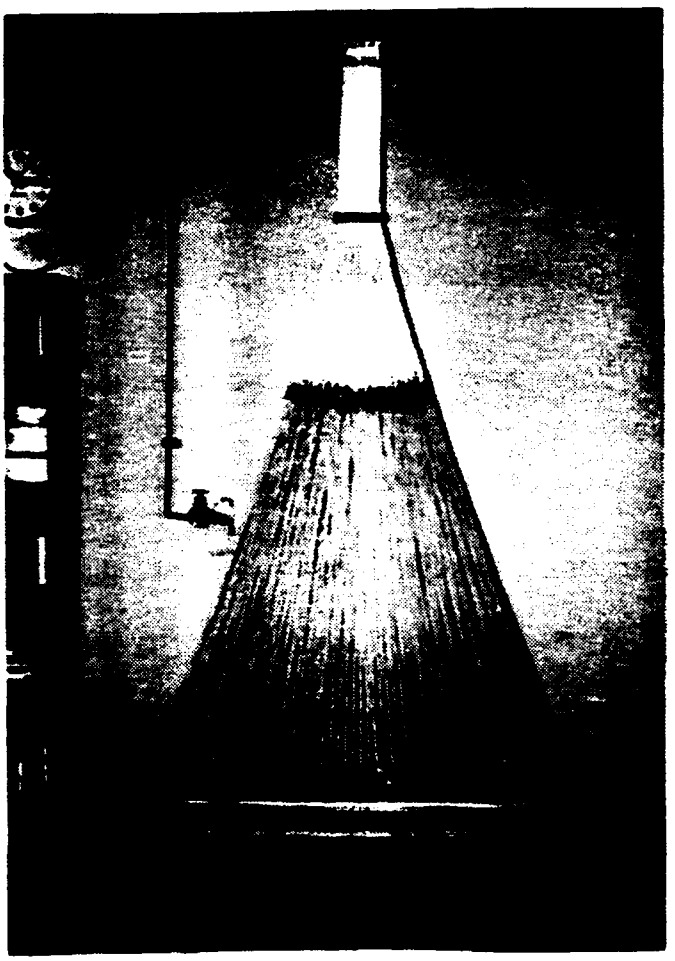

Figure 6: 4-Step Braiding Loom for a 1.0 inch Thick Sample

The targeted sizes of the test specimens were flat plates 6 inches by 6 inches having thicknesses of either 0.3, 0.5 or 1.0 inch. In order to manufacture a fiber preform of the correct dimensions, it was necessary to calculate the proper number of fiber tow and determine the size of the of braiding loom. The total number of tow is related to the the various parameters by:

$$\text{number of tow} = (A_p)\,(D_f)\,(V_f)\,(\cos(\text{theta}))\,(9 \times 10^5) / \text{den}$$

where
- A_p is the cross sectional area (cm^2) of the preform
- D_f is the fiber density (g/cm^3)
- V_f is the theoretical fiber volume fraction
- theta is the surface braid angle
- den is the linear density of tow in denier (g/9000m)

As seen from the above equation, the number of tow is inversely proportional to the size of the tow. Because the size of the loom and time for manufacture increases dramatically as the number of tow is increased, a large tow size was used. The remaining process parameters for braiding the preforms were calculated and are given in Table 1.

TABLE 1: Manufacturing Process Parameters for the Braiding of Test Specimen

Fiber - Type 30 E-Glass with 123 yd/pound yield

Number of tow per bobbin - 2

Projected fiber volume fraction - 0.50

Surface braid angle - 20 degrees

Preform Thickness	Tracks	Columns
0.3 inch	3	53
0.5 inch	5	53
1.0 inch	10	53

In order to compare the braided structures to laminate structures, preforms manufactured of unidirectional angle-ply laminates were designed to be similar to the braided specimen. The design utilized a similar fiber type, tow size, fiber angle, fiber volume fraction, and specimen size. The process parameters for manufacturing the unidirectional laminates are shown in Table 2.

TABLE 2: Manufacturing Process Parameters for Preforming Laminates

Fiber - Type 30 E-Glass with 123 yd/pound yield

Projected fiber volume fraction - .50

Surface fiber angle - 20 degrees

Preform Thickness	Laminates	Tow per Laminate
0.3 inch	3	106
0.5 inch	5	106
1.0 inch	10	106

In order to maintain the proper fiber orientation while making the preforms, a small loom was assembled as shown in Figure 7.

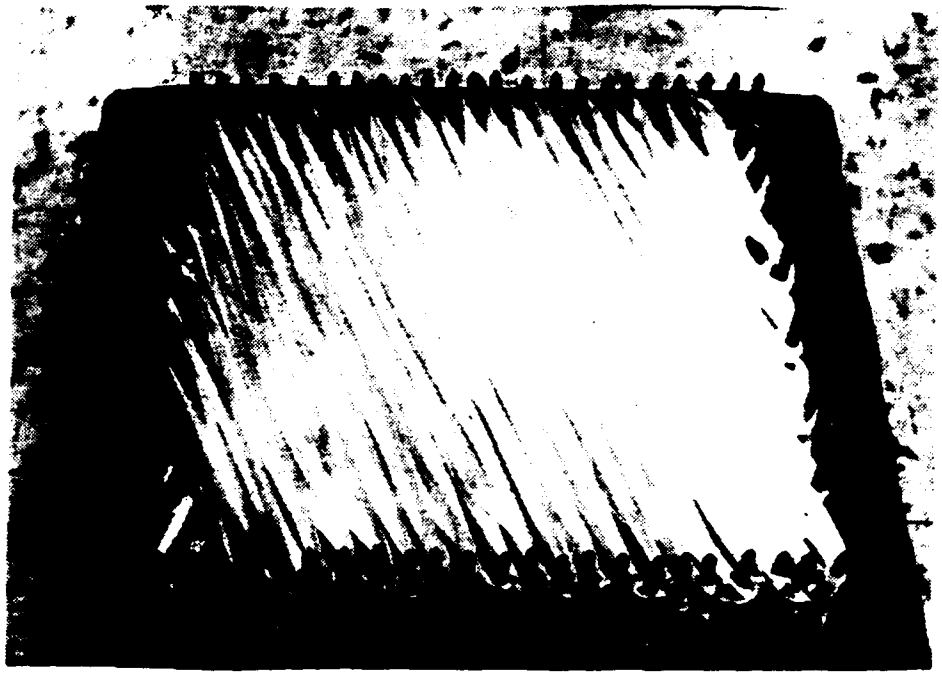

Figure 7: Loom for Manufacturing Preforms for angle-ply Laminates

3.2 Composite Manufacturing

3.2.1 Compression Molding

To convert the preform from its dry state which is flexible and conforming into a rigid structure, a resin or matrix material must be introduced into the space between the fibers. Not only does the resin have to surround and hold the yarn bundles together but it must penetrate and "wet-out" the individual fibers within each yarn. Once the resin is in place, it is cured or hardened, producing a rigid, light weight, strong composite.

If proper wetting is not obtained, the formation of voids will occur, leading to a poor fiber/matrix interface. It is this interface that is responsible for transferring the stresses from the matrix material to the load bearing fibers. A composite with improper wetting and hence poor interfacial bonding will have poor mechanical properties.

One method of introducing resin matrix material into the fibrous preform is by a compression molding technique as shown in

Figure 8. The preform is placed in the bottom tool with a surplus of resin. This assembly is then evacuated to degas and remove trapped air between the fibers and resin. The top portion of the tool is seated into the bottom and the two pressed together, forcing the resin to flow through the fibrous structure. The complete assembly is then placed into a vacuum oven where it is degassed again and heated to the required temperature for a proper cure cycle for a particular resin system.

Initial test samples were produced by compression molding techniques; however, poor wetting was obtained resulting in an appreciable amount of "fiber wash-out". Fiber wash-out is fiber movement caused by the flow of the resin, and since the focus of this study is on fiber architecture it is essential that the fibers preserve their original geometry. After exhausting the available variations of the process variables of this impregnation technique, it was decided to use an alternate one, resin transfer molding (RTM) [33].

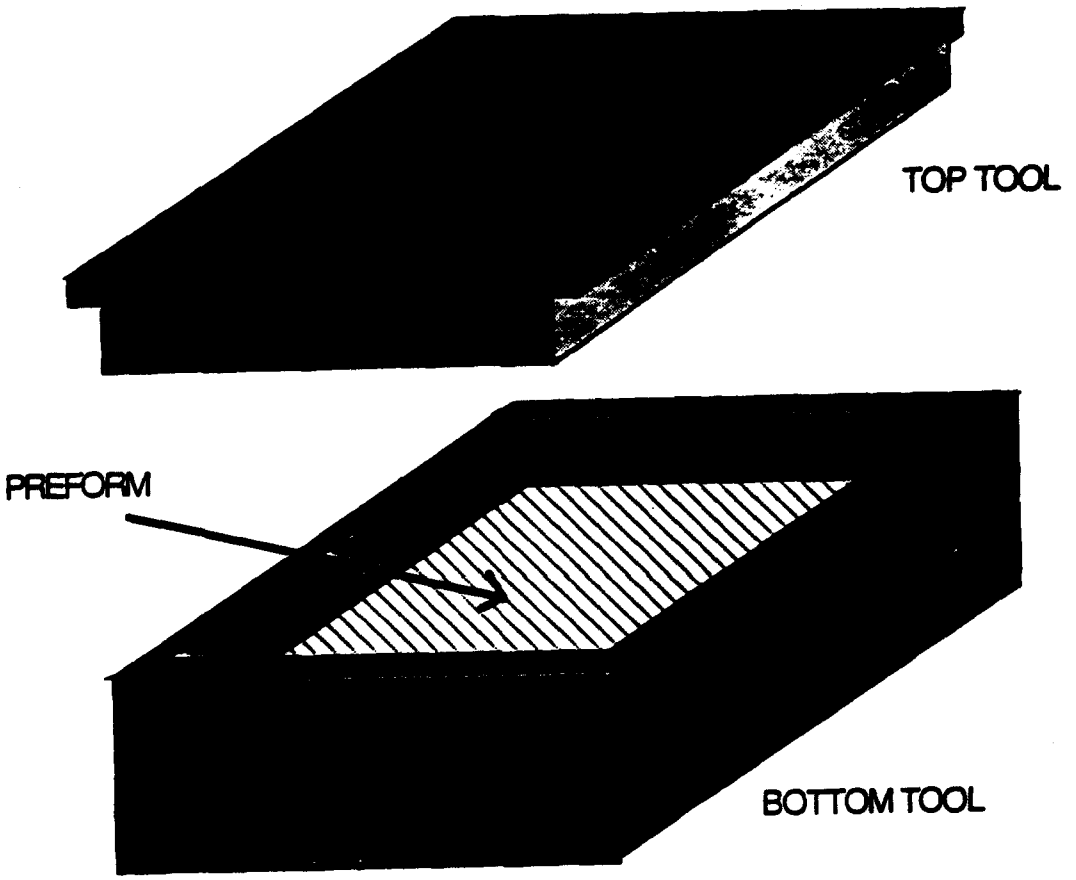

FIGURE 8: Schematic of a Compression Molding Technique

3.2.2 Resin Transfer Molding

Resin transfer molding, RTM, is a manufacturing process for composite materials in which the fibrous preformed reinforcement is placed in a closed die mold and is penetrated by pre-catalyzed resin using pressurized injection. RTM is widely used in the industry as a net-shape manufacturing technique for composite materials because of its relatively low tooling costs, short cycle times, control of component shape, quality, and reproducibility.

The RTM equipment and arrangement used in this study is shown in Figures 9 and 10. On the left in Figure 9 is a vacuum source and resin trap used to evacuate the entire system before the resin is injected. The center is the compression molding tooling modified by inserting the necessary inlet and outlet ports. On the right is a compressed air source and the pressurized vessel in which the catalyzed resin is placed before being degassed and injected into the mold.

All the samples used in this investigation were manufactured by the equipment described, following identical procedures. The

parameters that were investigated and optimized for producing high quality parts are: mold geometry, port locations and number, resin characteristics, mold temperature, injection pressure, vacuum assistance, and flow rate. After many design modifications and process variations, a system was established that produced high quality composites. The finalized standard operating procedure that was employed during the manufacture of each sample is as follows:

Standard Operational Procedures

For Resin Transfer Molding

1. Dry the preform at 110 degrees Celsius for one hour and place into the tool at room temperature.

2. Connect the vacuum source and resin tank. Mix the resin with catalyst and place into the resin tank. Apply vacuum to the entire system for 15 minutes in order to remove all air from the preform and to degas the resin.

3. Initiate resin flow by gradually pressurizing the resin tank while vacuum remained at the exit ports. Increase pressure to 10 psi and

hold until flow is seen at the exit ports.

4. Close the exit port and disconnect the vacuum source. Increase pressure to 60 psi.

5. Open the exit port slightly to allow a moderate flow of resin through the tool. Continue flow until the air bubbles cease to exit the tool.

6. Close the exit port and maintain injection pressure for one hour to allow for shrinkage during cure.

7. Seal all ports, disconnect all lines and place the entire tool into an oven at 80 degrees Celsius for 4 hours.

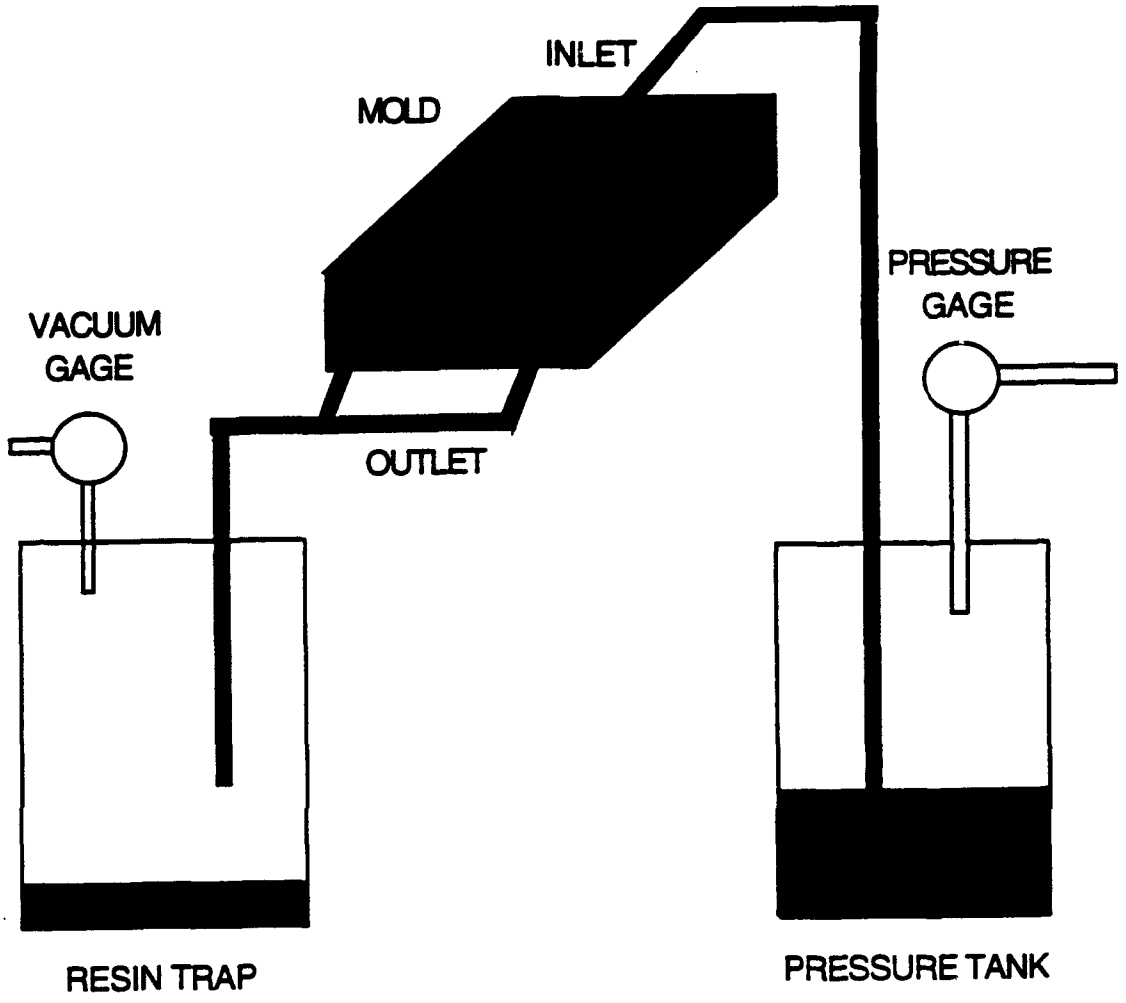

FIGURE 9: Schematic of a Resin Transfer Molding

Technique

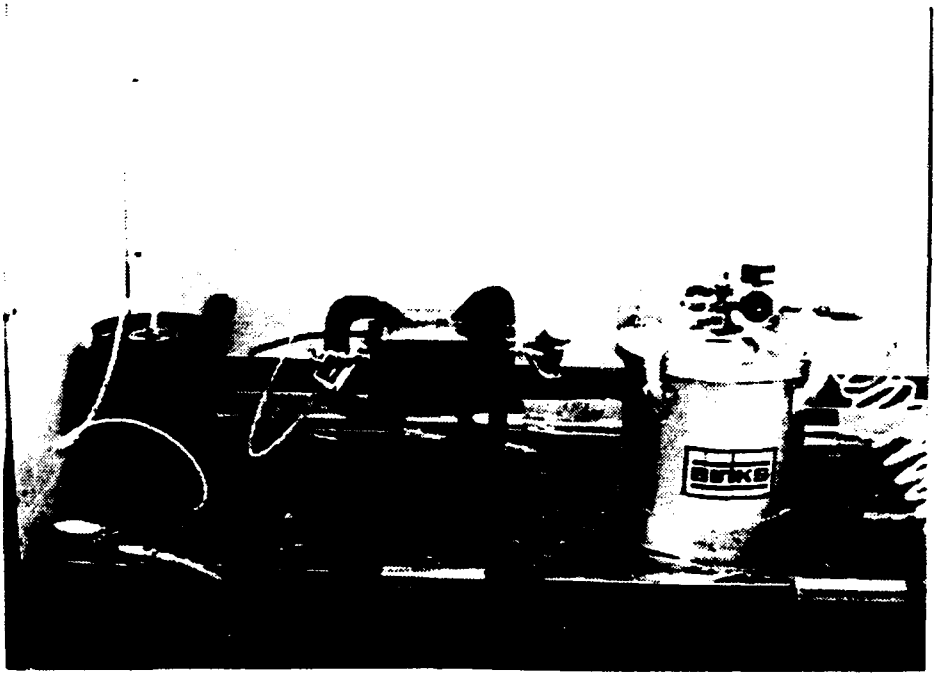

Figure 10: Photograph of the Resin Transfer Molding Equipment used in this Study

CHAPTER 4

Instrumented Drop Weight Testing

4.1 Test Procedure

All impact tests were performed on a Dynatup model 8140 instrumented impact tester in conjunction with a Dynatup model 730-I data acquisition system driven by an IBM PC-30. The equipment has the capability of using cross head weights ranging from 600 lbs. - 1750 lbs. with a maximum velocity of 21.8 ft/s. This gives a maximum available impact energy of 13125 ft-lbs. It is necessary to mention that the equipment does not incorporate a rebound break to prohibit multiple hits. The data acquisition system records a complete history of load and energy versus time or deflection during the impact event. The results can be displayed, printed and stored. The entire arrangement, including the impact tester, tup, sample holder, and computer equipment, is shown in Figure 11.

Figure 11: Complete System for Instrumented Drop Weight Impact Testing

The many variables associated with an impact test can be adjusted to yield an impact event closely resembling an environment in which the material is to be used. In this case, however, there is no direct application for the material being tested; rather the purpose is the characterization of the impact response and failure modes as a function of the fiber architecture. Therefore, the test geometry and parameters were fixed for testing all cases under identical conditions.

Given the specimen, a flat plate 6 in. by 6 in., the test fixture geometry was the first variable to be established. Initial tests were conducted using a sample holding fixture having a 5 in. by 5 in. unsupported area with a clamped 0.5 in. border as had been utilized in a previous study [21]. It was observed that during impact the sample slipped from the clamps. Work was done by another researcher utilizing a round test geometry to yield a simplified test geometry [26]. A new holder was designed using a larger more rigid clamped area with an unsupported circular area 4.5 in. in diameter as shown in Figure 12. Tests showed no slipping of the sample during impact, giving reproducible results.

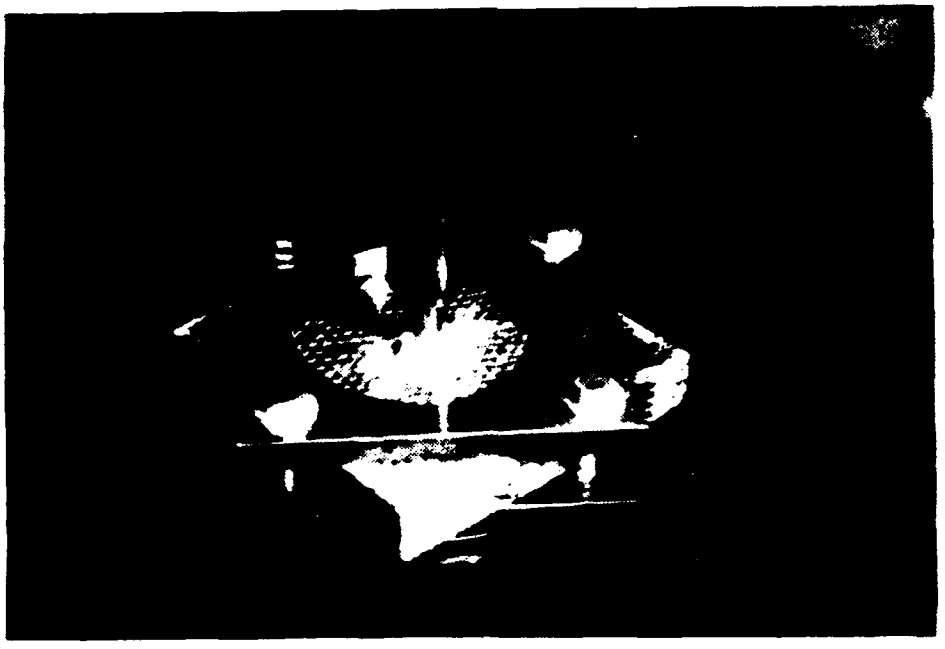

Figure 12: Specimen Holder for Impact Testing

The remaining test parameters were established considering that the impact energy should be greater than needed to penetrate the toughest of the samples while not exceeding the load cell capabilities. Through initial testing, it was found that the combination of parameters listed below in Table 3 is suitable.

TABLE 3: Test Conditions for Drop Weight Instrumented Impact Testing

Cross head weight	605 lbs
Impact velocity	10 ft/sec
Total impact energy	907.5 ft-lbs
Indenter geometry	0.5 in. diameter hemisphere
Test area	4.5 in. diameter

4.2 Test Matrix

Two materials were examined: 1) a 1x1x1 three dimensional braided E-glass/vinylester composite 2) a 20/20 cross ply laminate also of E-glass/vinylester. Both materials were manufactured into plates having nominal thicknesses of either 0.3, 0.5, or 1.0 in. giving a 2x3

test matrix. At least three samples in each category were tested, all under identical conditions.

Design of Experiment

	Fiber Architecture	
Specimen Thickness	3-D Braid	Angle-Ply
0.3 in.	X	X
0.5 in.	X	X
1.0 in.	X	X

Chapter 5

As Manufactured Quality

In order to assure the validity of the test results, the quality of each manufactured panel was inspected prior to testing. Both void volume determination and x-ray analysis were conducted on each sample.

5.1 Void Content

The void content of a composite may significantly affect its mechanical properties. The knowledge of the void volume is desirable for estimating the quality of composites, screening for defective samples, and interpreting the results of mechanical testing.

The void content of each sample was determined by following the procedures detailed in ASTM D-2734, Standard Test for Void Content of Reinforced Plastics. The results of the void content analysis are listed in Table 4. One sample had a measured void volume in excess

of 5% and was rejected. All of the remaining samples had void content's below 5% with most below 2%.

TABLE 4: ASTM D-2734 VOID CONTENT OF COMPOSITES

Sample	Thick. (in.)	Fiber (w/o)	Resin (w/o)	Void Volume (%)	Fiber (v/o)
1	0.3	73.3	26.7	0.40	55.0
2	0.3	70.9	29.1	0.38	52.0
3	0.3	73.9	26.1	0.13	55.9
10	0.5	69.5	30.5	2.29	49.4
11	0.5	70.4	29.6	1.36	50.9
12	0.5	72.8	27.2	1.71	53.7
20	1	67.0	33.0	2.23	46.6
21	1	68.3	31.7	5.56	46.4
22	1	66.9	33.1	2.90	46.1
23	1	66.7	33.3	0.20	47.3
24	1	69.3	30.7	0.30	50.1
30	0.3	71.3	28.7	0.88	52.2
31	0.3	67.5	32.5	0.64	48.0
32	0.3	71.2	28.8	2.30	51.4
33	0.3	67.7	32.3	1.36	47.8
40	0.5	66.3	33.7	1.42	46.2
41	0.5	70.9	29.1	0.79	51.9
42	0.5	68.9	31.1	2.56	48.6
43	0.5	70.5	29.5	1.66	50.9
50	1	69.8	30.2	0.62	50.5
51	1	69.2	30.8	1.82	49.3
52	1	71.6	28.4	3.75	51.2
60	0.4	69.4	30.6	1.54	49.6

The void content measurement indicates the volume percentage of voids throughout the entire sample. It does not reveal the position, size or distribution of the voids. In order to determine the distribution of the existing voids, methods such as ultrasonic or x-ray techniques need be applied.

5.2 X-ray Transmission NDE

Several techniques to characterize the as-manufactured quality of the samples were tried; *ultrasonic C-scan, dye penetrant, and x-ray* transmission. Because of the complex fiber orientations as well as time constraints, ultrasonics and dye penetrant testing were eliminated. X-ray transmission, shown in Figure 13, emerged as the only viable option because of its simplicity and speed. The x-rays are directed toward the x-y plane of the test sample. The x-rays passing through the sample cause a Kodak lanex screen to fluoresce. The image is viewed with a video camera, enhanced with an IBM computer and displayed on a monitor. The validity of the x-ray transmission was confirmed by examining several samples using both ultrasonic and x-ray techniques with similar results. All of the remaining samples were x-rayed to verify their quality.

Permanent records for each test in the form of a video recording and photographs were taken.

Figures 14 and 15 are typical examples of x-ray photographs of a braided sample and an unidirectional sample, respectively. They illustrate two points in particular. There is a homogeneous distribution of the resin and also an uniform fiber structure throughout the plane. Figure 16 shows an example of a sample that was rejected as the result of x-ray inspection. The top center of the sample has a large void, possibly due to air entrapped during the resin injection.

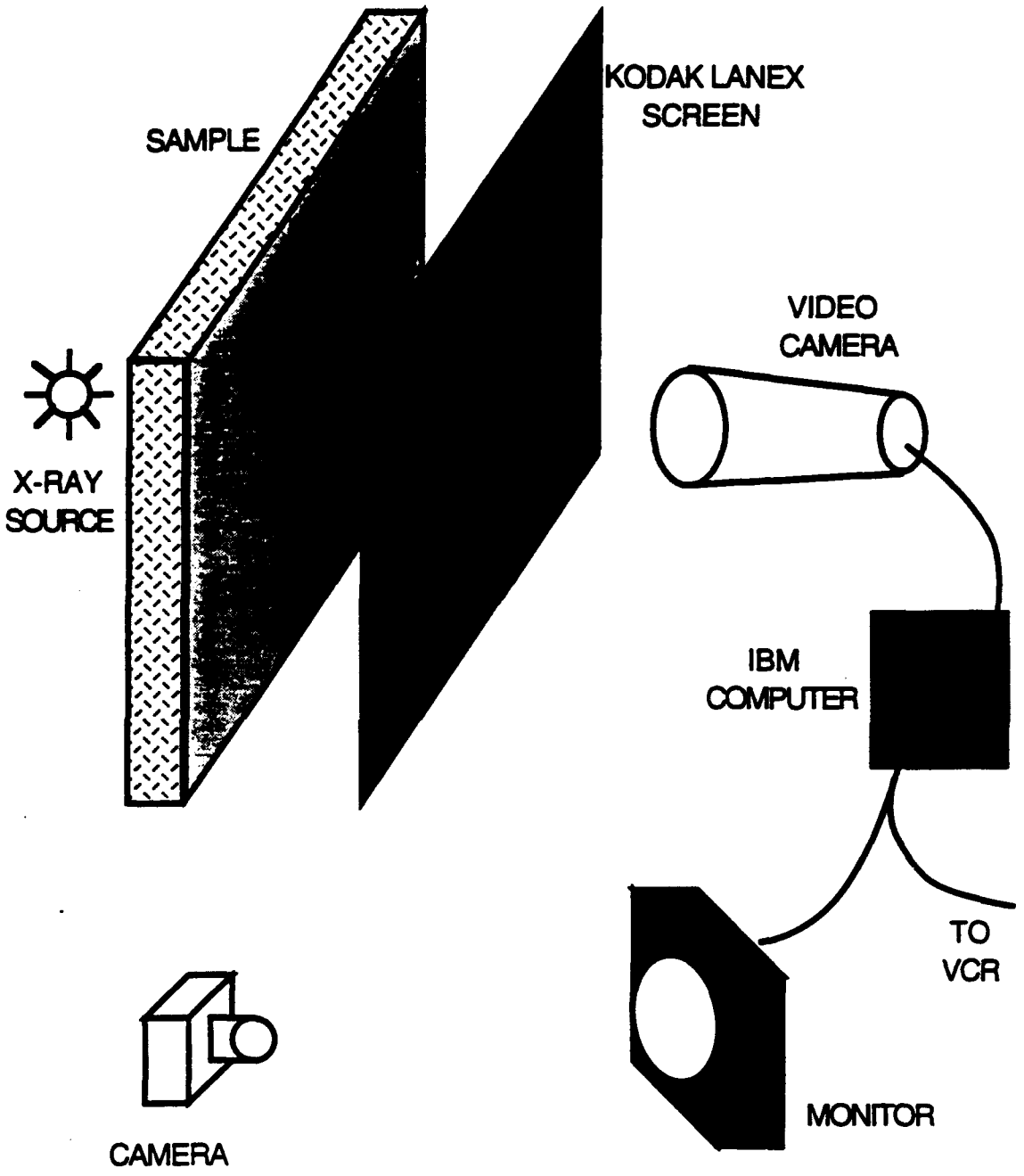

Figure 13: Schematic for X-Ray Transmission Non-Destructive Evaluation

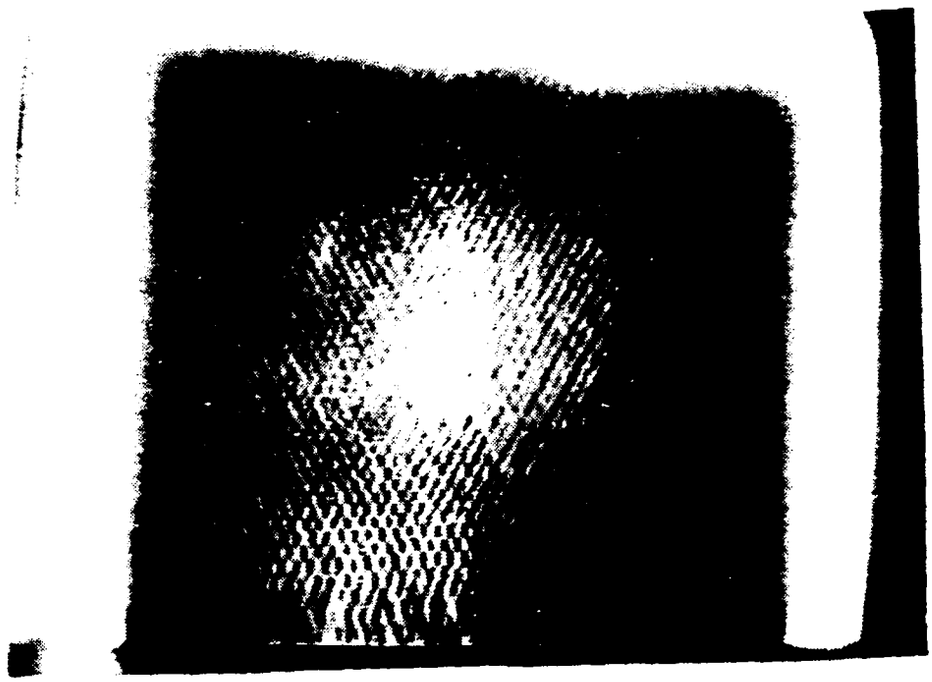

Figure 14: Photograph of a Typical Braided Composite Using X-Ray Transmission

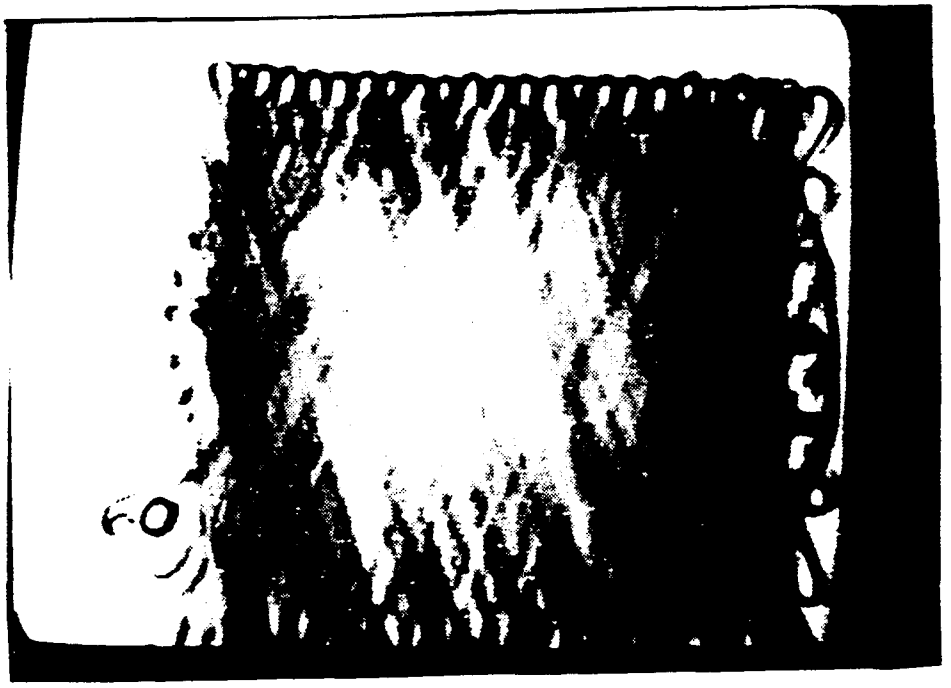

Figure 15: Photograph of a Typical Laminate Composite Using X-Ray Transmission

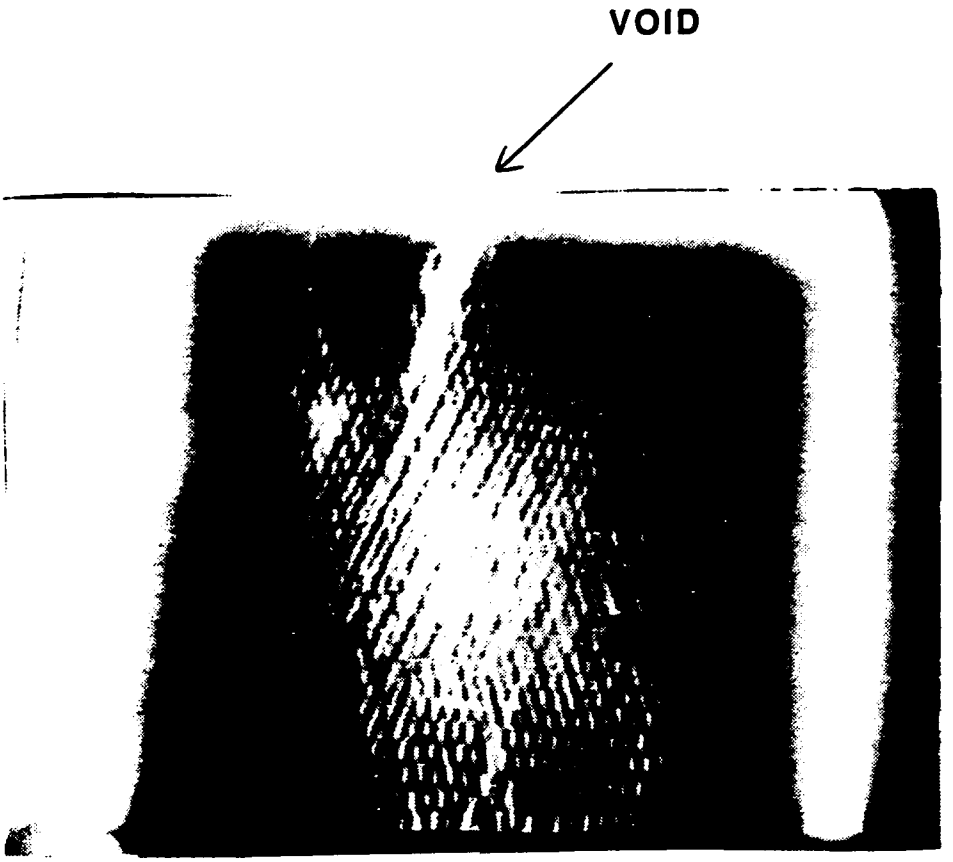

Figure 16: Example of a Rejected Sample Due to a Void Detected by X-Ray Transmission

Chapter 6

Results and Discussion

6.1 *Impact Data*

Using a drop weight instrumented impact test, a large quantity of data can be collected during a single impact event. These data are usually presented in the form of dynamic response curves: load and energy as a function of time or displacement as shown in Figure 17. Various features of the response curve can be related to specific physical observations [21], illustrating the potential of instrumented impact testing. It is clear that the amount of data obtained from conventional non-instrumented impact testing corresponds to only a small portion of that available.

Results from conventional testing may correspond to a single point along the response curve, such as the total energy for penetration, E_t. Not only do conventional test methods provide a limited amount of data, they are very time consuming and can be very costly due to their "go/no go" test procedures.

Figure 17: TYPICAL IMPACT RESPONSE CURVES

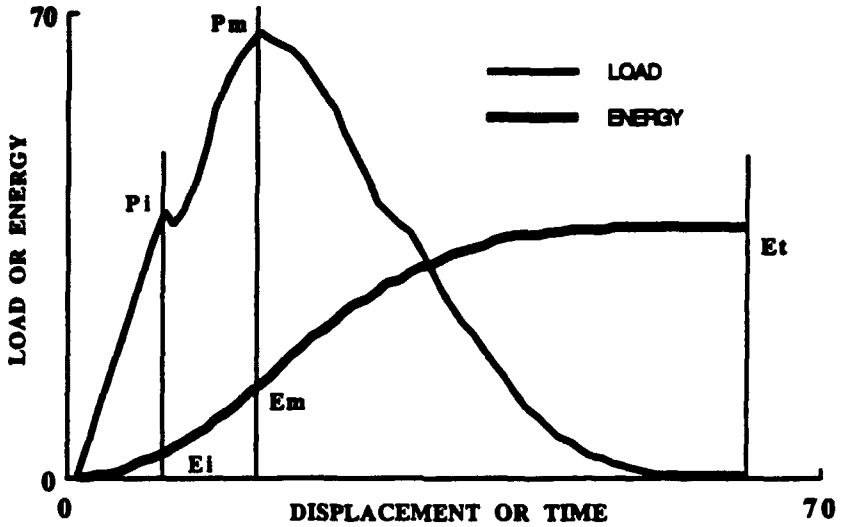

Each of the critical points on the curve has been associated with a distinct physical occurrence in the test sample and can be significant, depending on the design constraints for a specific application. The following will describe the relationship of the

critical points on the impact response curve and the physical occurrences.

If the retained strength after impact is a major consideration, then the energy at which the first fiber damage occurs, is significant. This point, Ei, has been normally attributed to correlate with the onset of fiber damage [21] which can detrimentally effect after impact properties. The energy in excess of E_i must be accounted for by such physical phenomena as fiber breakage and matrix cracking. If the energy of the impacting object is less than E_i, fiber damage would not be initiated and the loss of strength will probably be minimal. Impacts greater than E_i will damage fibers and greatly reduce the material's pre-impact properties.

Under other considerations, where the appearance of visible surface damage or the presence of a through-the-thickness crack is critical, the energy at maximum load can be used as a design criterion. It has been shown that E_m is the energy required to initiate a crack and propagate it through the thickness of the sample [21].

One last example is a non-structural components, such as a protective barrier, in which the intention is to prohibit complete

penetration. In this case E_t, the total energy absorbed during complete penetration may be the dominant feature for design considerations.

In this study there were two classes of impact response patterns associated with the different fiber architecture as exemplified in Figures 18 and 19. These correspond to braid and laminate responses, respectively. For these materials the characteristic response curves can be divided into four regions as shown in the figures. The first region starts as the tup contacts the sample and loading begins. As seen from the loading curves, the initial loading rate is generally linear until an abrupt but small decrease in load occurs at P_i. This point is observed at relatively low deformation levels and is known as the incipient damage point, generally back face cracking [21].

Figure 18: GENERAL IMPACT RESPONSE OF BRAIDED COMPOSITES

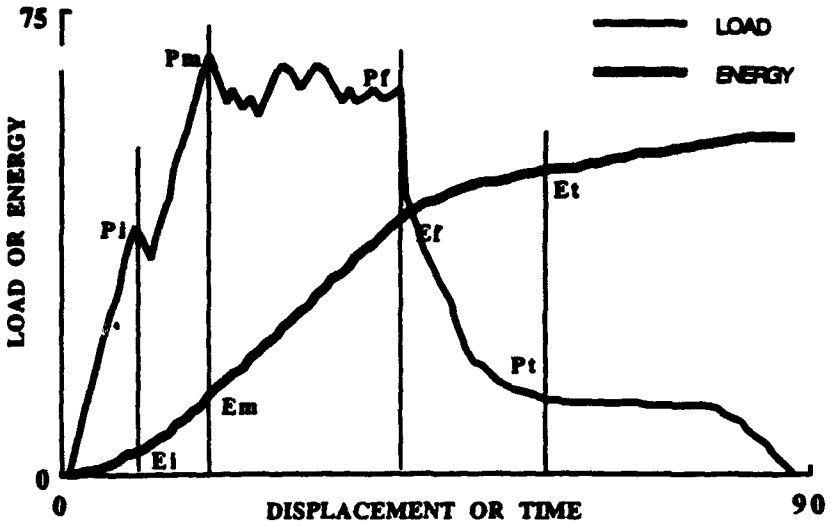

Figure 19: GENERAL IMPACT RESPONSE OF LAMINATE COMPOSITES

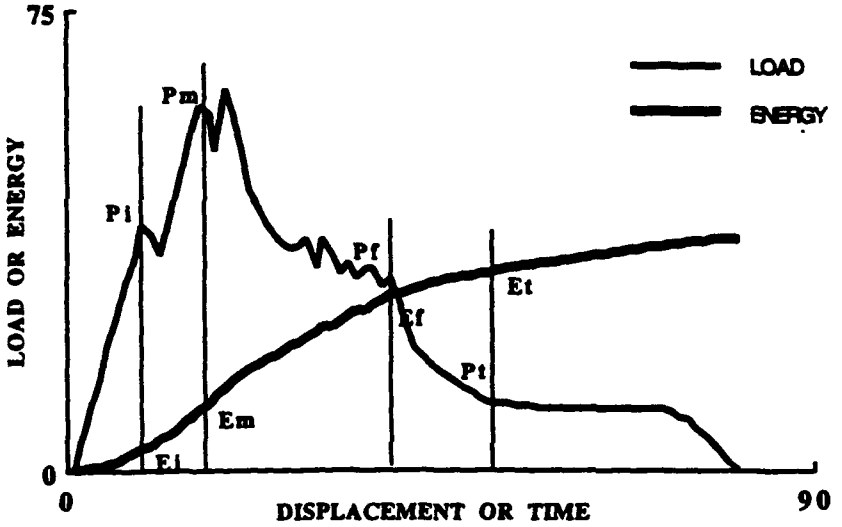

In the second region the back face crack propagates through the thickness of the sample while the load increases linearly up to its maximum point, P_m. After this point, the braided and laminate samples behave differently. The load response for the braided samples consist of a wide plateau with a series of irregular peaks and valleys near its maximum value followed by a rapid decrease. The response curve for the laminate samples has an immediate but gradual reduction in load with only a few small peaks and valleys after P_m. This extended failure mode requires an additional point to be assigned at the region in which the load begins to rapidly decrease or fail, P_f. In both cases after P_f, the load decreases to a constant level, P_t, which represents the shear force of the tup passing through the sample.

In Table 5, the load and energy values associated with each of the four points described above are listed. They were grouped in terms of fiber architecture and sample thickness. The average and standard deviation for each group are calculated and listed.

For comparison, the impact energy absorbed is plotted in Figure 20. The braided composites have a higher level of energy absorption than the laminate composites at each point for each of the three

TABLE 5: LOAD AND ENERGY VALUES FROM IMPACT TEST

ID	TYPE	THICK (in.)	LOAD (lbs.)	ENG. (ft-lb)	LOAD (lbs.)	ENG. (ft-lb)	LOAD (lbs.)	ENG. (ft-lb)	LOAD (lbs.)	ENG. (ft-lb)
1	BRAID	0.3	2437	11	3916	58	3793	167	446	217
2	BRAID	0.3	4142	50	4143	50	3158	150	452	168
3	BRAID	0.3	4420	56	4420	56	3220	153	322	175
	AVERAGE		3666	39	4160	55	3390	156	407	187
	Std. Dev.		1074	25	252	5	350	9	73	27
10	BRAID	0.5	9273	126	9274	126	5727	393	616	494
11	BRAID	0.5	7516	68	7516	68	4813	260	562	323
12	BRAID	0.5	5100	55	7972	136	6773	360	778	459
	AVERAGE		7296	83	8254	110	5771	338	652	425
	Std. Dev.		2095	38	912	37	981	69	112	90
20	BRAID	1.0	6549	22	14376	123	12527	620	1396	858
24	BRAID	1.0	9112	35	17071	222	15318	721	2029	931
	AVERAGE		7830	28	15723	173	13922	671	1713	894
	Std. Dev.		1812	9	1906	70	1973	72	448	52
30	LAM.	0.3	1897	10	3773	68	1412	130	306	137
31	LAM.	0.3	1650	12	3225	78	1230	132	450	138
32	LAM.	0.3	2699	19	3773	57	2068	107	246	135
33	LAM.	0.3	2023	15	2869	68	2868	98	624	149
	AVERAGE		2067	14	3410	68	1895	117	407	140
	Std. Dev.		449	4	444	8	742	17	168	6
41	LAM.	0.5	5098	40	5098	65	2525	232	717	281
42	LAM.	0.5	3420	27	3500	82	3790	162	776	232
43	LAM.	0.5	4709	24	5947	86	4689	194	1091	315
	AVERAGE		4409	30	4849	78	3668	196	861	276
	Std. Dev.		879	8	1243	11	1087	35	201	42
50	LAM.	1.0	7952	23	12500	133	11000	220	1504	588
51	LAM.	1.0	6886	22	10752	93	11250	210	1554	577
52	LAM.	1.0	3439	32	5750	125	4274	342	1686	448
	AVERAGE		6092	26	9667	117	8841	257	1581	538
	Std. Dev.		2359	5	3503	21	3957	73	94	78

thicknesses. The critical points of each response curve were compared and examined in more detail as shown in Figures 21-24.

At point P_i, the difference of the absorbed energy between the braided and laminated composites in the case of the 0.3" and 0.5" thick samples appear to be large but minimal for the 1.0" samples. This is not a true representation because there was not a distinct P_i for 2 out of 3 of the braided composites at the 0.3" and 0.5" thicknesses and P_m was used as P_i. If we use the sole data point from each size, 11 ft-lbs for the 0.3" sample and 55 ft-lbs and for the 0.5" thick sample, there is little difference between the braided and laminated composites.

At point P_m the difference in the amount of absorbed energy between the two materials was minimal with the absorbed energy of the braided samples slightly higher than that of the laminated samples. At point P_f the difference increased for all cases, with the braided samples absorbing much more energy than the laminated samples. This difference was maintained through P_t.

The region, between points P_m and P_f on the impact response curve, corresponds to the large plateau following the peak load. It was this

FIGURE 20: ABSORBED IMPACT ENERGY (BRAID VS LAMINATE)

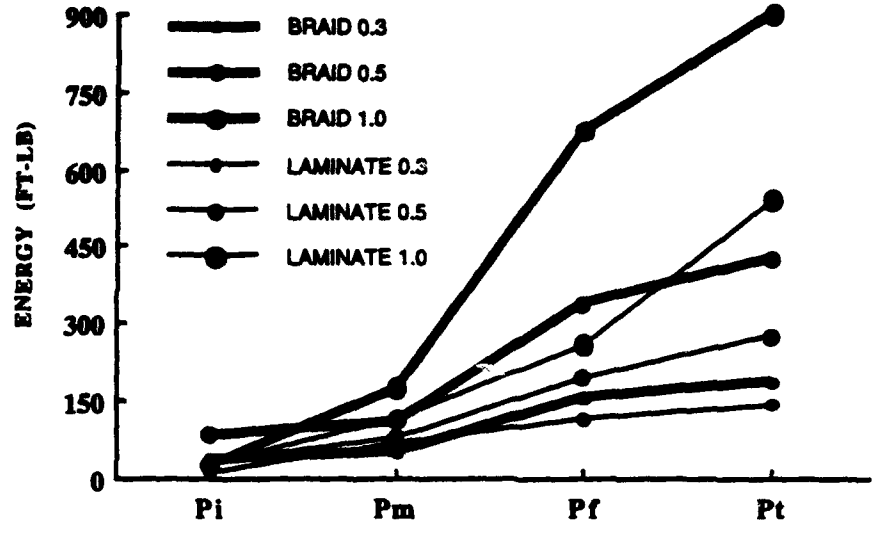

FIGURE 21: ENERGY ABSORBED AT Pi
BRAID VS LAMINATE

FIGURE 22: ENERGY ABSORBED AT Pm
BRAID VS LAMINATE

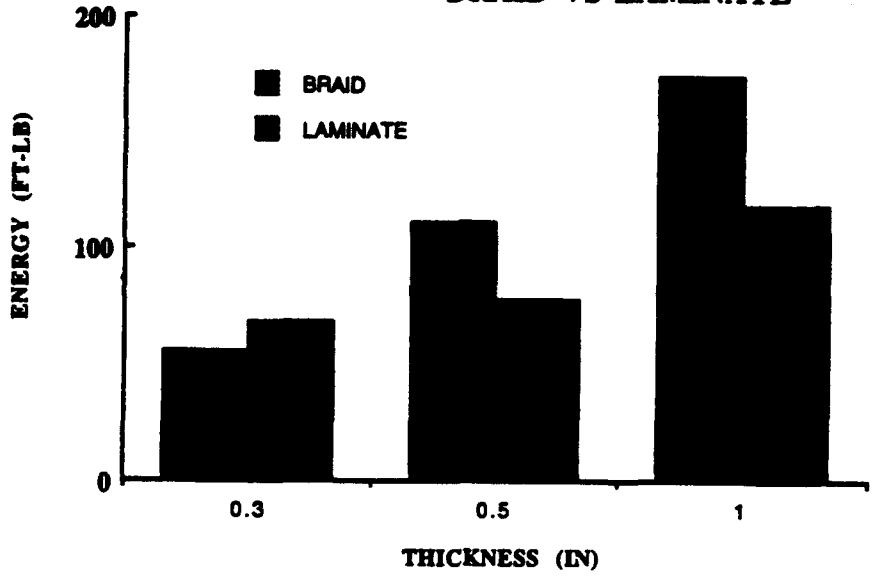

FIGURE 23: ENERGY ABSORBED AT Pf
BRAID VS LAMINATE

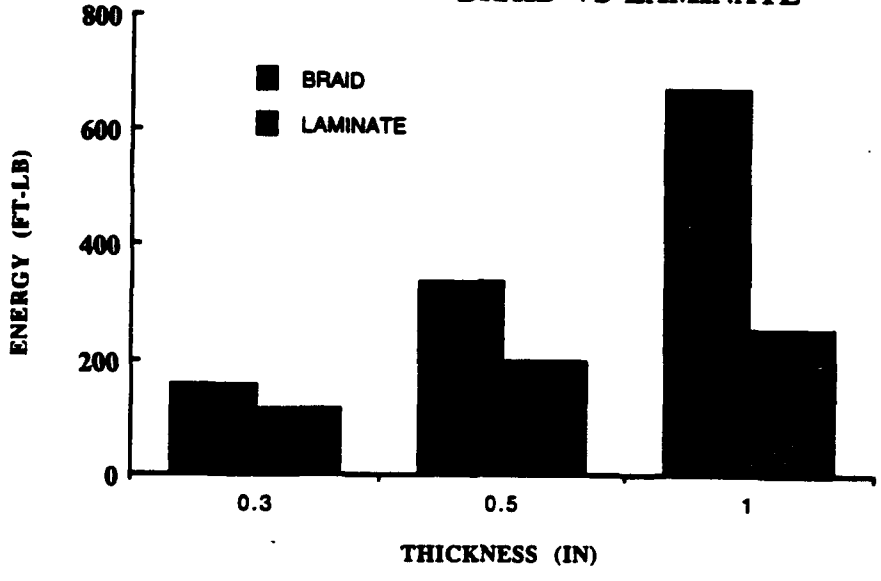

FIGURE 24: ENERGY ABSORBED AT Pt BRAID VS LAMINATE

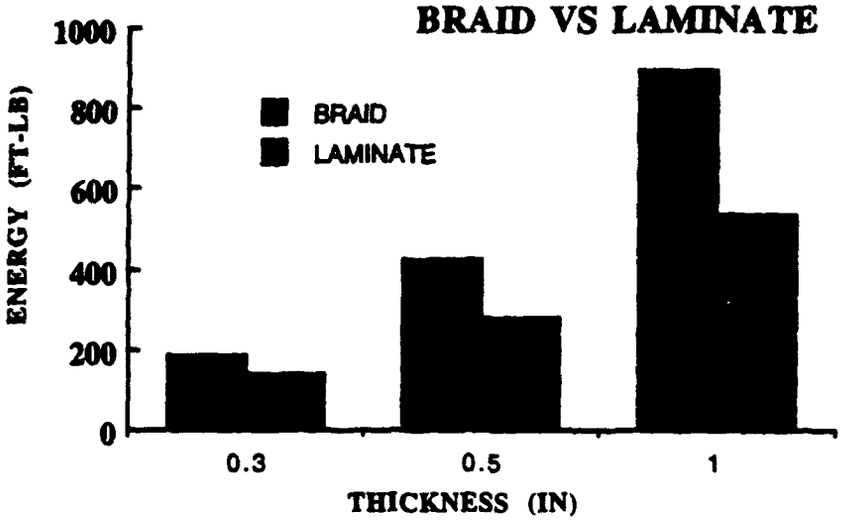

region in which the braided samples had the largest differential increase over the laminate samples. For the braided samples, this plateau was quite wide at a high loading and accounted for the majority of the energy absorbed. The plateau in the response curve of the laminate samples was very small or nonexistent and was immediately followed by a decrease in load. Because of the lower load level and shorter duration of the load response curve of the laminate composites, considerably less energy was absorbed.

In Figures 25 and 26 the effect of the thickness on the absorbed energy is shown separately for the braided and laminate composites. The percent increase in total absorbed energy of the braided composites over that of the laminate composites for the 0.3, 0.5, and 1.0 inch thick samples is 33.6%, 54.0%, and 66.2%; respectively. The larger difference in the case of the thicker samples may be attributed to the increase in fiber interlacing with the thicker sample size.

FIGURE 25: EFFECT OF PLATE THICKNESS ON ABSORBED IMPACT ENERGY OF BRAIDED COMPOSITES

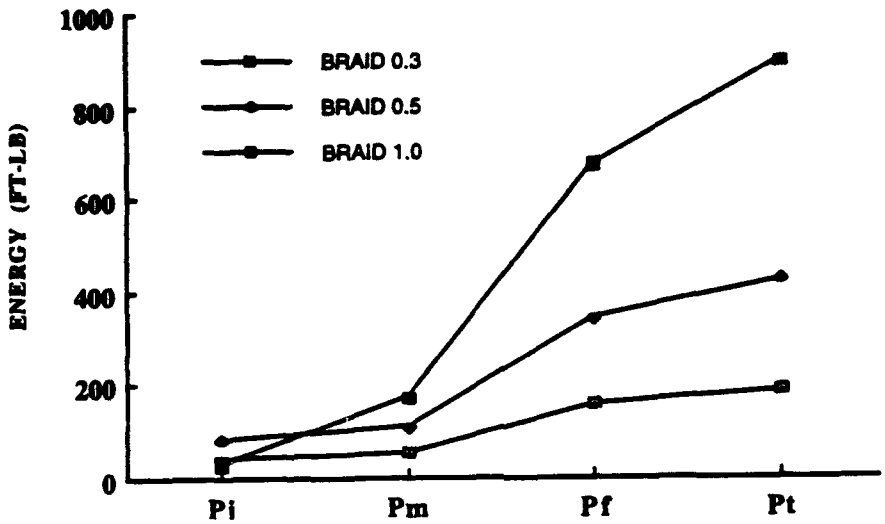

FIGURE 26: EFFECT OF PLATE THICKNESS ON ABSORBED IMPACT ENERGY OF LAMINATE COMPOSITES

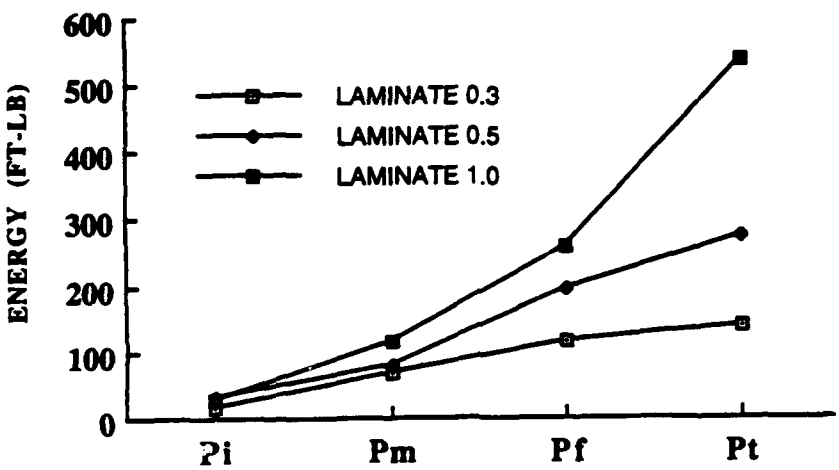

6.2 Damage Assessment

The resultant damage following impact testing was characterized utilizing light transmission and microscopic examination. Light transmission provides a global view of the extent of the damaged area while microscopic examination gives insight into the failure mechanisms.

6.2.1 Light Transmission

A light transmission technique was developed to quantify the extent of damage in each sample. The apparatus consists of a light source, video camera, video recorder, monitor and photographic camera as seen in Figure 27. This method utilizes similar principles to the x-ray transmission technique discussed previously, except that an incandescent light source replaces the x-ray source and the lanex screen is not needed because the transmitted light can be seen directly. In this case a light source is used rather than the x-ray source to enable the observance of discontinuities, such as fiber/matrix debonding, matrix cracking and fiber cracking. The discontinuities impede the light transmitted by diffraction and reflection. A permanent record in the form of video recording and

photographs was taken for each sample.

Examples of typical images obtained from light transmission examination of damaged braided and laminate samples are shown in Figures 28 and 29, respectively. The dark areas in the photographs represent areas in which light could not be transmitted because of discontinuities in the material and these define the region of damage. Several samples were sectioned, polished, and examined microscopically in order to identify the damage shown in light transmission and verify its validity. There was a small amount of matrix cracking present at the outer fringes of the damage area that were not clearly observed by light transmission. The damaged area of each sample was measured from the photographs taken with light transmission and tabulated in Table 6.

From Table 6, the damage area for the braided composites is seen to be less than the laminate composites for all sample thicknesses. Visual examination clearly shows this, as seen in Figure 30. This is a macro-photograph showing an example of the impact damage for samples of each thickness and fiber architecture. It can be seen that the braided composite tends to limit the extent of damaged area more effectively than the laminate composites.

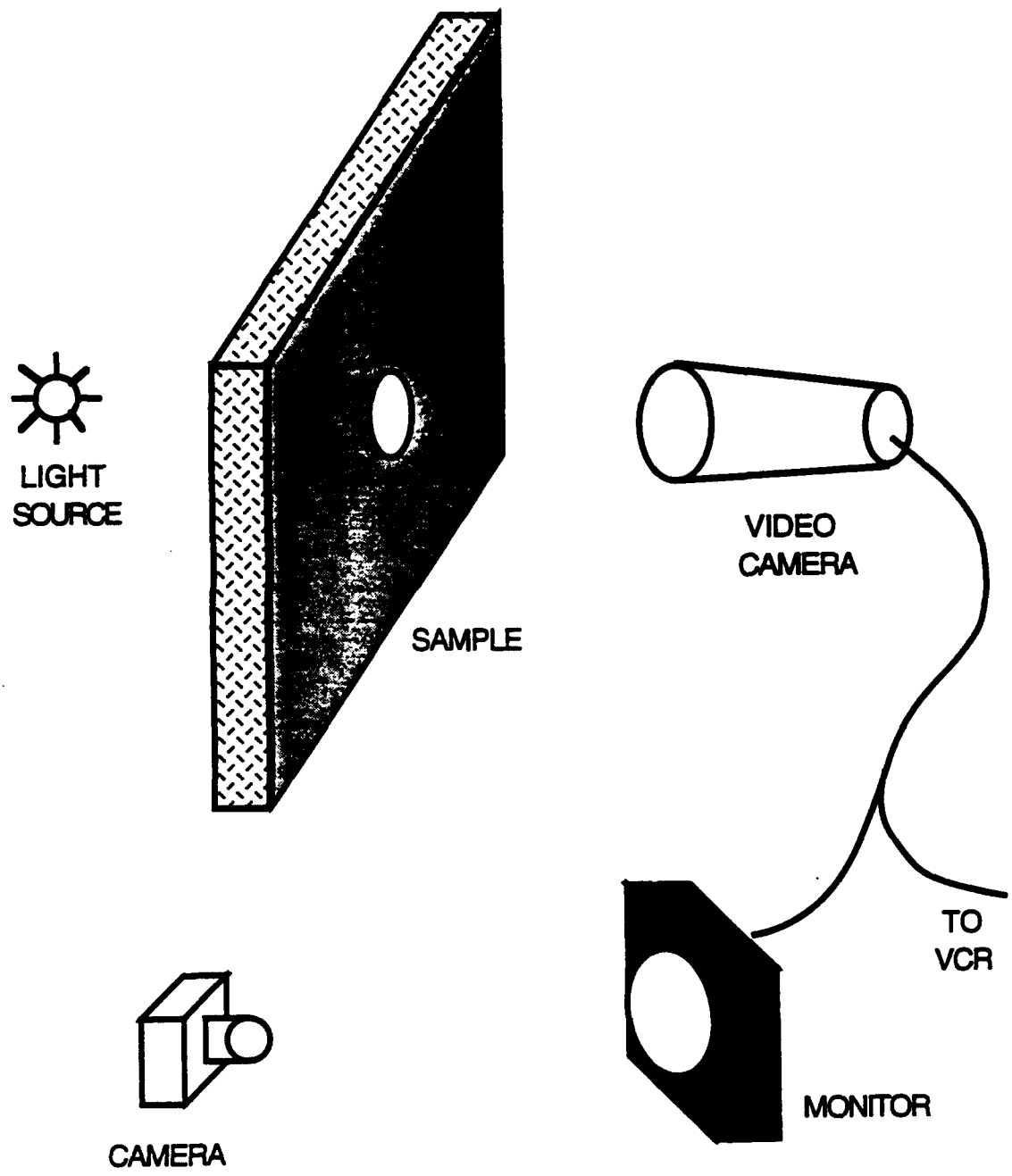

Figure 27: Schematic Diagram for Light Transmission Non-Destructive Evaluation of Damaged Composites

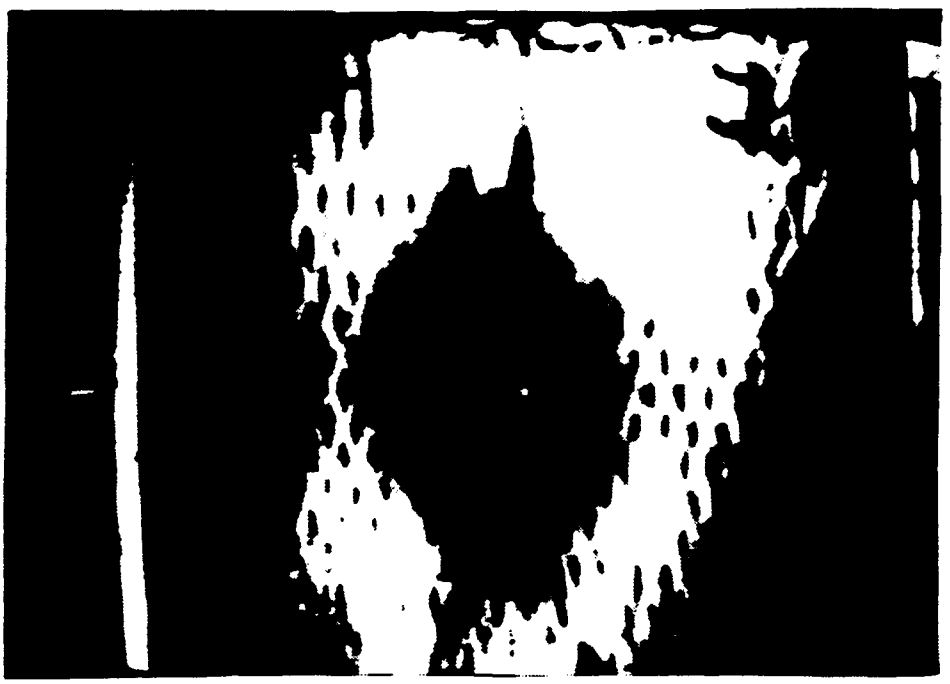

Figure 28: Damaged Region of a Braided Composite Using Light Transmission

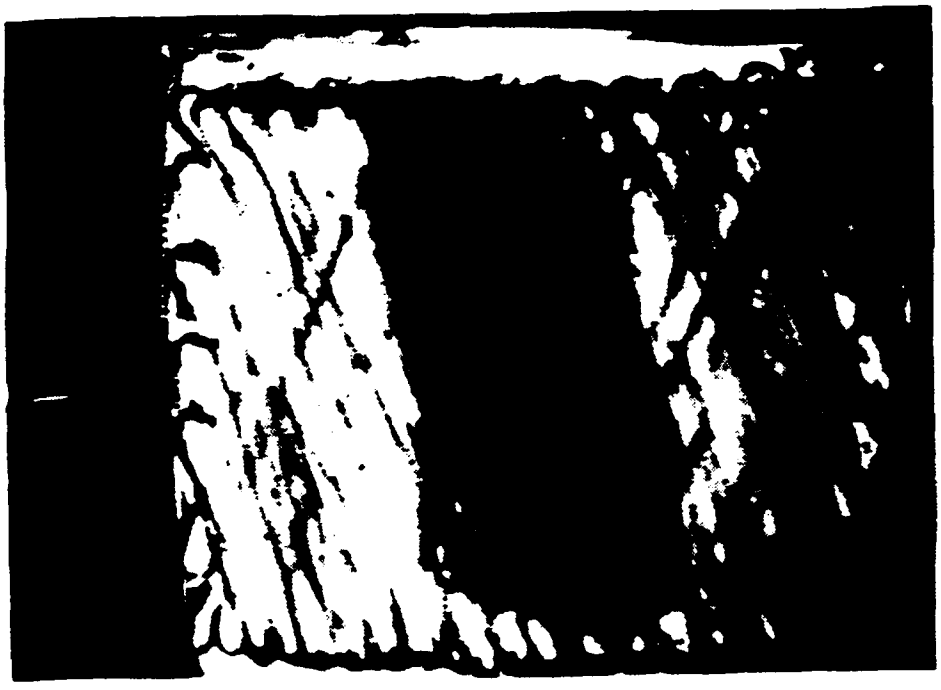

Figure 29: Damaged Region of a Laminate Composite Using Light Transmission

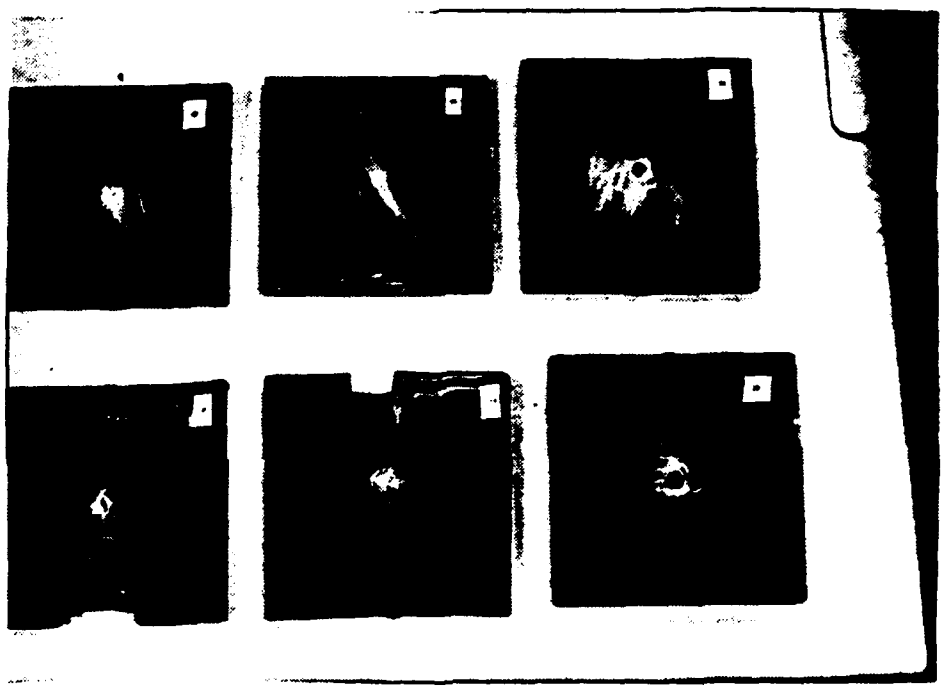

Figure 30: Photograph of Impacted Surface Showing Damaged Area. Top Row (Left to Right) 0.3 in. Laminate, 0.5 in. Laminate, 1.0 in. Laminate. Bottom Row (Left to Right) 0.3 in. Braid, 0.5 in. Braid, 1.0 in. Braid

TABLE 6: Damage Assessment from Light Transmission

SAMPLE ID	TYPE	THICKNESS INCH	DAMAGE AREA (in^2)
1	BRAID	0.3	8.00
2	BRAID	0.3	8.25
3	BRAID	0.3	7.88
		AVERAGE	8.04
10	BRAID	0.5	7.75
11	BRAID	0.5	7.50
12	BRAID	0.5	7.00
		AVERAGE	7.42
20	BRAID	1	5.25
22	BRAID	1	6.12
24	BRAID	1	5.63
		AVERAGE	5.67
30	LAMINATE	0.3	9.50
31	LAMINATE	0.3	8.80
32	LAMINATE	0.3	10.33
33	LAMINATE	0.3	9.25
		AVERAGE	9.47
40	LAMINATE	0.5	8.25
41	LAMINATE	0.5	7.44
42	LAMINATE	0.5	10.68
43	LAMINATE	0.5	9.25
		AVERAGE	8.91
50	LAMINATE	1	13.75
51	LAMINATE	1	11.87
52	LAMINATE	1	11.50
	AVERAGE		12.37

Figure 30 also shows that the penetration hole on the 1.0 inch thick samples remained open while the holes of the thinner samples closed upon removal of the indenter. This can be attributed to the higher degree of flexibility of the thinner samples where they are subject to more bending.

The damage area data was roughly normalized by multiplying the damage area by the sample thickness in order to show a comparison over a range of thicknesses. Figure 31 shows the specific damage area for the braided and laminate composites as a function of absorbed impact energy. In both cases, a linear relationship was found between the specific damage area and impact energy as was observed in previous studies [34]. Although both materials exhibit a linear relationship, the slope for the braided composites is much lower than the slope for the laminate composites. The braided sample exhibit a more efficient means of absorbing impact energy. This is an indication that the energy absorbing mechanisms for the two materials is probably different.

6.2.2 Examination of Damage

Impacted test samples from each type composite were cross

sectioned in both the transverse and the longitudinal directions, transverse being perpendicular to the primary fiber direction and longitudinal being parallel to the primary fiber direction. They were polished by ordinary metallographic techniques using a 1 micron diamond paste and left unetched. Both macroscopic and microscopic examination were used to evaluate the extent of damage and the failure mode.

FIGURE 31: SPECIFIC DAMAGE AREA VERSUS ABSORBED IMPACT ENERGY

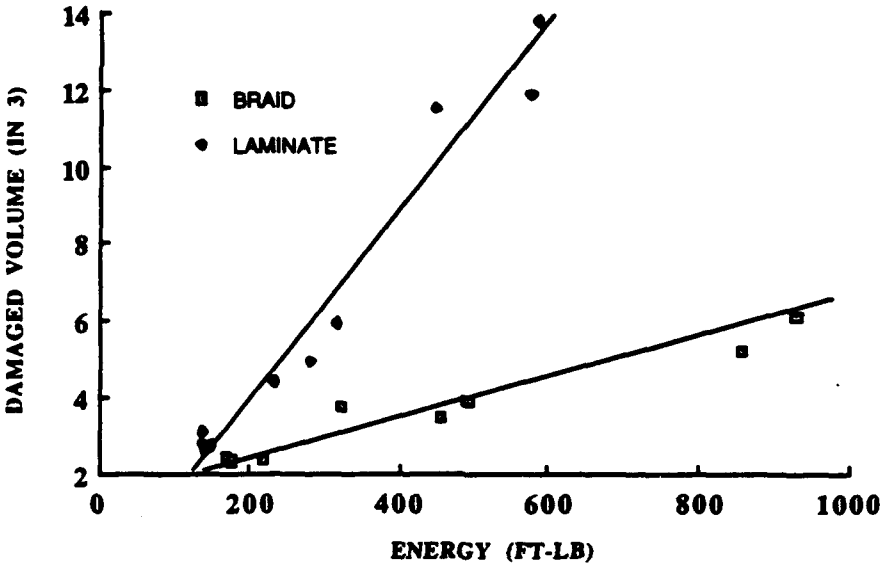

Microscopic examination was used to classify the types of damage depicted in the images produced with the light transmission technique. It was evident from the cross sectioned samples that the

dark images from the light transmission for the laminate composites largely represented areas of delamination. For the braided samples, these dark areas represented gross debonding between individual tow along with some fiber breakage.

Figures 32 and 33 show the impacted surfaces of 0.3 inch thick braided and laminate composites. In the case of all the braided composites, it appears that the cracks were initiated at the site of impact and primarily followed along the interfaces between tow bundles in the direction of fiber reinforcement. The 3-D braided structure is intensely interlaced forming a complex path for crack propagation, therefore acting as a network of crack arrestors. The constant alteration of the path of crack propagation, along with a great deal of branching and crazing, yields a dense area of damage and causes a large quantity of energy to be absorbed in a small area.

For the laminate composites, the cracks again appear to be initiated at the impact site but follow the interfaces between laminate layers. This differs from the braided composites because the interlaminar cracking occurs in the planes between each laminate layer. The crack propagation is not forced to deviate from its initial plane and therefore the crack grows with relative ease, requiring a

large area to absorb a given quantity of energy.

Longitudinal and transverse sections of 1.0 inch thick samples of braided and laminate composites are compared in Figure 34 and 35. The longitudinal views show that the laminate composite has cracking between each laminate extending a distance of over 2 inches from the impact site. The braided sample has a localized but intensive damaged zone near the impact site extending outward approximately 0.5 inches. In the transverse view, the laminate sample exhibits cracking between the layers and also within them, extending laterally up to 1.5 inches. The braided sample did not show any sign of damage outside of the penetrated hole in the transverse direction.

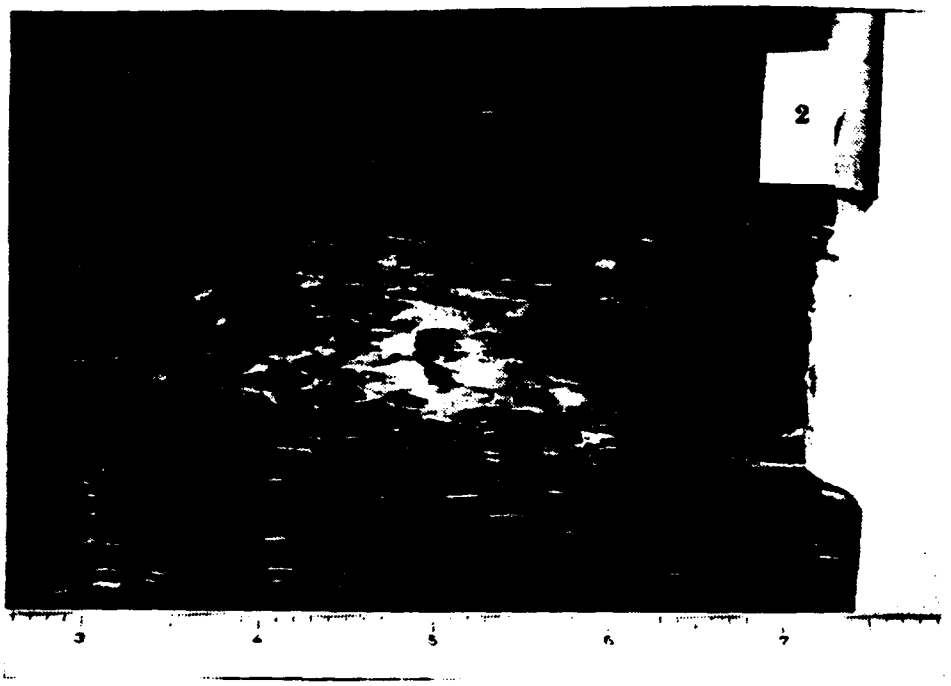

Figure 32: Impacted Surface of a 0.3 in. Braided Composite

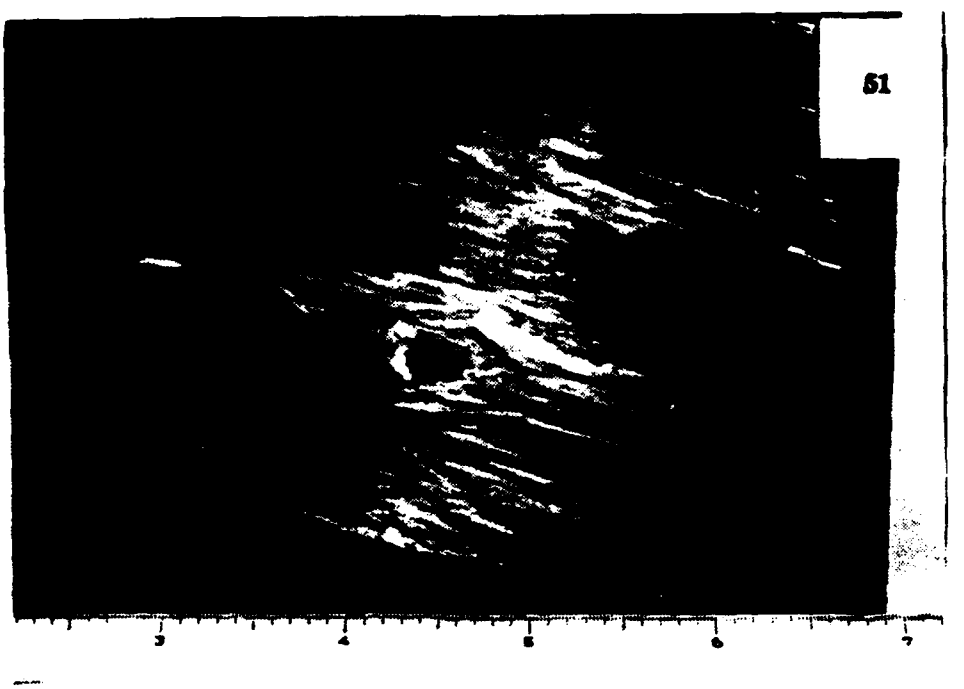

Figure 33: Impacted Surface of a 0.3 in. Laminate Composite

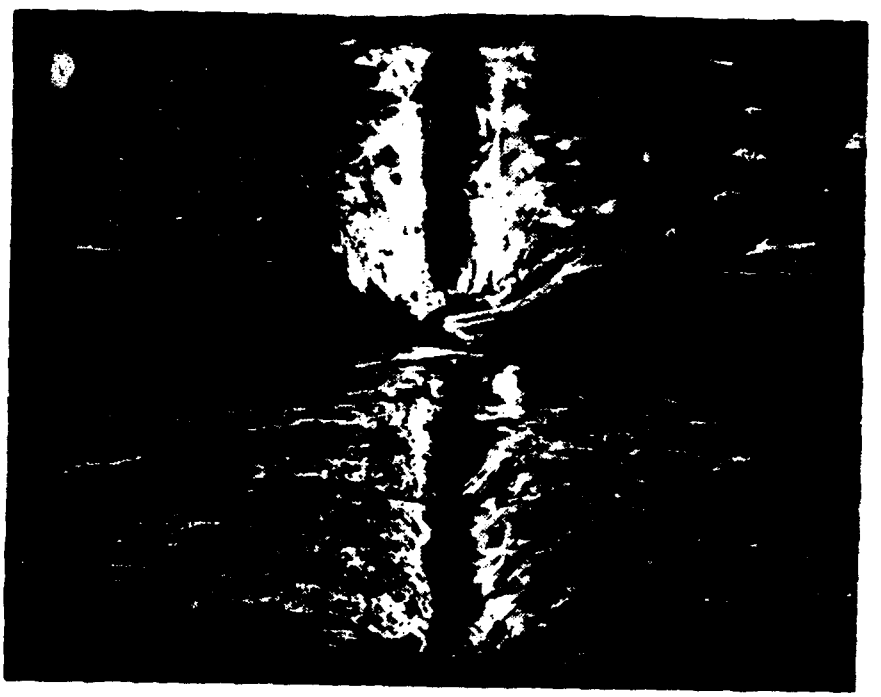

Figure 34: Longitudinal Section of 1.0 in. Samples

Top - Braid; Bottom - Laminate

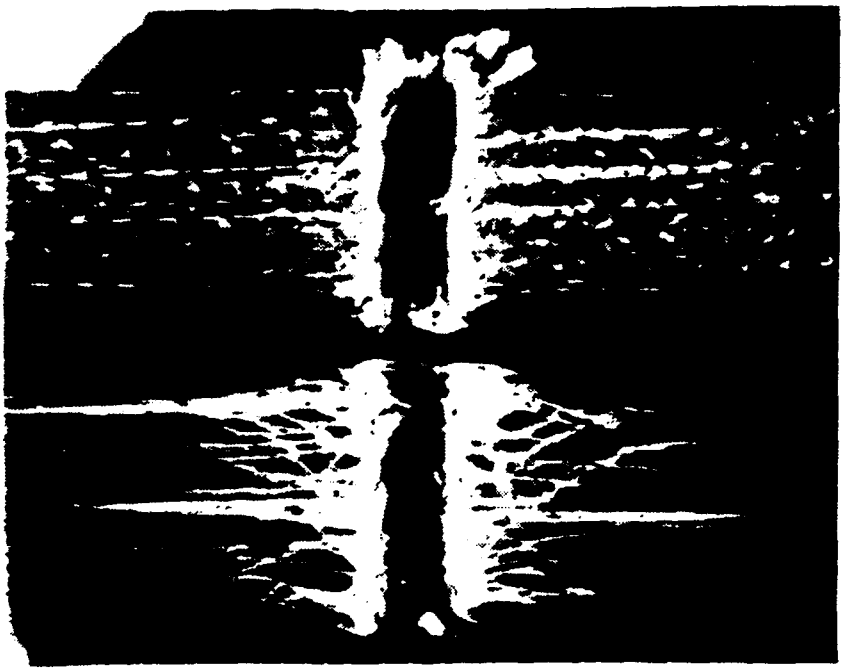

Figure 35: Transverse Section of 1.0 in. Sample

Top - Braid; Bottom - Laminate

Chapter 7

Conclusions and Recommendations

7.1 Conclusions

An instrumented impact test was utilized to characterize the impact behavior of composite plates. It was found that the impact response cannot be characterized by any individual parameter, but rather the entire load/energy impact response curve must be considered. This must be evaluated in conjunction with a determination of the damaged area and failure mechanisms in order to fully assess the impact behavior of composites.

Two types of composite materials were utilized to isolate the influence of the fiber reinforcement in the through-the- thickness direction on the impact response: 1) a 1x1x1 Euclidian 3-D braided structure and 2) a ±20 degree angle-ply laminate. The construction of the fibrous reinforcement of the two composites were similar except that the laminated samples had reinforcement only in the x-y plane where the braided samples had reinforcement with an

additional "z" component, which can be seen in Figure 36. In a comparison between the 3-D braid and ±20 angle-ply composites, the braid absorbed a higher level of energy under identical impact conditions. This is most evident in the later portion of the impact response, where the braid exhibits an extended plateau on the load curve.

The improved damage tolerance of the braided composites can be attributed to their interlacing network of reinforcing fibers. Laminates traditionally have relatively weak interlaminar layers and low through the thickness strength. This allows crack formation and easy propagation between the reinforcing layers. The "z" component of the fibers in the braided composites not only eliminates the interlaminar layers but also sets up a network of sites for crack deflection throughout the material.

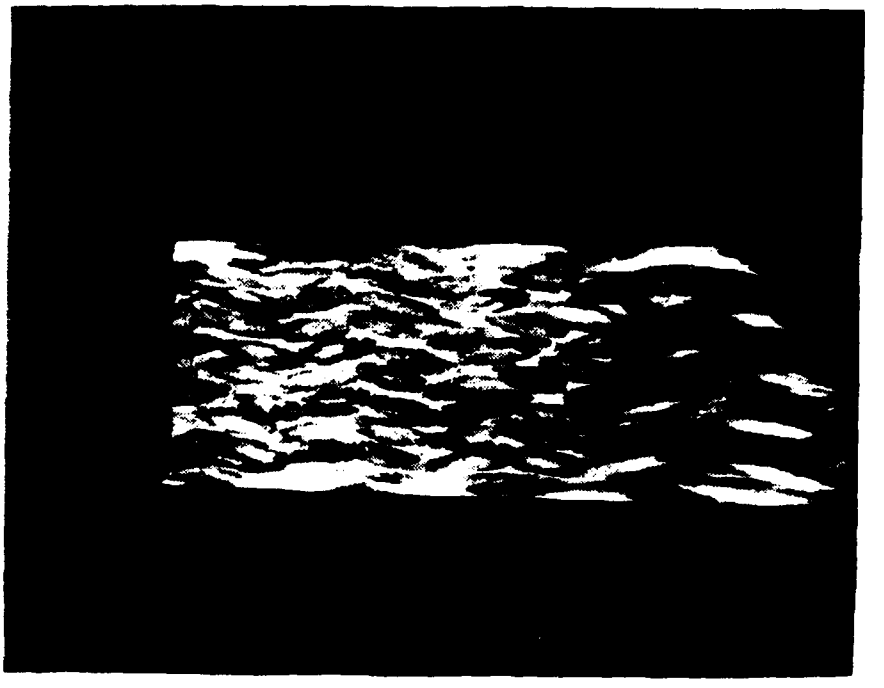

Figure 36: Transverse Section of 1.0 in. Braided Sample Showing the Level of Reinforcement in the "z" Direction

The percent increase in total absorbed energy of the braided composites versus the laminate composites for the 0.3, 0.5, and 1.0 inch thick samples is 33.6%, 54.0%, and 66.2%; respectively. The data show a correlation between the thickness and the improvement of damage tolerance of the braided composites versus the laminated composites.

This can be explained by the increased degree of interlacing of the braided composites as the thickness is increased. Figure 37 shows the cross section of a 0.3 in. braided sample. The 0.3 in. braided preforms had three columns in the braiding process, which essentially creates three intertwined layers through the thickness. As seen below, the top and bottom layers, because of the boundary conditions, do not have a large "z" component. As the thickness of the sample increases, the effect of the boundary conditions are decreased because the top and bottom layers with their reduced z-component reinforcement become a smaller percentage of the over all reinforcement. Therefore a relatively greater increase in "z" direction reinforcement occurs as the composite thickness increases.

Figure 37: Cross Section of 0.3" Thick Braided Sample

It was also shown that the braided samples absorbed higher levels of energy within a smaller area of damage propagation. This can be attributed to a difference in failure mode between the two materials. The angle-ply laminate failed primarily by delamination, cracks propagating between each lamina. This is essentially matrix cracking in an unrestricted direction and requires a low amount of energy. The braided material failed by cracks propagating between fiber tow. Since the tow are interlaced in a complex architecture, a network of crack arrestors is inherent in the material. There is no easy path for the cracks to propagate.

There are several by-products of this thesis that are of importance such as the non-destructive evaluation techniques using x-ray and light transmission that were designed and verified. Since X-ray absorption is a function of density, X-ray transmission was utilized in the detection of voids and the evaluation of fiber placement. Light transmission works well in detecting discontinuities such as delamination and cracks in composite plates. The transmission techniques proved to be extremely rapid and reliable.

7.2 Recommendations

Manufacturing techniques were developed to make the fiber preforms and consolidate them by resin transfer molding. It was found that this could be accomplished with a limited amount of hardware and expense; however, the procedures were extremely labor intensive. If future work is to be conducted on a larger scale, an automated means of manufacturing 3-D braided preform must be developed. Not only is the method in this study extremely labor intensive, but also the quality of the preforms may vary with variations in operator procedures.

This study has shown that the interlacing of the fiber in the through-the-thickness direction is an effective method of improving damage tolerance. Future work should be conducted in the development of new fiber architecture with higher levels of interlacing. This 3-D structures should also be compared other existing composite structures such as fabric laminates, 2-D, 2.5-D and angle interlock systems.

It has been explained that the critical points along the impact response curve have been cited to correlate to specific physical

phenomena occurring in the sample. The cited report dealt with thin laminate composites, under 0.25 inches thick. It would be of interest to determine if the same phenomena occur in thicker samples as well as with different fiber architectures.

BIBLIOGRAPHY

BIBLIOGRAPHY

1. Buynak, C.F., Moran, T. I. and Donaldson, S., "Characterization of Impact Damage in Composites", SAMPE Journal, March/April, 1988

2. Chang, F.K., Choi, H.Y. and Jeng, S.T., "Characterization of Impact Damage in Laminated Composites", SAMPE Journal, January/February, 1990

3. Gandhe, G.V., Griffin, O.H., "Post-Impact Characterization of Interleaved Composite Materials", SAMPE Quarterly, v20, 1989

4. Ko, F.K., Hartman, D. "Impact Behavior of 2-D and 3-D Glass/Epoxy Composites", SAMPE Journal, July/August, 1986

5. Gause, L.W., Alper, J.M., "Structural Properties of Braided Graphite/Epoxy Composites", Journal of Composites Technology and Research, v9 n4, 1987

6. Verpoest I., et al., "2.5D and 3D Fabrics for Delamination Resistant Composite Laminates And Sandwich Structures", SAMPE conference, 1988, Milano

7. Ko, F.K., and Koczak, M., "Structural Toughening of Glass Matrix Composites by 3-D Fiber Architecture", Ceramic Engineering, Science and Processing, v3, 1987

8. Proceedings of the 2nd Textile Structural Composite Symposium, Drexel University, February 10-11, 1987

9. Ko, F.K., Razavi, A., Rogers, H.C., "An Evaluation of the Failure Behavior of 3-D Braided FP/Aluminum-Lithium Composites Under Static and Dynamic Blanking", ASTM, STP 964, 1988

10. Adams, A.F., Zimmerman, R.S., "Static and Impact

Performance of Polyethylene Fiber/Graphite Fiber Hybrid Composites", SAMPE Journal, November/December, 1986

11. Nolet, S.C., Sandusky, P.M., "Impact Resistant Hybrid Composite for Aircraft Leading Edge", SAMPE Quaterly, July, 1986

12. Ko, F.K., and Pastore, C.M., "Workshop on Braiding Technology", 4th Textile Structural Composites Symposium, Drexel University, Phila., PA, 1989

13. Ko, F.K., "Three Dimensional Fabrics for Composites", Textile Structural Composites, Elsevier Science Publishers, 1989

14. Erturk, T. etal., "Tailoring Interphase Properties for Damage Containment in Graphite/Aluminum Metal Matrix Composites", MIT, Cambridge, MA

15. Mullen, J.V., "Influence of Fiber Property Variation on Composite Failure Mechanisms", ASTM STP 521, 1973

16. Jang, B.Z., Chen, L.C., et al., "The Response of Fibrous Composites to Loading", Polymer Composites, v11, 1990

17. Chawla, K.K., Composite Materials, Springer-Verlag, N.Y., 1987

18. Prosser, R.A., "Penetration of Nylon Ballistic Panels by Fragment Stimulating Projectiles", Textile Research Institute, March, 1988

19. Toland, R.H., "Failure Modes in Impact-Loaded Composite Materials", Failure Modes in Composites, Proceedings of the Symposium 1972, Sponsored by The Metallurgical Society, Boston, MA

20. Liu, D. and Malvern, L.E., "Matrix Cracking in Impacted Glass/Epoxy Plates", Journal Of Composite Materials, v21, July 1987

21. Wardle, M.W., Tokarsky, E.W., "Drop Weight Impact Testing of Laminates Reinforced with Kevlar Aramid Fibers, E-Glass, and Graphite", Composite Tech Review, v5 n1, 1983

22. Winkel, J.D. and Adams, D.F., "Instrumented Drop Weight Impact Testing of angle-ply and Fabric Composites", Composites, v16, n4, October 1985

23. Ireland, D.R., "Proceedings and Problems Associated with Reliable Control of the Instrumented Impact Test", ASTM STP 563, 1973

24. Beaumont, P.W., et al., "Foreign Object Impact Damage to Composites", ASTM STP 568, 1975

25. Vasudev, A. and Mehlman, M., "A Comparative Study of the Ballistic Performance of Glass Reinforced Plastic Materials", SAMPE Quarterly, v18 n4, July 1987

26. Zukas, J.A., et al., Impact Dynamics, John Wiley And Sons, N.Y., 1982

27. Pinnel, M.F. and Sjoblom,P.O., Low Velocity Impact Testing of Thermoplastic and Thermoset Matrix Composite Materials, WRDC-TR-90-4078, Wright-Patterson Air Force Base, Ohio, 1988

28. Wei, L. and Shiekh, A.E., "The Effect of Processes and Processing Parameters on 3-D Braided Preforms for Composites", SAMPE Quarterly, v19 n4, July 1988

29. Sjoblom, P.O., Hartness, J.T. and Cordell, T.M., "On Low Velocity Impact Testing of Composite Materials", Journal of Composite Materials, v22, 1988

30. Moore, D.R., Prediger, R.S., "A Study of Low-Energy Impact of Continuous Carbon-Fibers-Reinforced Composites",

Polymer Composition, v9 n5, 1988

31. Agarwal, B.D., and Broutman, L.J., Analysis and Performance of Fiber Composites, John Wiley and Sons, N.Y., 1980

32. Adams, D.F., "Impact Response of Polymer - Matrix Composite Materials", Composite Materials, ASTM STP 617, 1977

33. Hayward, J.S. and Harris, B., "Effect of Process Variables on the Quality of RTM Mouldings", SAMPE Journal, v26 n3, 1990

34. Hong, S. and Liu, D., "On the Relationship Between Impact Energy and Delamination Area", Experimental Mechanics, June, 1989

APPENDIX A

IMPACT LOAD/ENERGY RESPONSE CURVES

Appendix A: Impact Load/Energy Response Curves

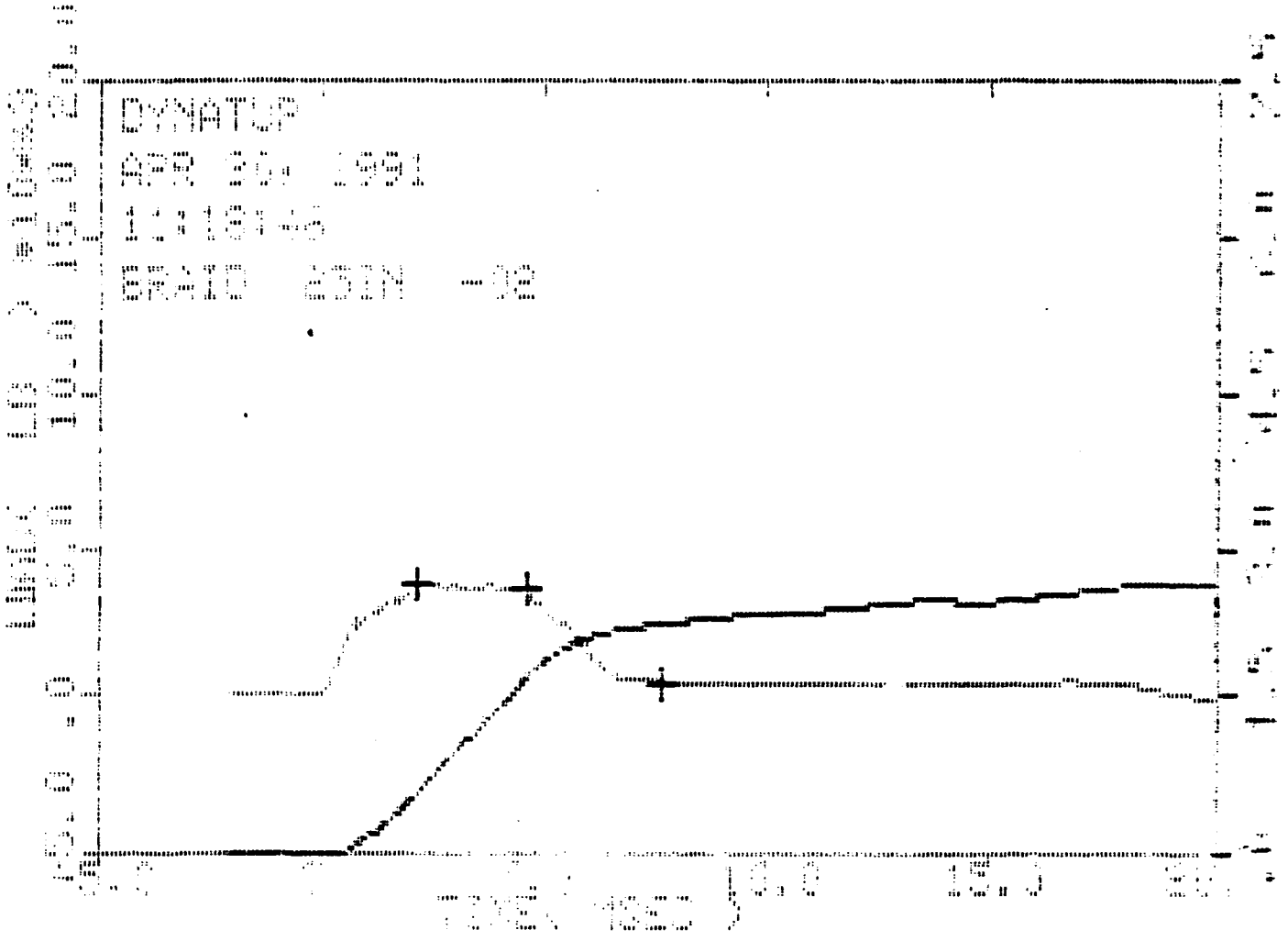

Specimen Id.	Temperature T	Slope lb/in	Velocity ft/sec	Time msec	Load lb	Energy ft-lb	Deflect inch
BRAID 45in -0% 71.3V .0%							
Impact:		11.78			1270.11		
Yield:			.00	.00	.00	.00	
Maximum Load:			2.35	3973.05	67.58	.33	
Failure(.00%):			.00	.00	.00	.00	
Energy After Max Load:					202.99		
Total Energy:			19.50		270.57	2.61	
Pt. 1:		11.58	2.15	3916.16	58.45	.30	
Pt. 2:		11.13	4.60	3792.89	166.68	.64	
Pt. 3:		10.98	7.65	445.66	217.48	1.04	

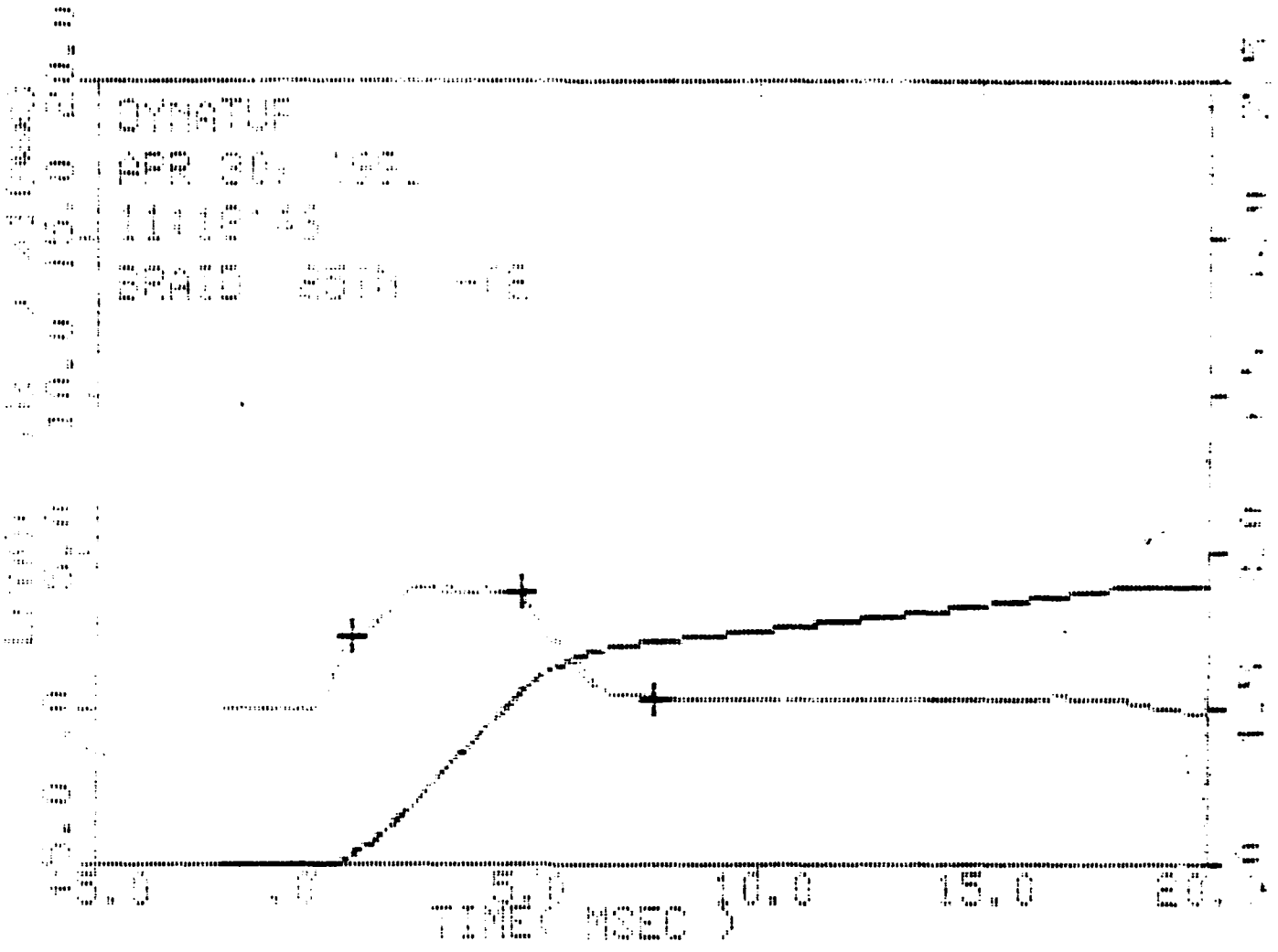

Specimen Id.	Temperature F	Slope lb/in	Velocity ft/sec	Time msec	Load lb	Energy ft-lb	Deflect inch
BRAID .25IN -02	72.00	.000					
Impact:			11.76			1270.11	
Yield:				.00	.00	.00	.00
Maximum Load:				2.35	3973.05	67.58	.33
Failure(.00%):				.00	.00	.00	.00
Energy After Max Load:						202.99	
Total Energy:				19.50		270.57	2.61
pt 1:			11.76	.80	2436.93	10.60	.11
pt 2:			11.13	4.60	3792.89	166.65	.64
pt 3:			10.98	7.60	455.15	217.23	1.03

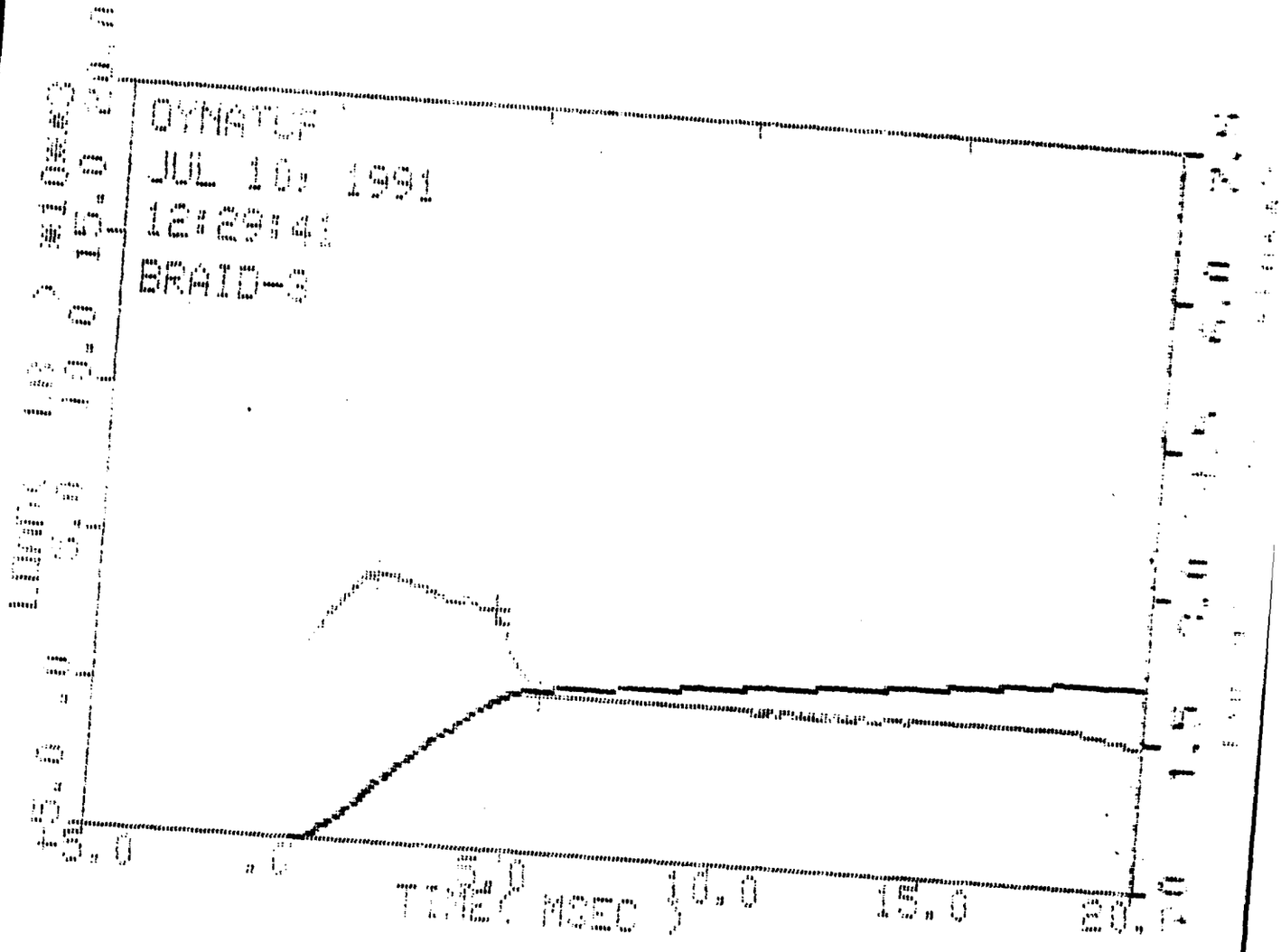

Specimen Id.	Temperature F	Slope lb/in	Velocity ft/sec	Time msec	Load lb	Energy ft-lb	Deflect inch
BRAID-3	75.00	.000					
Impact:			10.06			911.99	
Yield:				.00	.00	.00	
Maximum Load:				1.85	4172.05	57.96	.00
Failure(.00%):				.00	.00	.00	.22
Energy After Max Load:						152.92	.00
Total Energy:				19.62		210.88	
Pt. 1:			9.83	1.65	4142.53	49.83	2.23
Pt. 2:			9.35	4.50	3158.35	149.74	.20
Pt. 3:			9.28	5.70	452.63	167.58	.52
							.66

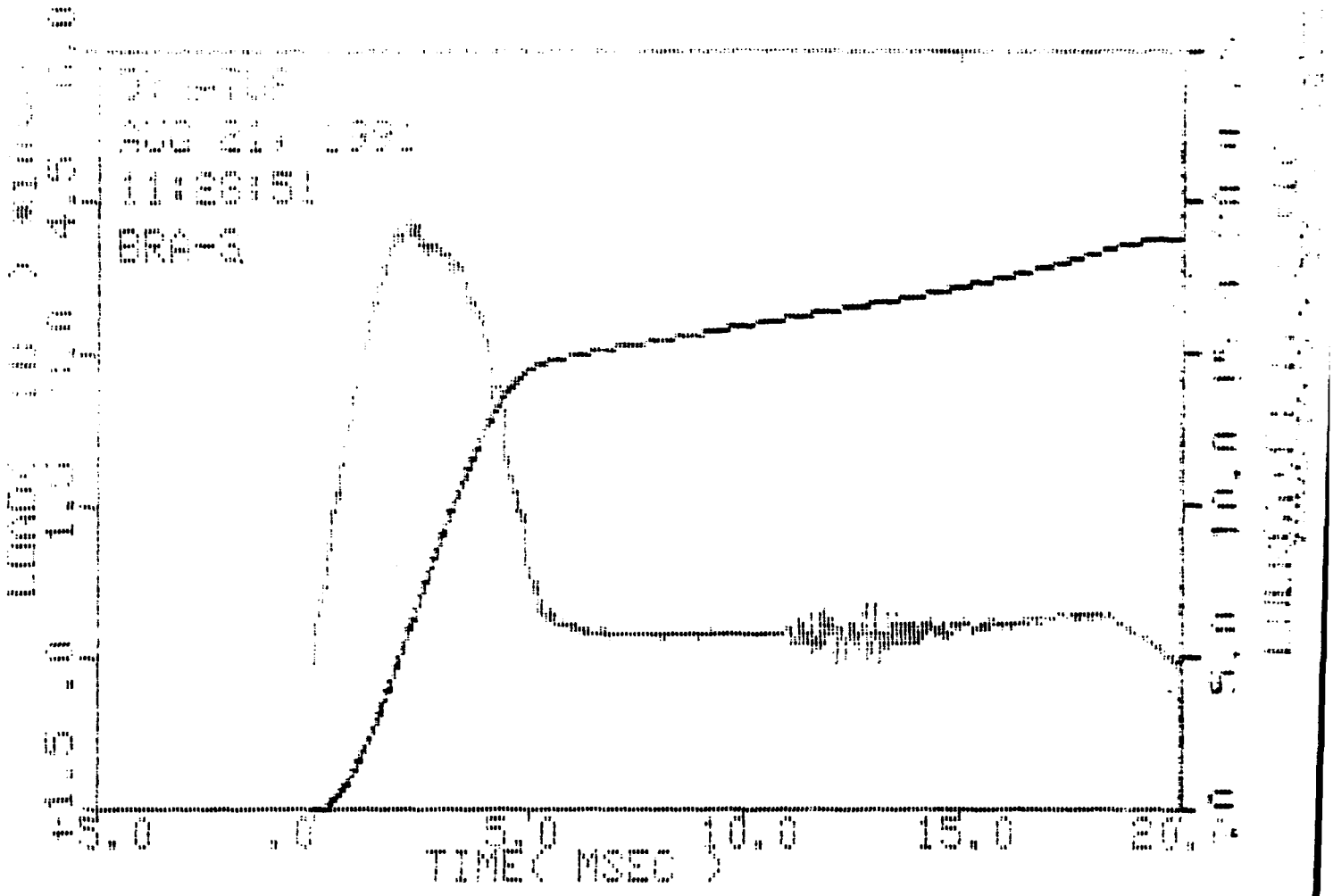

Specimen Id	Temp (f)	Veloc. (ft/sec)	Impact Energy (ft-lb)	Time (msec) Max Ld	Time (msec) Total	Load (lb) Max	Energy (ft-lb) Maxld	Energy (ft-lb) Total
bra-3	75.	10.12	922.40	2.27	12.10	4313.7	61.962	165.488

Filter No.= 1. No Smoothing.
Comments:

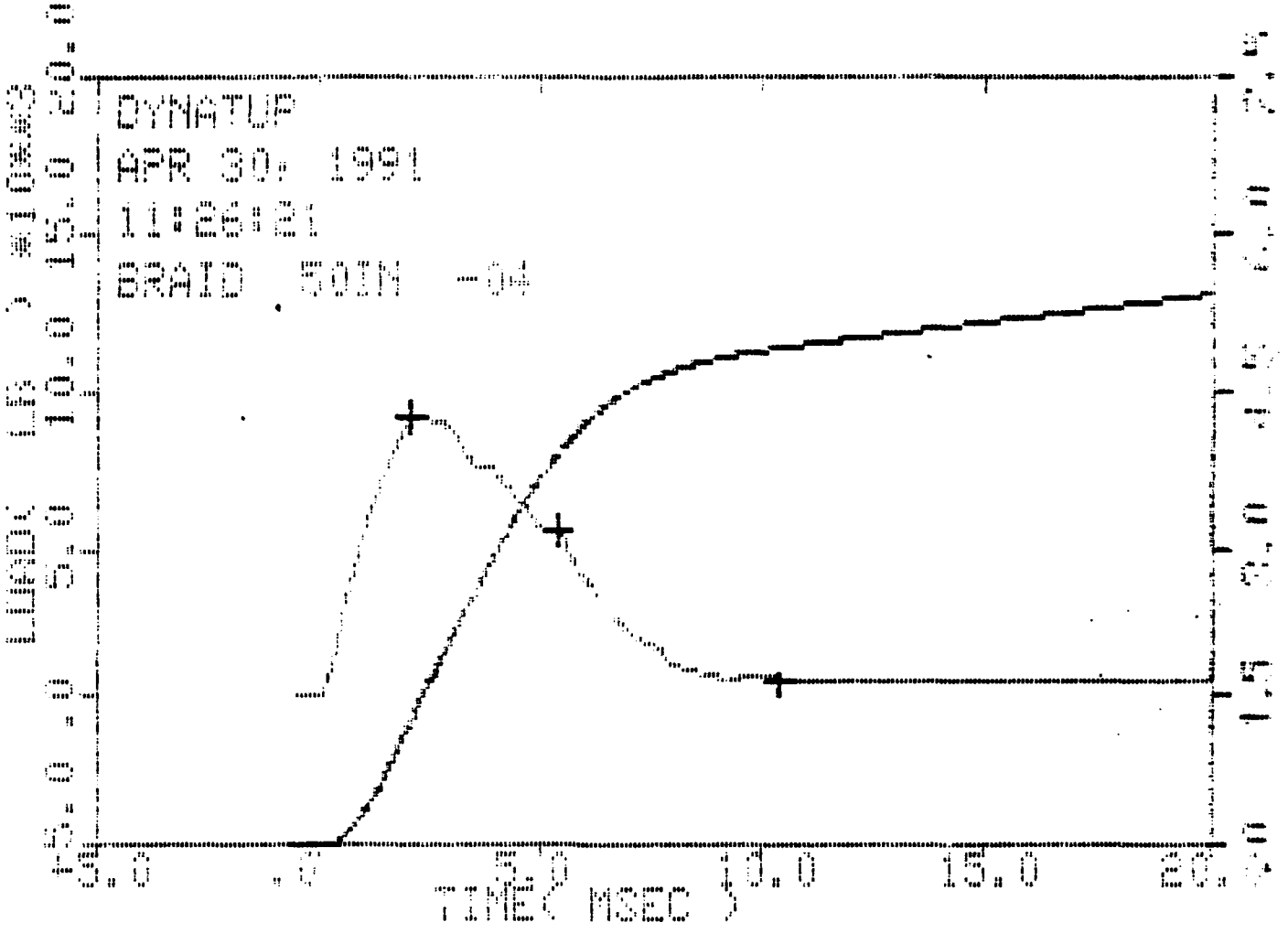

Specimen Id.	Temperature F	Slope lb/in	Velocity ft/sec	Time msec	Load lb	Energy ft-lb	Deflect inch
BRAID .50IN -04	72.00	.000					
Impact:			11.73			1259.62	
Yield:				.00	.00	.00	.00
Maximum Load:				2.20	9330.50	136.77	.30
Failure(.00%):				.00	.00	.00	.00
Energy After Max Load:						414.97	
Total Energy:				21.90		551.74	2.60
Pt. 1:			11.20	2.10	9273.61	126.38	.29
Pt. 2:			9.92	5.40	5727.26	393.55	.71
Pt. 3:			7.52	10.40	616.34	493.91	1.29

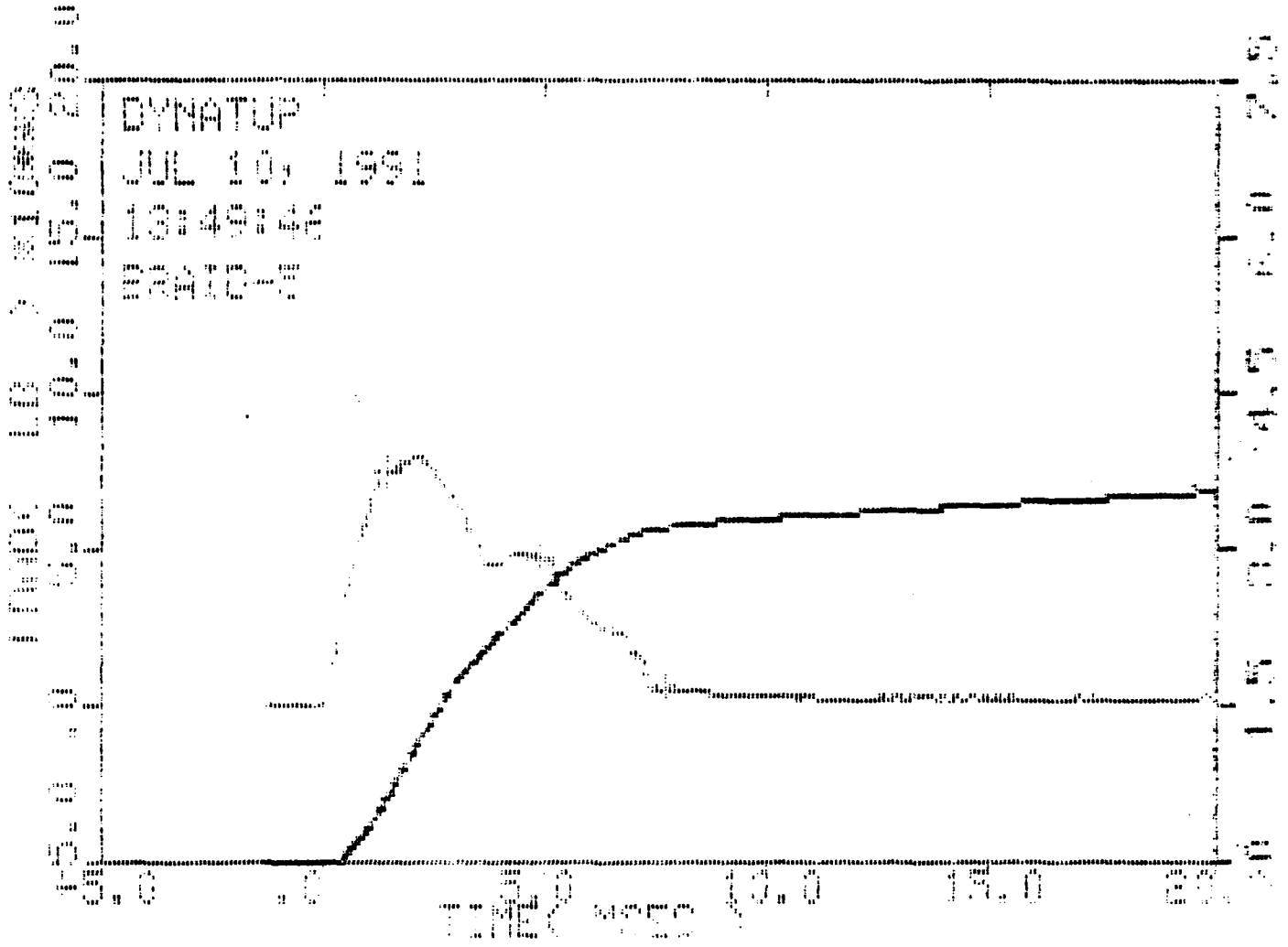

Specimen Id.	Temperature °F	Slope lb/in	Velocity ft/sec	Time msec	Load lb	Energy ft-lb	Deflection inch
3PNJB-3	77.10	1060					
Impact:		10.03				910.27	
Yield:				.00	.00	.00	.00
Maximum Load:				2.20	9019.44	118.63	.35
Failure(.00%):				.00	.00	.00	.00
Energy After Max Load:						242.63	
Total Energy:				21.95		361.45	2.27
Pt. 1:			4.72	1.32	7516.38	68.25	.18
Pt. 2:			9.67	4.90	4813.64	260.00	.55
Pt. 3:			8.04	7.70	562.25	323.04	.84

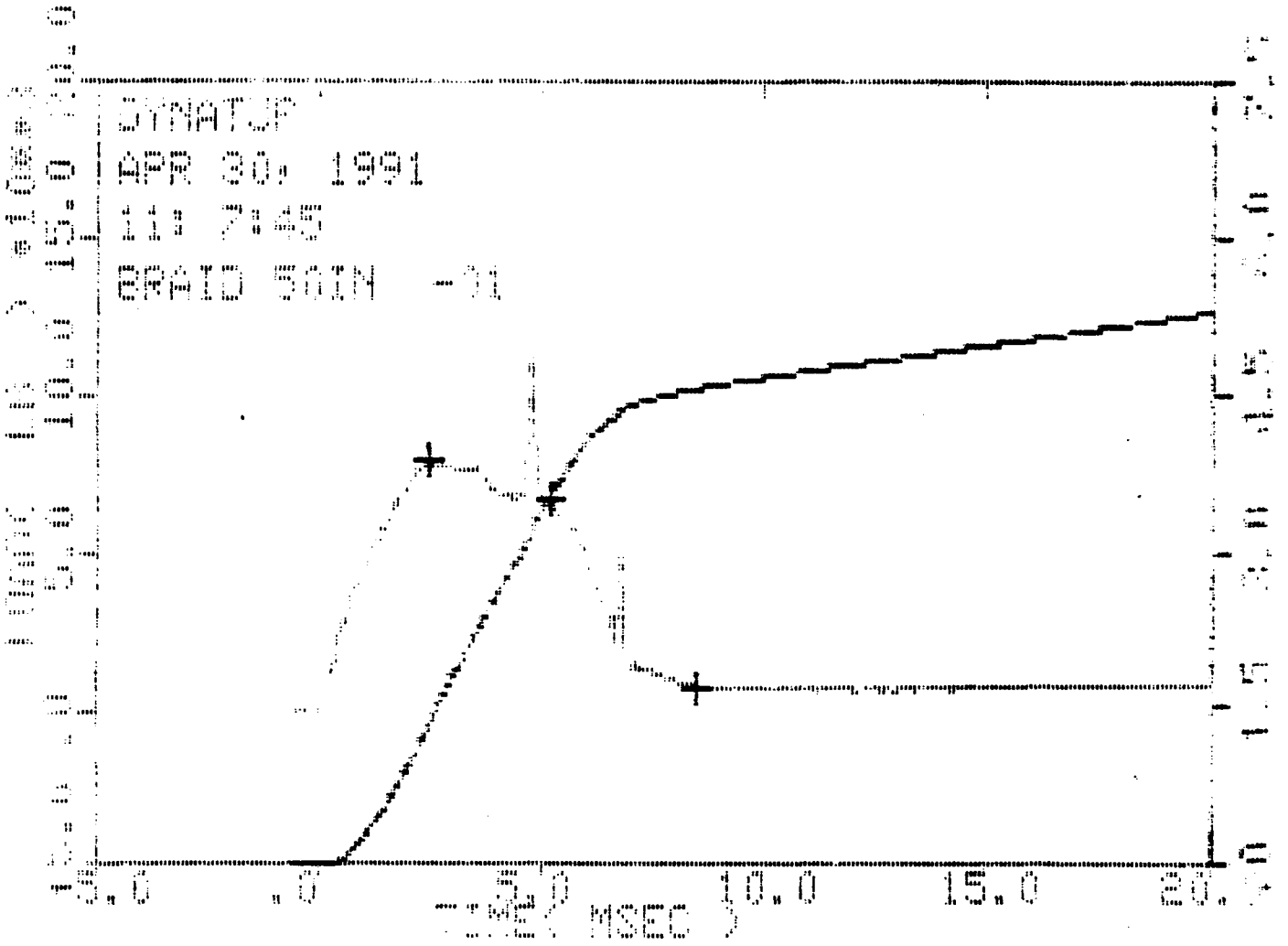

Specimen Id.	Temperature F	Slope lb/in	Velocity ft/sec	Time msec	Load lb	Energy ft-lb	Deflect inch
BRAID 50IN -01	72.00	.000					
Impact:			11.74			1260.78	
Yield:				.00	.00	.00	.00
Maximum Load:				4.77	11364.61	325.20	.64
Failure(.00%):				.00	.00	.00	.00
Energy After Max Load:						213.33	
Total Energy:				21.80		538.53	2.62
Pt. 1:			11.17	2.45	7972.30	135.67	.34
Pt. 2:			10.11	5.22	6773.23	360.10	.69
Pt. 3:			9.67	8.52	777.88	458.84	1.08

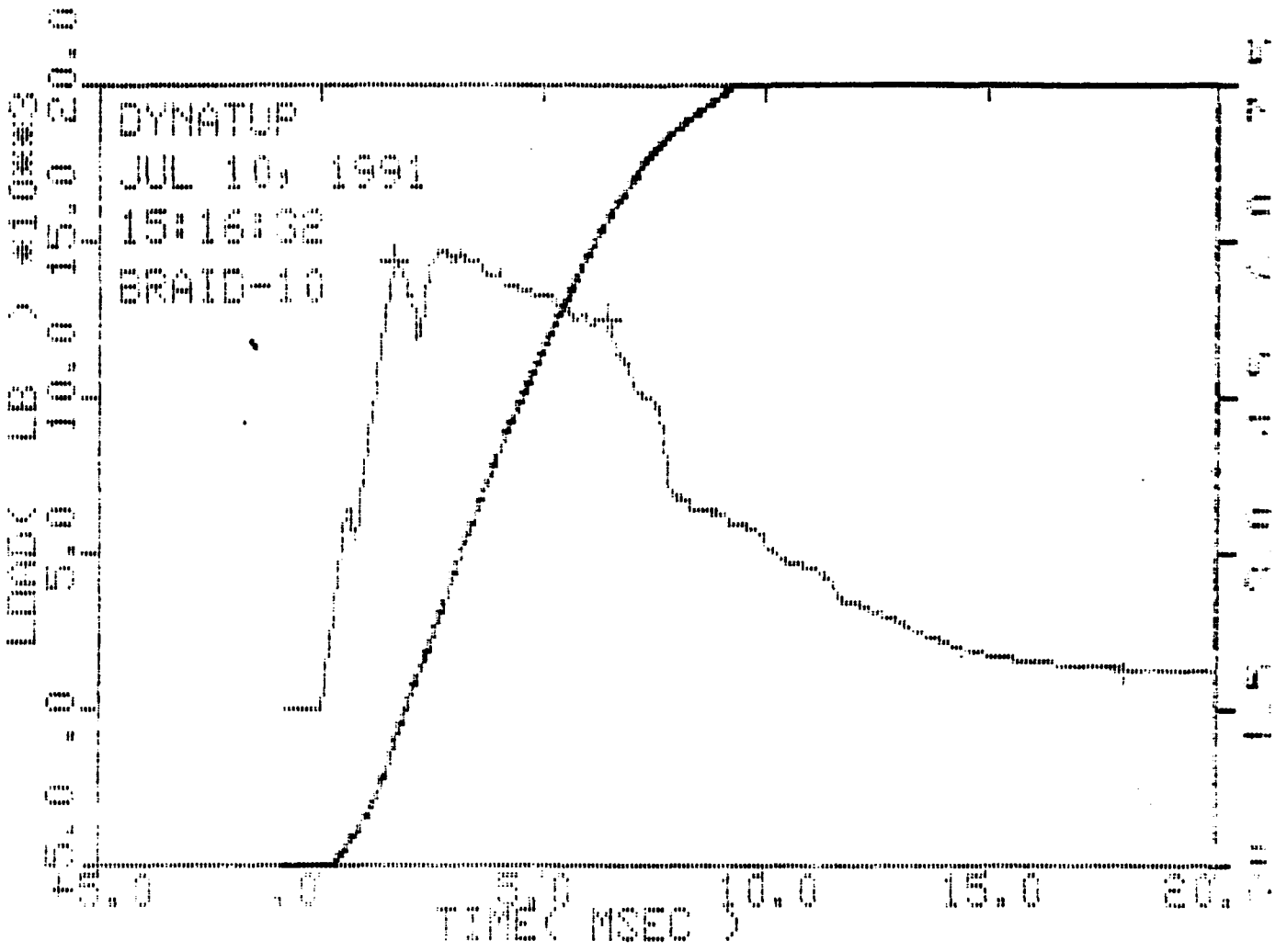

Specimen Id.	Temperature F	Slope lb/in	Velocity ft/sec	Time msec	Load lb	Energy ft-lb	Deflect inch
BRAID-10	75.00	.000					
Impact:			10.09			917.21	
Yield:				.00	.00	.00	.00
Maximum Load:				2.75	14628.16	251.05	.32
Failure(.00%):				.00	.00	.00	.00
Energy After Max Load:						636.68	
Total Energy:				24.70		887.73	1.52
Pt. 1:			9.44	1.73	14375.84	123.40	.20
Pt. 2:			6.03	6.45	12527.24	620.18	.64
Pt. 3:			3.64	16.02	1396.29	857.73	1.24

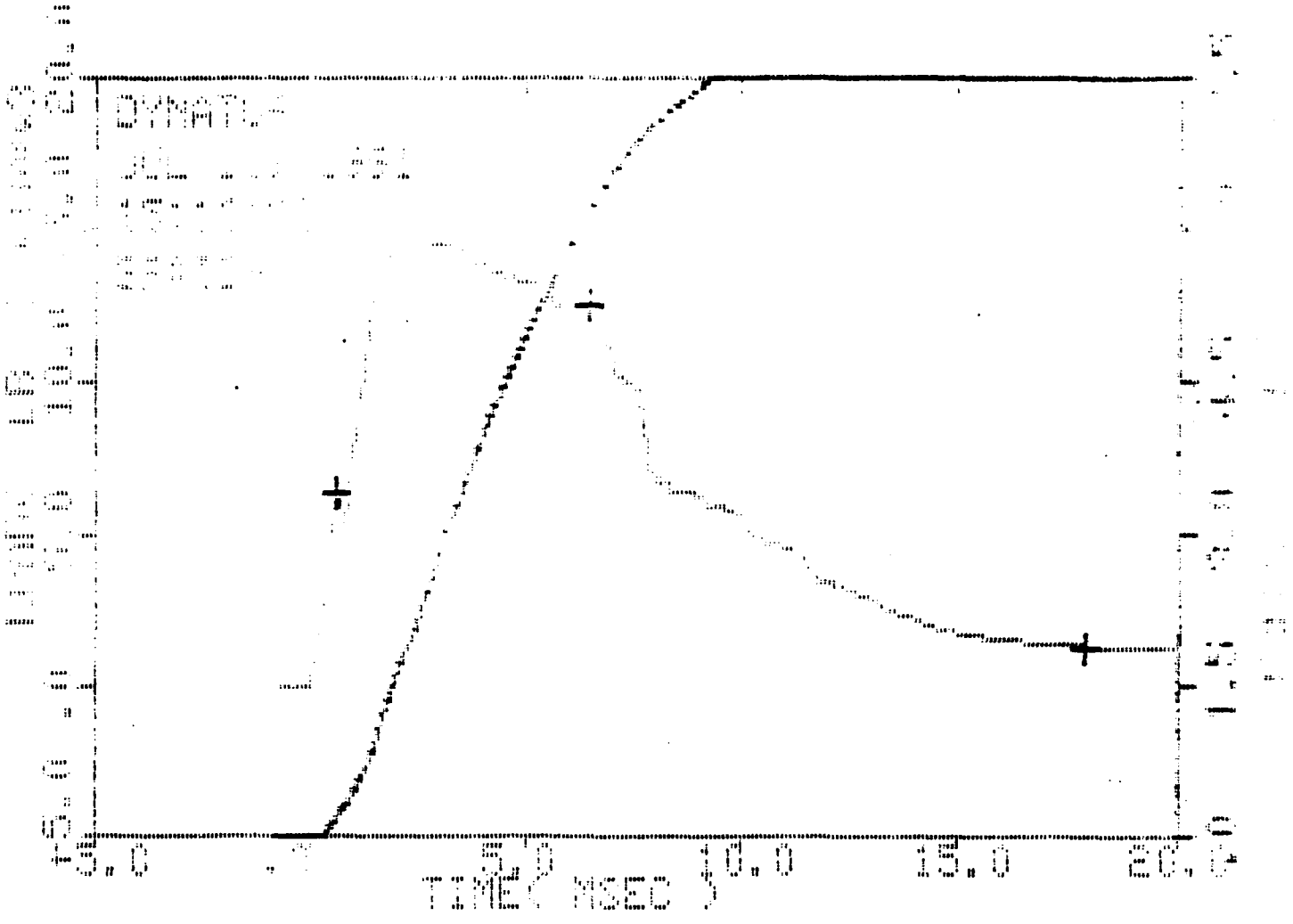

Specimen Id.	Temperature F	Slope lb/in	Velocity ft/sec	Time msec	Load lb	Energy ft-lb	Deflect inch
BRAID-10	75.00	.000					
Impact:			10.09			917.21	
Yield:				.00	.00	.00	.00
Maximum Load:				2.75	14828.16	251.05	.32
Failure(.00%):				.00	.00	.00	.00
Energy After Max Load:						636.68	
Total Energy:				24.70		887.73	1.52
pt 1:			9.99	.65	6548.78	22.14	.08
pt 2:			6.03	6.45	12527.24	620.18	.64
pt 3:			3.65	17.90	1406.12	857.09	1.24

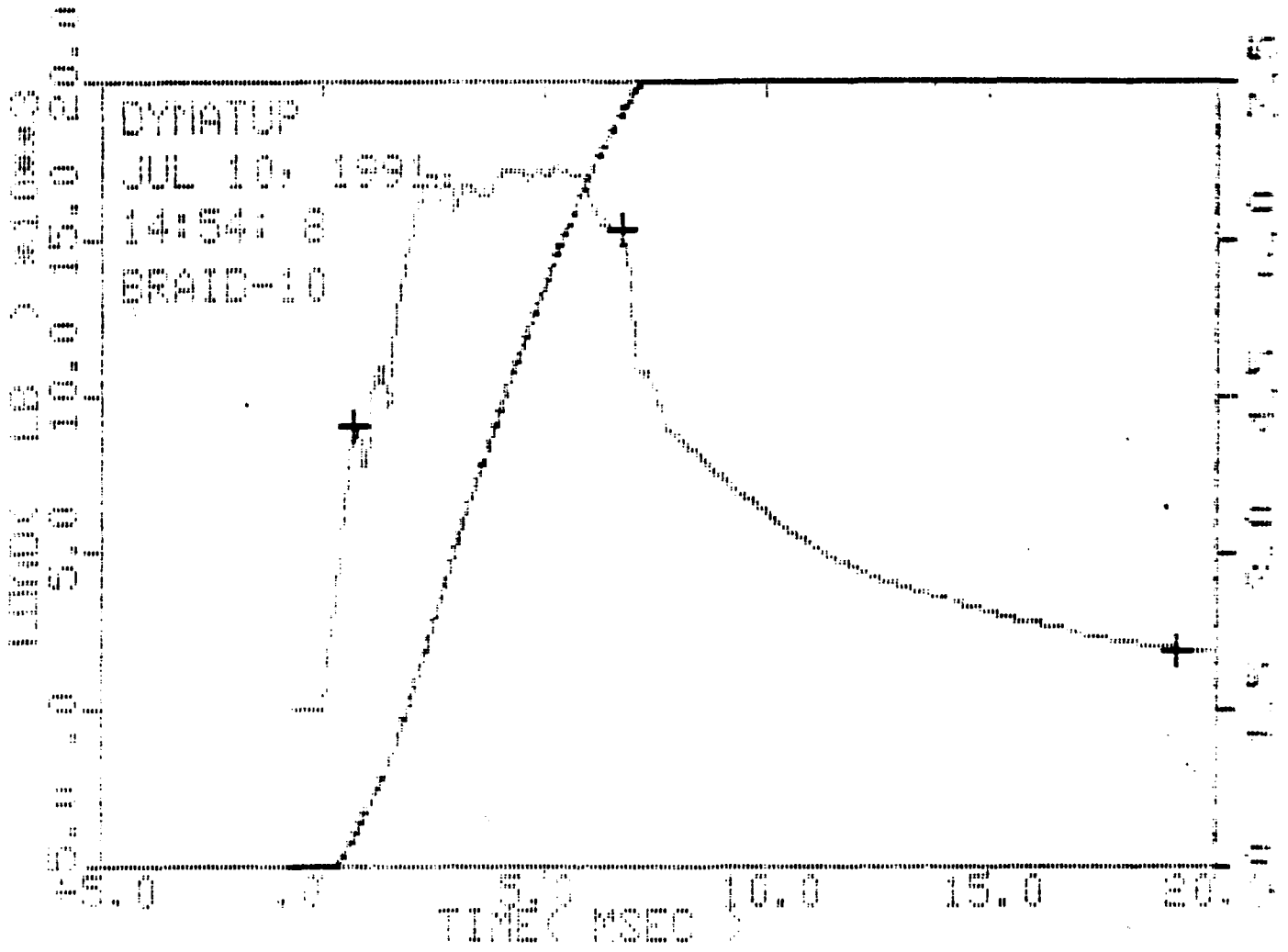

Specimen Id.	Temperature f	Slope lb/in	Velocity ft/sec	Time msec	Load lb	Energy ft-lb	Deflect inch
BRAID-10	75.00	.000					
Impact:			10.06			912.48	
Yield:				.00	.00	.00	.00
Maximum Load:				5.28	17336.55	588.70	.54
Failure(.00%):				.00	.00	.00	.00
Energy After Max Load:						360.23	
Total Energy:				24.85		948.93	1.19
pt 1:			9.89	.75	9111.69	34.52	.09
pt 2:			4.96	6.72	15317.50	721.35	.63
pt 3:			1.93	19.17	2029.20	930.78	1.07

27

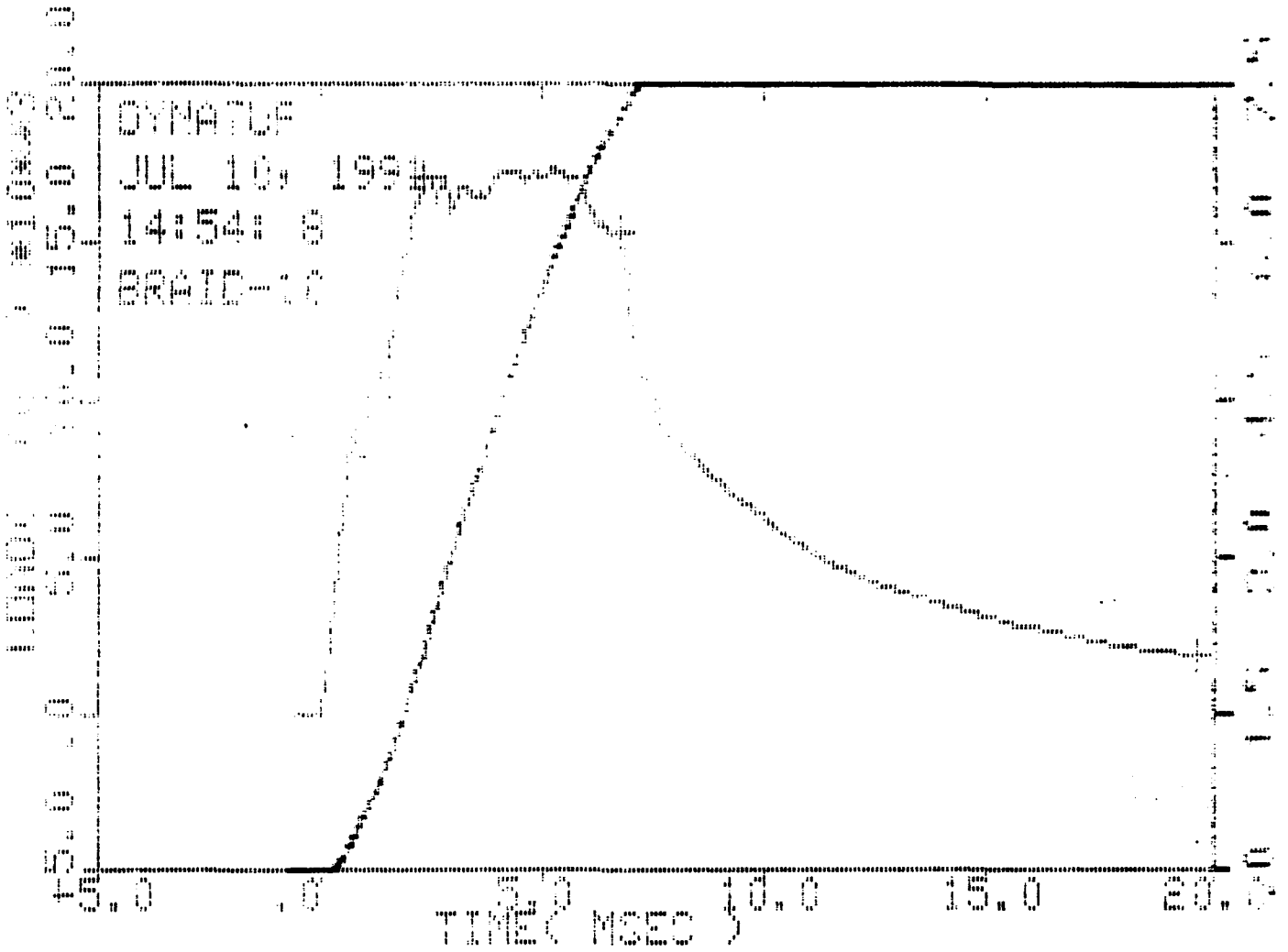

Specimen Id.	Temperature F	Slope lb/in	Velocity ft/sec	Time msec	Load lb	Energy ft-lb	Deflect inch
BRAID-10	75.00	.000					
Impact:			10.06			912.48	
Yield:				.00	.00	.00	.00
Maximum Load:				5.28	17356.55	588.70	.54
Failure(.00%):				.00	.00	.00	.00
Energy After Max Load:						360.23	
Total Energy:				24.85		948.93	1.19
Pt. 1:			8.84	2.40	17070.88	222.14	.28
Pt. 2:			4.96	6.72	15317.50	721.35	.63
Pt. 3:			1.89	19.65	1979.95	932.60	1.08

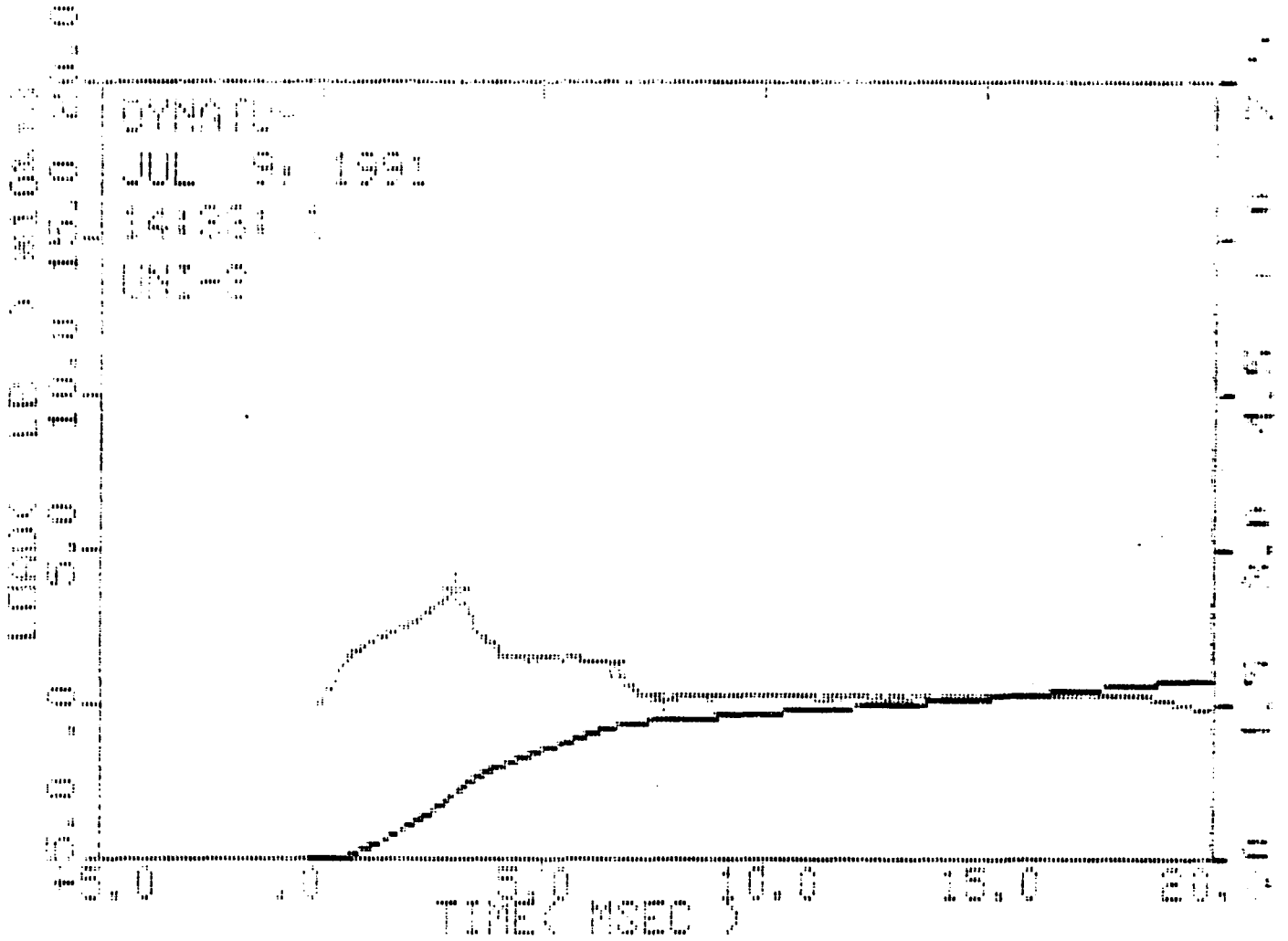

Specimen Id.	Temperature f	Slope lb/in	Velocity ft/sec	Time msec	Load lb	Energy ft-lb	Deflect inch
UNI-3	75.00	.000					
Impact:			9.92			887.01	
Yield:				.00	.00	.00	.00
Maximum Load:				3.10	3783.11	69.19	.37
Failure(.00%):				.00	.00	.00	.00
Energy After Max Load:						105.32	
Total Energy:				19.58		174.50	2.24
Pt. 1:			9.63	3.07	3773.24	68.28	.36
Pt. 2:			9.39	6.55	1412.49	129.73	.76
Pt. 3:			9.38	7.75	306.20	137.20	.89

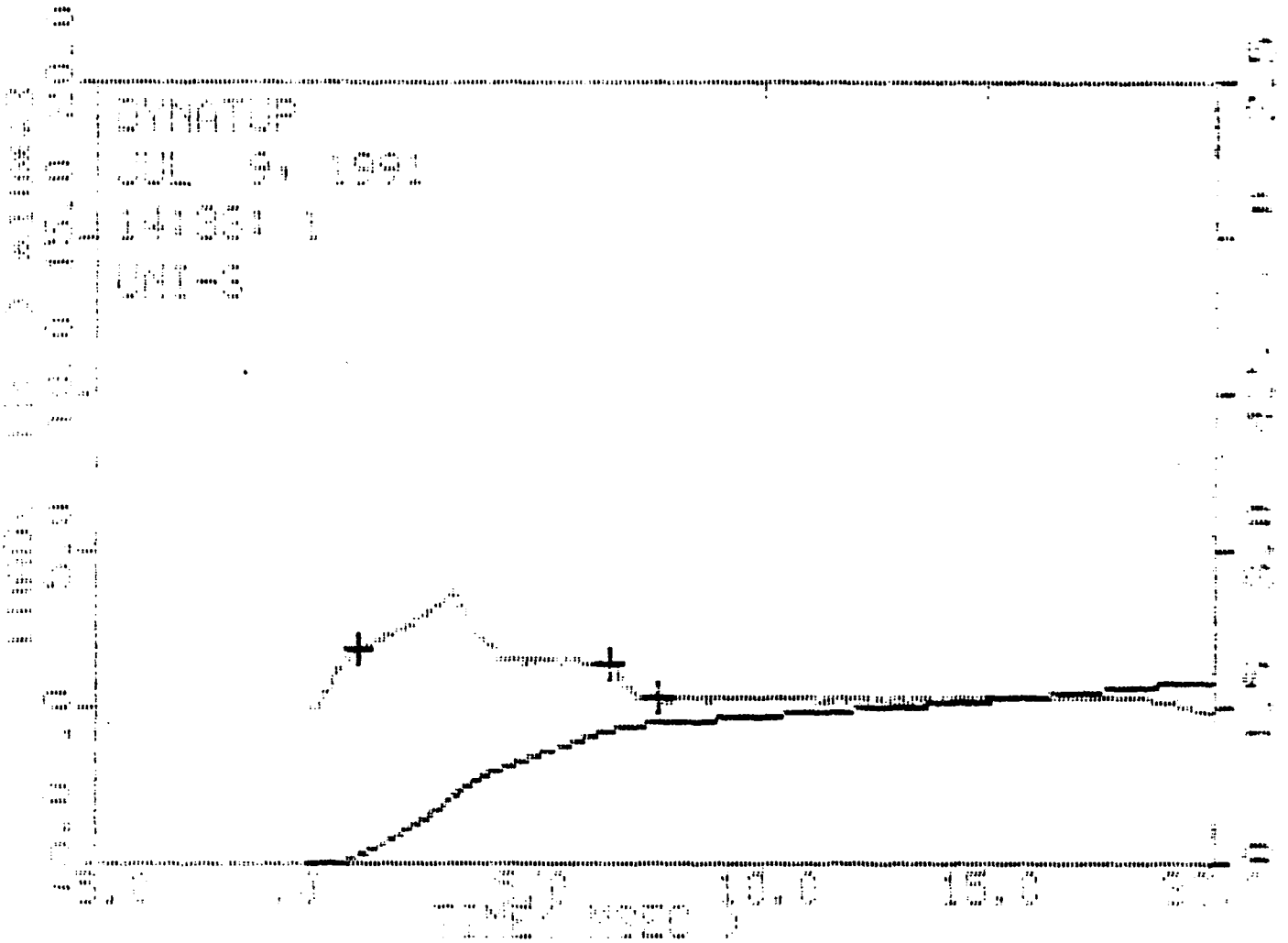

Specimen ID	Temperature °F	Start Velocity ft/sec	Time msec	Load lb	Energy ft-lb	Deflect inch
UNIT	75.00	.00				
Impact:		7.91			887.01	
Yield:			.00	.00	.00	.00
Maximum Load:			3.10	3783.11	69.19	.37
Failure: (.00%):			.00	.00	.00	.00
Energy After Max Load:					105.32	
Total Energy:			19.38		174.50	2.24
pt 1:		7.89	.93	1896.30	10.40	.11
pt 2:		7.89	6.55	1412.49	129.72	.76
pt 3:		7.88	7.62	325.96	136.97	.88

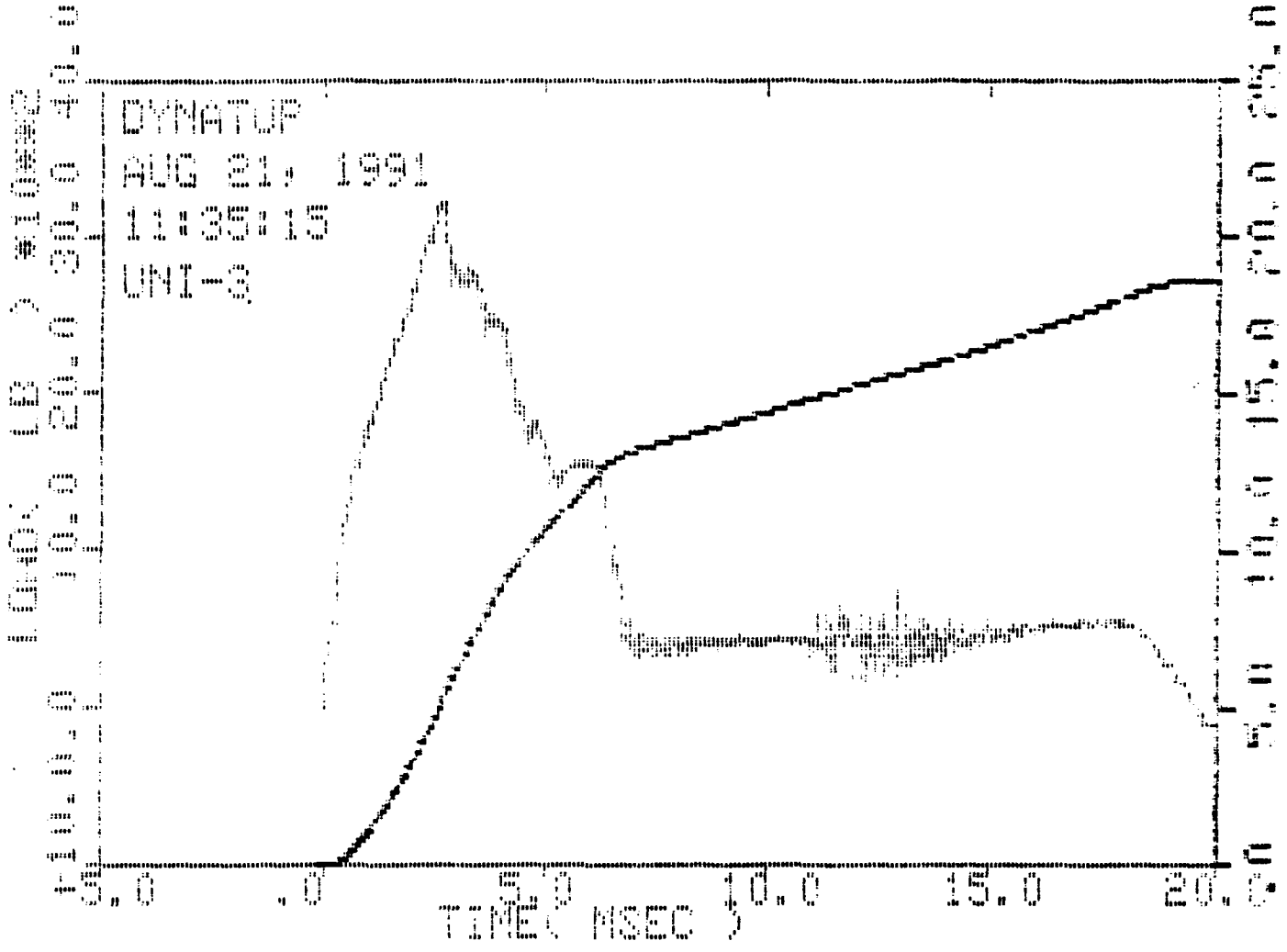

Specimen Id	Temp (F)	Impact Veloc. (ft/sec)	Impact Energy (ft-lb)	Time (msec) Max Ld	Time (msec) Total	Load (lb) Max	Energy (ft-lb) Maxld	Energy (ft-lb) Total
uni-3	75.	10.12	922.84	2.67	19.65	3237.3	53.100	187.320

Filter No.= 1, No Smoothing.
Comments:

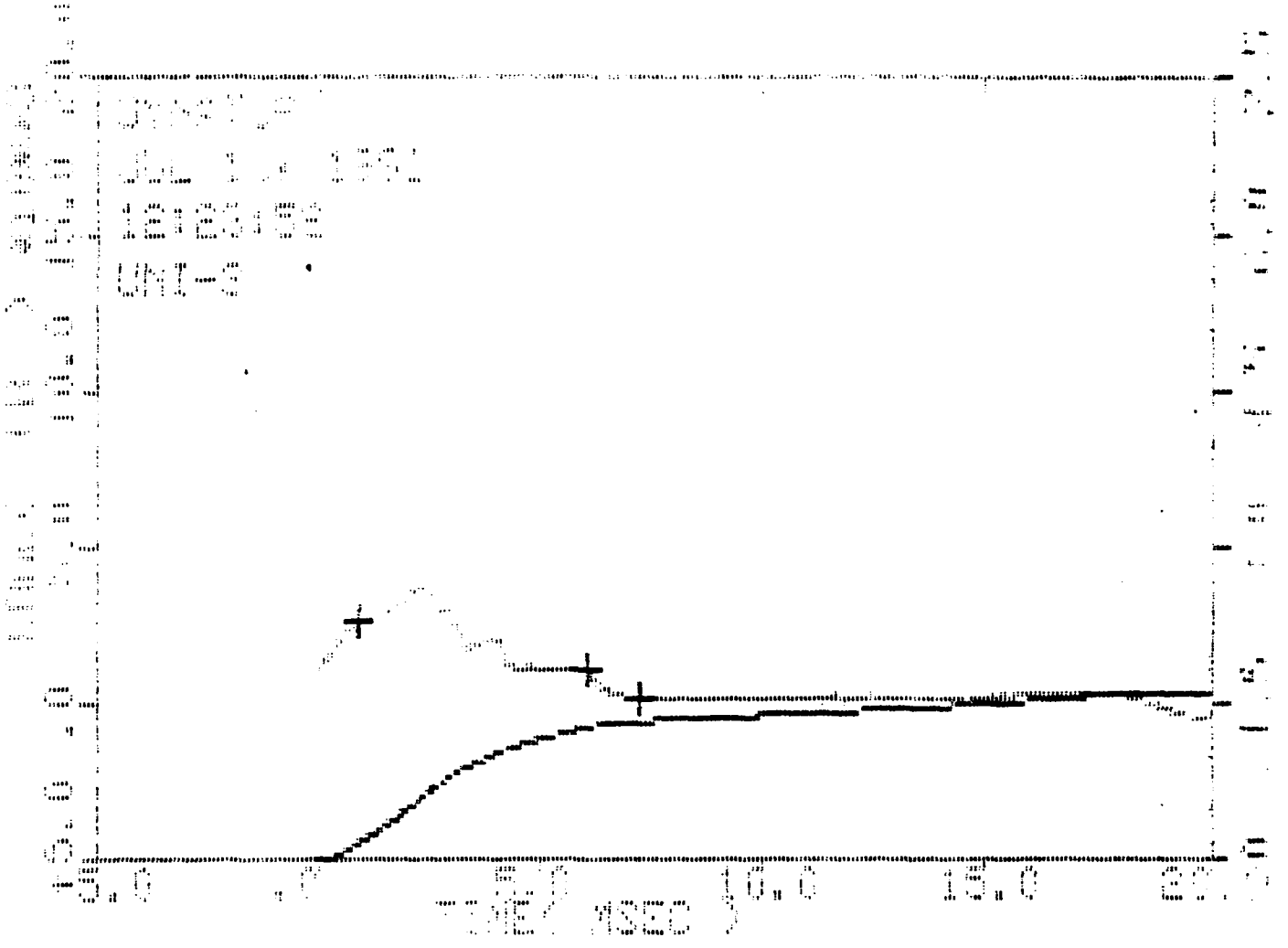

Specimen Id.	Temperature F	Slope lb/in	Velocity ft/sec	Time msec	Load lb	Energy ft-lb	Deflect inch
UNI-3	75.00	.000					
Impact:			10.06			909.77	
Yield:				.00	.00	.00	.00
Maximum Load:				2.35	3841.69	63.04	.28
Failure (.00%):				.00	.00	.00	.00
Energy After Max Load:						100.67	
Total Energy:				16.85		163.71	2.18
pt 1:			9.97	.95	2699.03	19.24	.13
pt 2:			9.51	6.05	1103.25	129.47	.71
pt 3:			9.01	7.30	206.86	135.49	.85

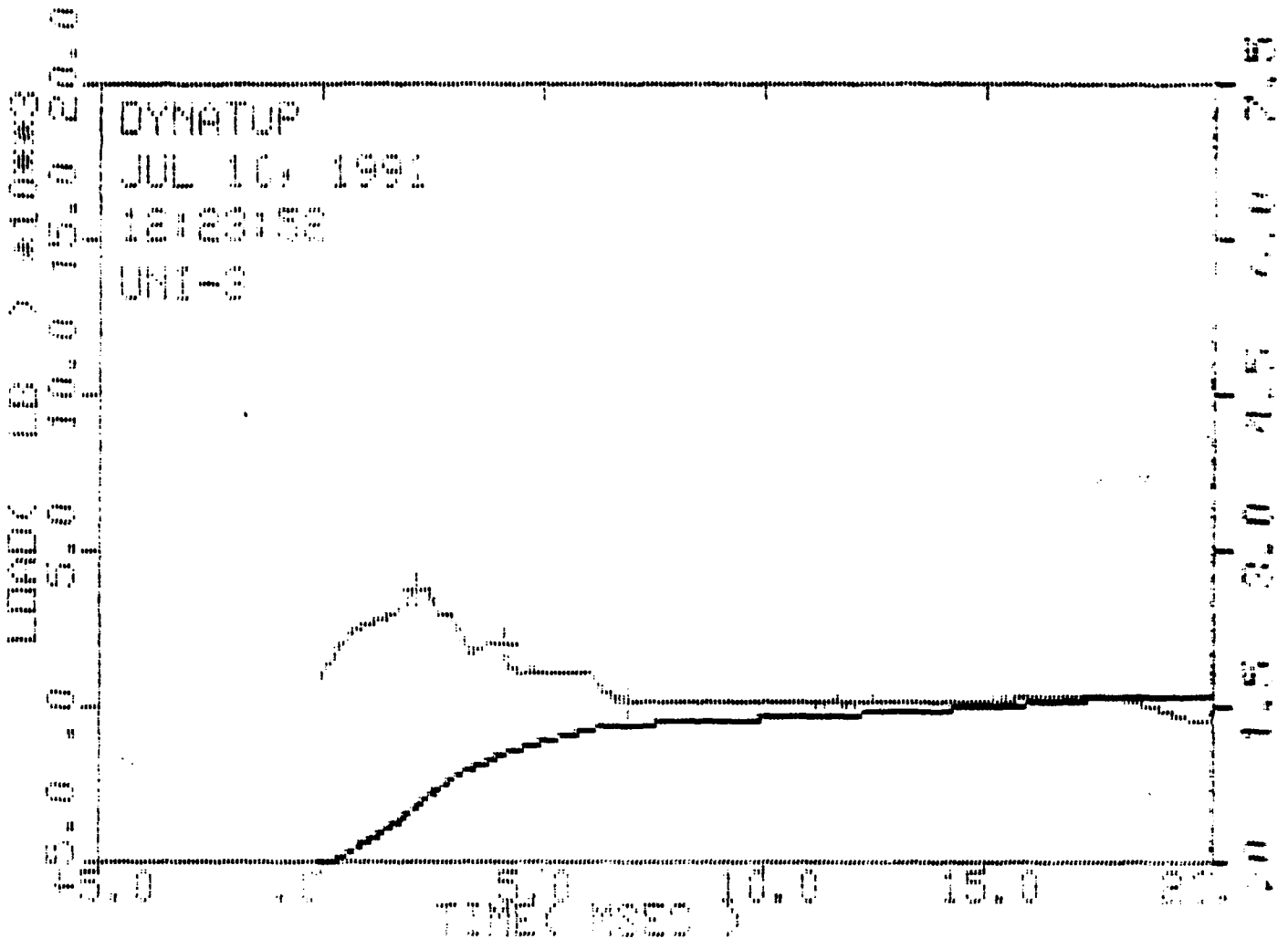

Specimen Id.	Temperature F	Slope lb/in	Velocity ft/sec	Time msec	Load lb	Energy ft-lb	Deflect inch
UNI-3	75.00	.000					
Impact:			10.03			909.77	
Yield:				.00	.00	.00	.00
Maximum Load:				2.35	3841.69	63.04	.28
Failure: .00%):				.00	.00	.00	.00
Energy After Max Load:						100.67	
Total Energy:				18.85		163.71	2.18
Pt. 1:			9.80	2.20	3772.73	57.48	.26
Pt. 2:			9.58	4.13	2068.60	106.90	.49
Pt. 3:			9.51	6.97	246.26	134.71	.81

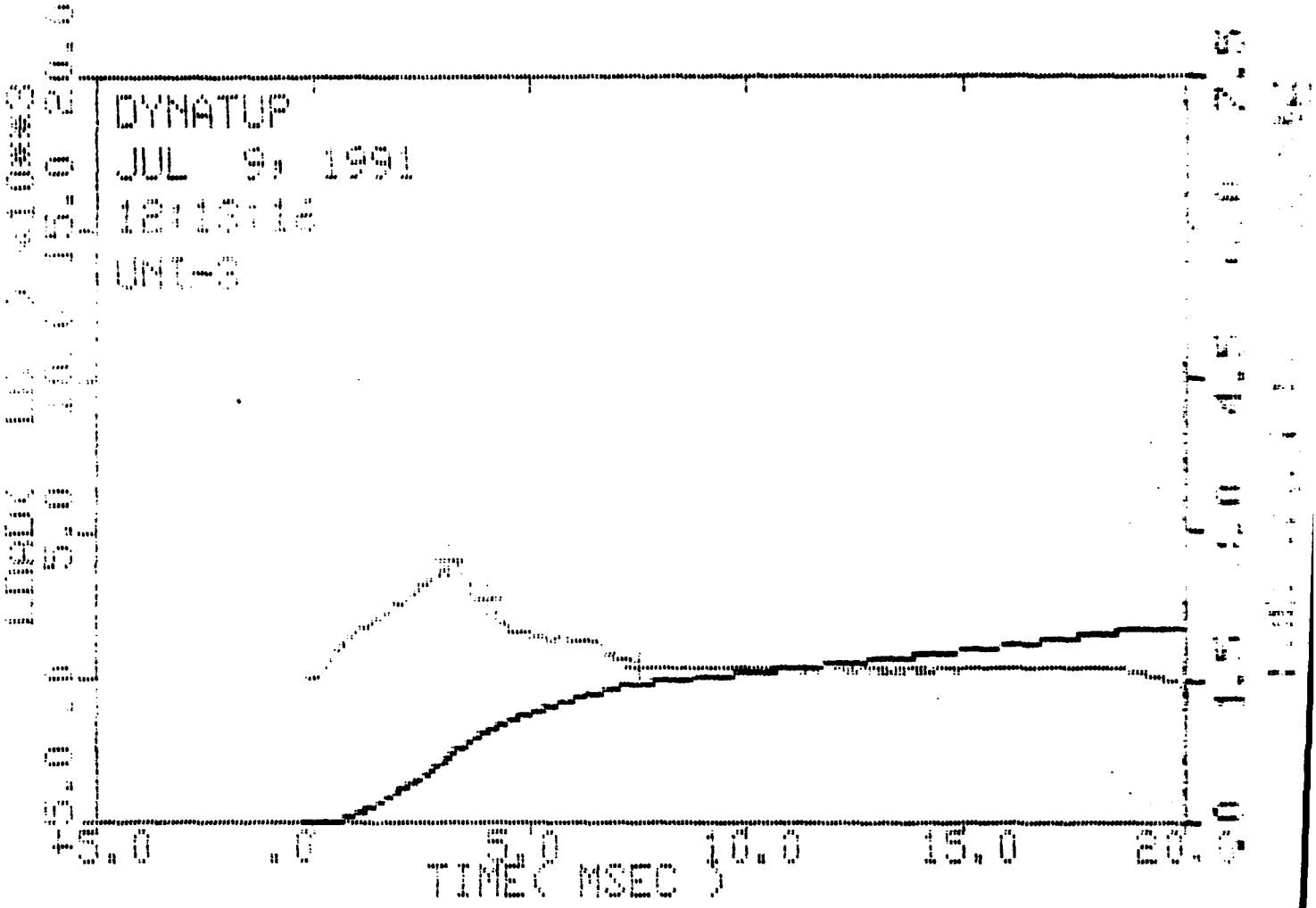

Specimen Id.	Temperature f	Slope lb/in	Velocity ft/sec	Time msec	Load lb	Energy ft-lb	Deflect inch
UNI-3	75.00	.000					
Impact:			9.95			892.32	
Yield:				.00	.00	.00	.00
Maximum Load:				3.25	4145.17	73.65	.38
Failure(.00%):				.00	.00	.00	.00
Energy After Max Load:						131.78	
Total Energy:				19.92		205.43	2.26
Pt. 1:			9.65	3.20	4089.85	71.66	.38
Pt. 2:			9.52	4.00	2868.82	97.33	.47
Pt. 3:			9.34	7.55	624.34	148.51	.87

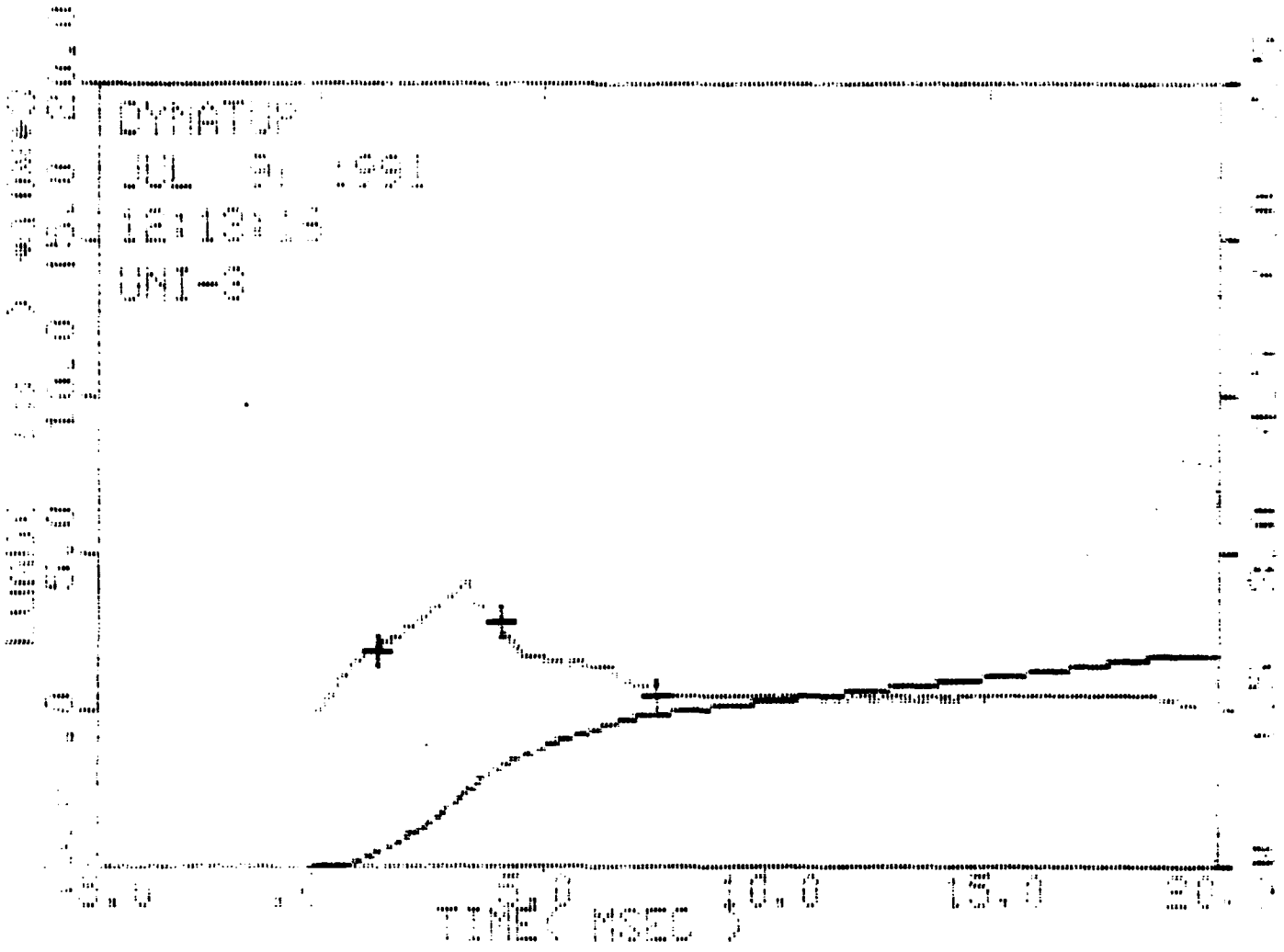

Specimen Id.	Temperature t	Slope lb/in	Velocity ft/sec	Time msec	Load lb	Energy ft-lb	Deflect inch
UNI-3	75.00	.000					
Impact:			9.93			892.32	
Yield:				.00	.00	.00	.00
Maximum Load:				3.25	4145.17	73.65	.38
Failure(.00%):				.00	.00	.00	.00
Energy After Max Load:						131.78	
Total Energy:				19.92		205.43	2.26
pt 1:			9.91	1.25	2023.19	14.73	.15
pt 2:			9.52	4.02	2821.40	98.20	.47
pt 3:			9.34	7.53	624.34	148.51	.87

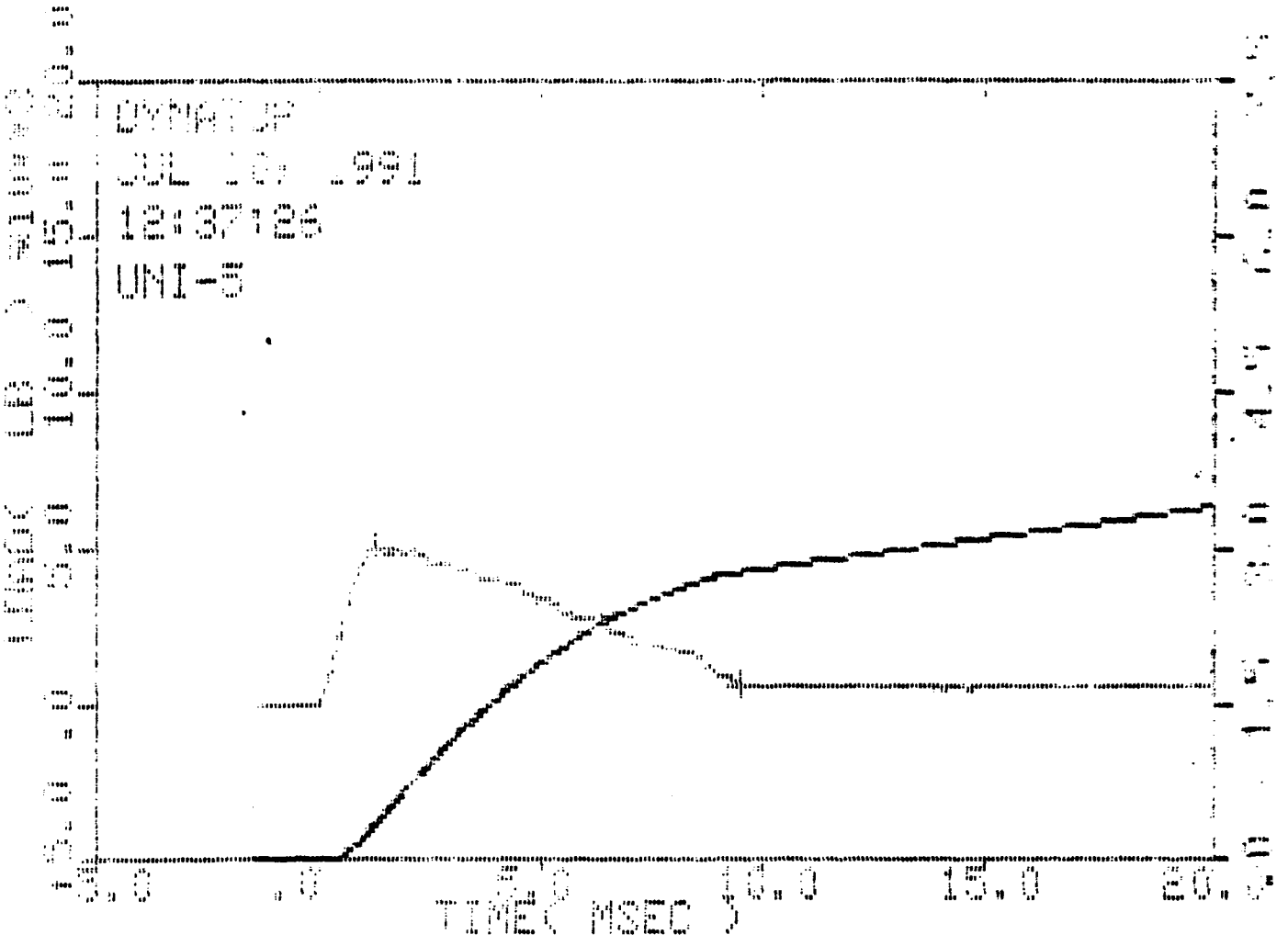

Specimen Id.	Temperature F	Slope lb/in	Velocity ft/sec	Time msec	Load lb	Energy ft-lb	Deflect inch
UNI-5	75.00	.000					
Impact:			10.05			910.68	
Yield:				.00	.00	.00	.00
Maximum Load:				1.35	3118.06	40.88	.16
Failure(.00%):				.00	.00	.00	.00
Energy After Max Load:						310.80	
Total Energy:				21.70		351.68	2.32
Pt. 1:			9.87	1.32	5098.41	39.62	.16
Pt. 2:			8.90	6.40	2524.65	232.49	.73
Pt. 3:			8.69	9.33	717.12	281.42	1.06

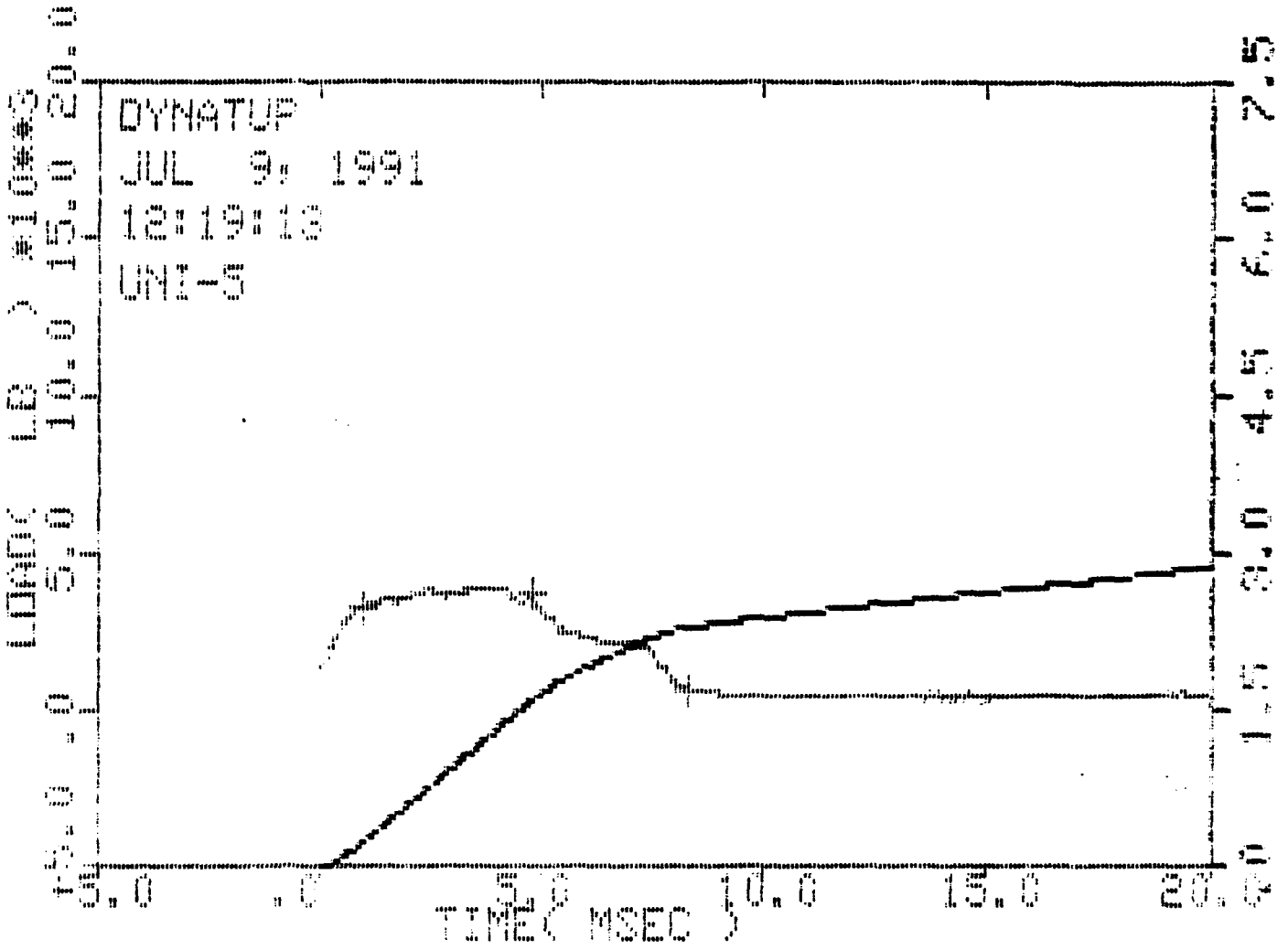

Specimen Id.	Temperature °	Slope lb/in	Velocity ft/sec	Time msec	Load lb	Energy ft-lb	Deflect inch
UNI-5	75.00	.000					
Impact:			9.95			891.53	
Yield:				.00	.00	.00	.00
Maximum Load:				2.52	4006.57	80.12	.30
Failure(.00%):				.00	.00	.00	.00
Energy After Max Load:						213.58	
Total Energy:				21.10		293.70	2.29
Pt. 1:			9.83	1.02	3419.57	26.55	.12
Pt. 2:			9.16	4.80	3789.89	161.87	.55
Pt. 3:			8.84	8.30	776.10	231.95	.93

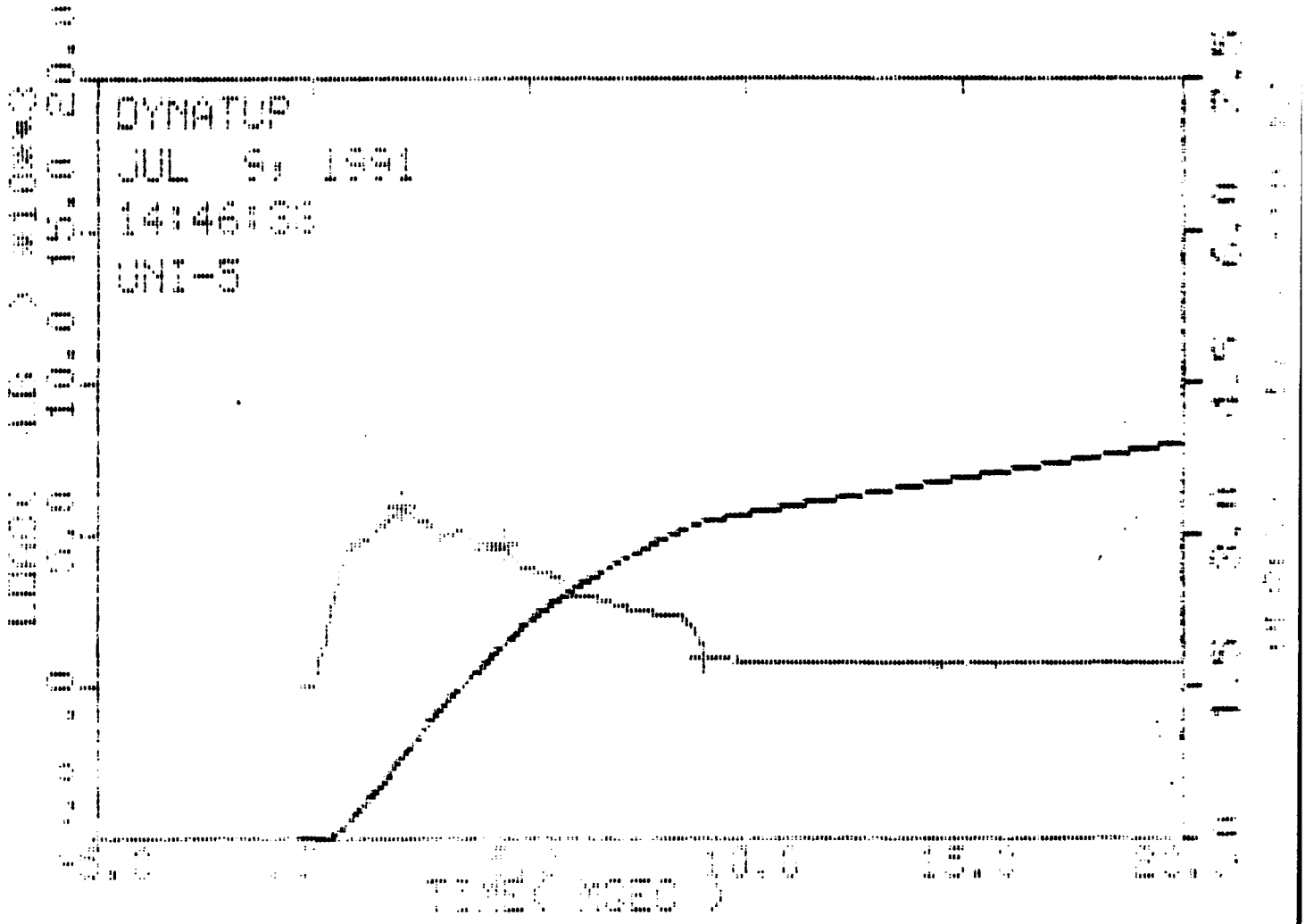

Specimen Id.	Temperature F	Slope lb/in	Velocity ft/sec	Time msec	Load lb	Energy ft-lb	Deflect incn
UNI-5	75.00	.000					
Impact:			9.96			894.62	
Yield:				.00	.00	.00	.00
Maximum Load:				2.15	5957.13	87.68	.25
Failure(.00%):				.00	.00	.00	.00
Energy After Max Load:						317.59	
Total Energy:				22.35		405.27	2.30
Pt. 1:			9.54	2.13	5947.30	86.26	.25
Pt. 2:			8.97	4.40	4689.03	193.99	.50
Pt. 3:			8.34	9.05	1091.16	314.98	.98

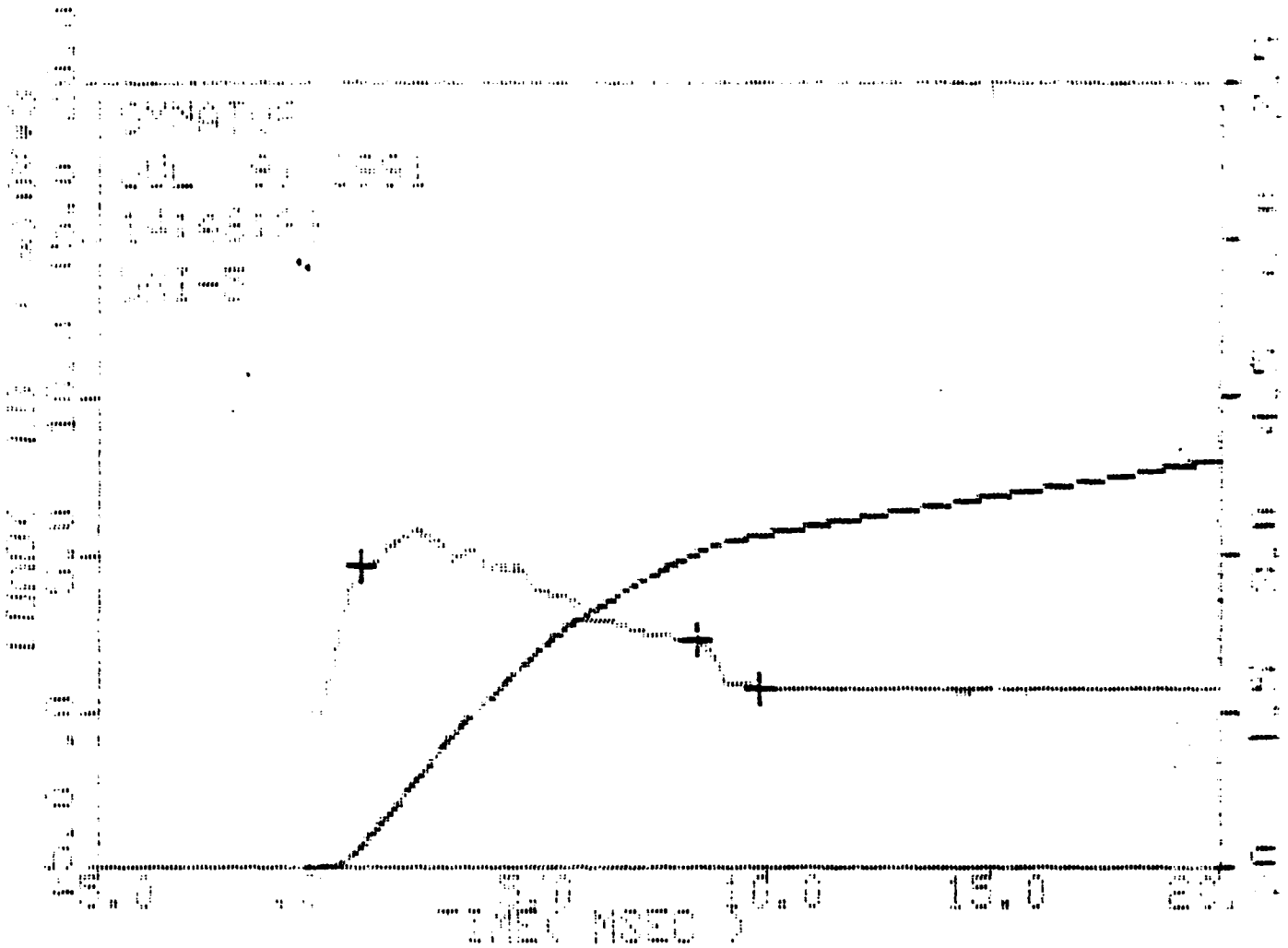

Specimen Id.	Temperature F	Slope lb/in	Velocity ft/sec	Time msec	Load lb	Energy ft-lb	Deflect inch
UNI-5	75.00	.000					
Impact:			9.96			894.62	
Yield:				.00	.00	.00	.00
Maximum Load:				2.15	5957.13	87.68	.25
Failure(.00%):				.00	.00	.00	.00
Energy After Max Load:						317.59	
Total Energy:				22.35		405.27	2.30
pt 1:			9.86	.93	4709.69	24.45	.11
pt 2:			9.39	8.43	2398.59	304.56	.92
pt 3:			8.82	9.82	933.87	321.31	1.06

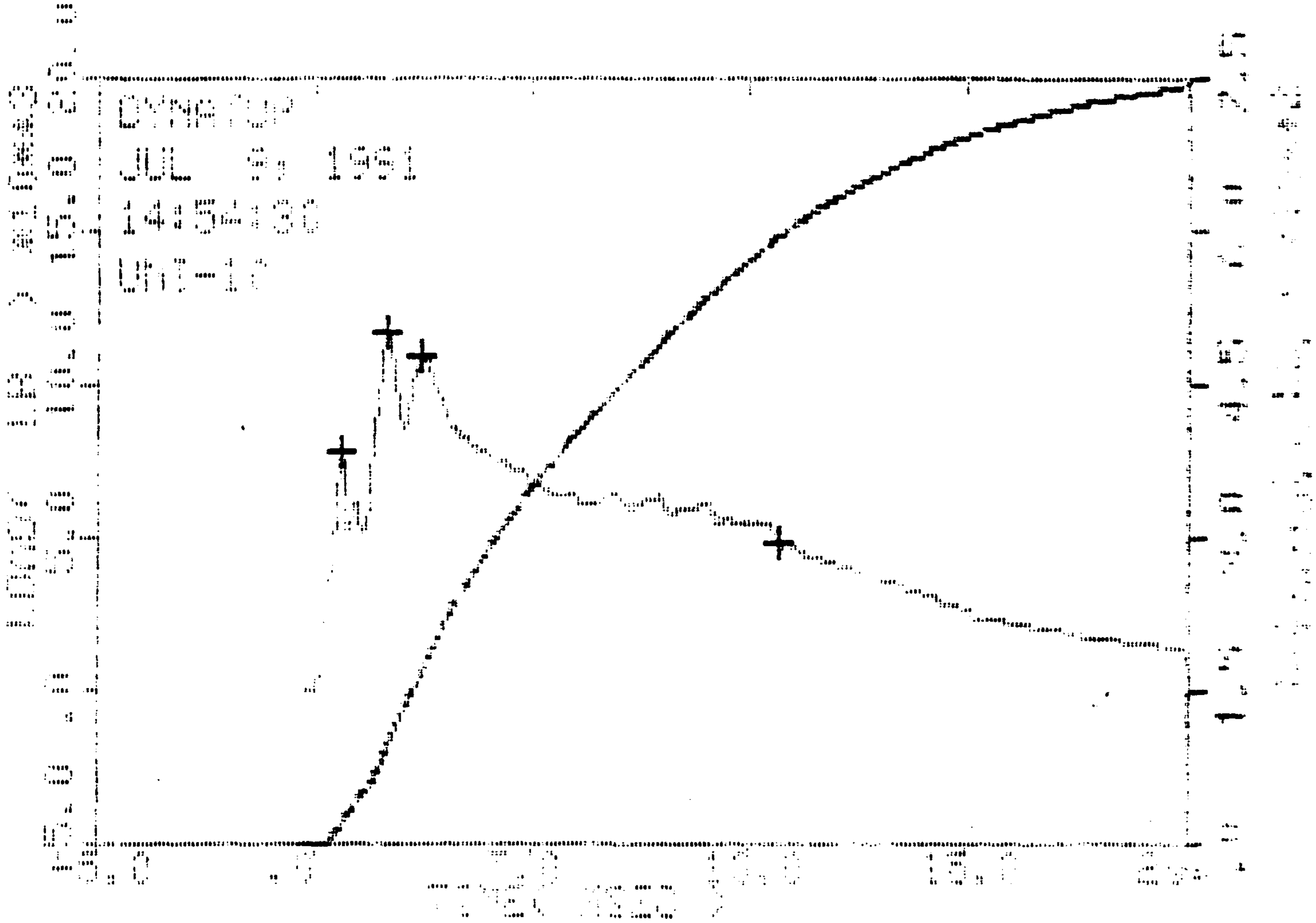

Specimen Id.	Temperature F	Slope lb/in	Velocity ft/sec	Time msec	Load lb	Energy ft-lb	Deflect. in.
UNI-10	75.00	[illegible]					
Impact:			[illegible]			[illegible]	
Yield:				.00	.00	.00	.00
Maximum Load:				[illegible].72	[illegible]	[illegible].54	[illegible]
Failure:				.00	.00	.00	.00
Energy After Max Load:						[illegible]0.22	
Total Energy:				20.22		[illegible]	1.7[illegible]
pt 1:			[illegible]	.60	7962.67	[illegible]	.08
pt 2:			[illegible]	[illegible].70	117[illegible]6.00	10[illegible]	.20
pt 3:			[illegible]	[illegible].30	109[illegible]0.73	[illegible]	.29
pt 4:			[illegible]	10.65	4574.11	[illegible]	1.03

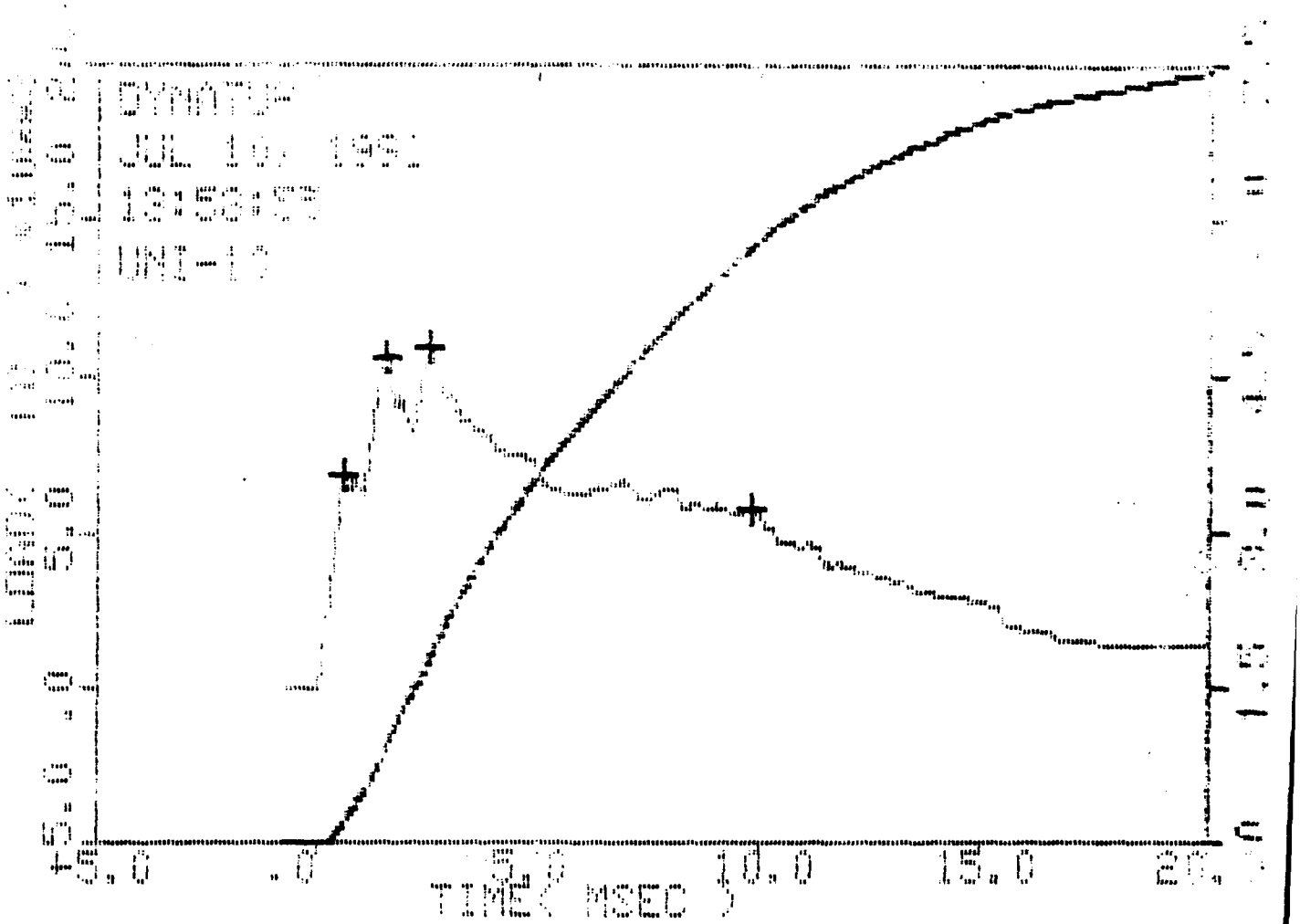

Specimen Id.	Temperature F	Slope lb/in	Velocity ft/sec	Time msec	Load lb	Energy ft-lb	Deflect inch
UNI-10	75.00	.000					
Impact:			10.07			913.58	
Yield:				.00	.00	.00	.00
Maximum Load:				2.52	11037.10	177.50	.29
Failure(.00%):				.00	.00	.00	.00
Energy After Max Load:						604.82	
Total Energy:				24.85		782.32	1.96
pt 1:			9.97	.63	6944.91	20.71	.08
pt 2:			9.57	1.62	10722.31	97.86	.19
pt 3:			9.08	2.60	10958.40	185.01	.30
pt 4:			6.53	9.80	5813.66	576.44	.97

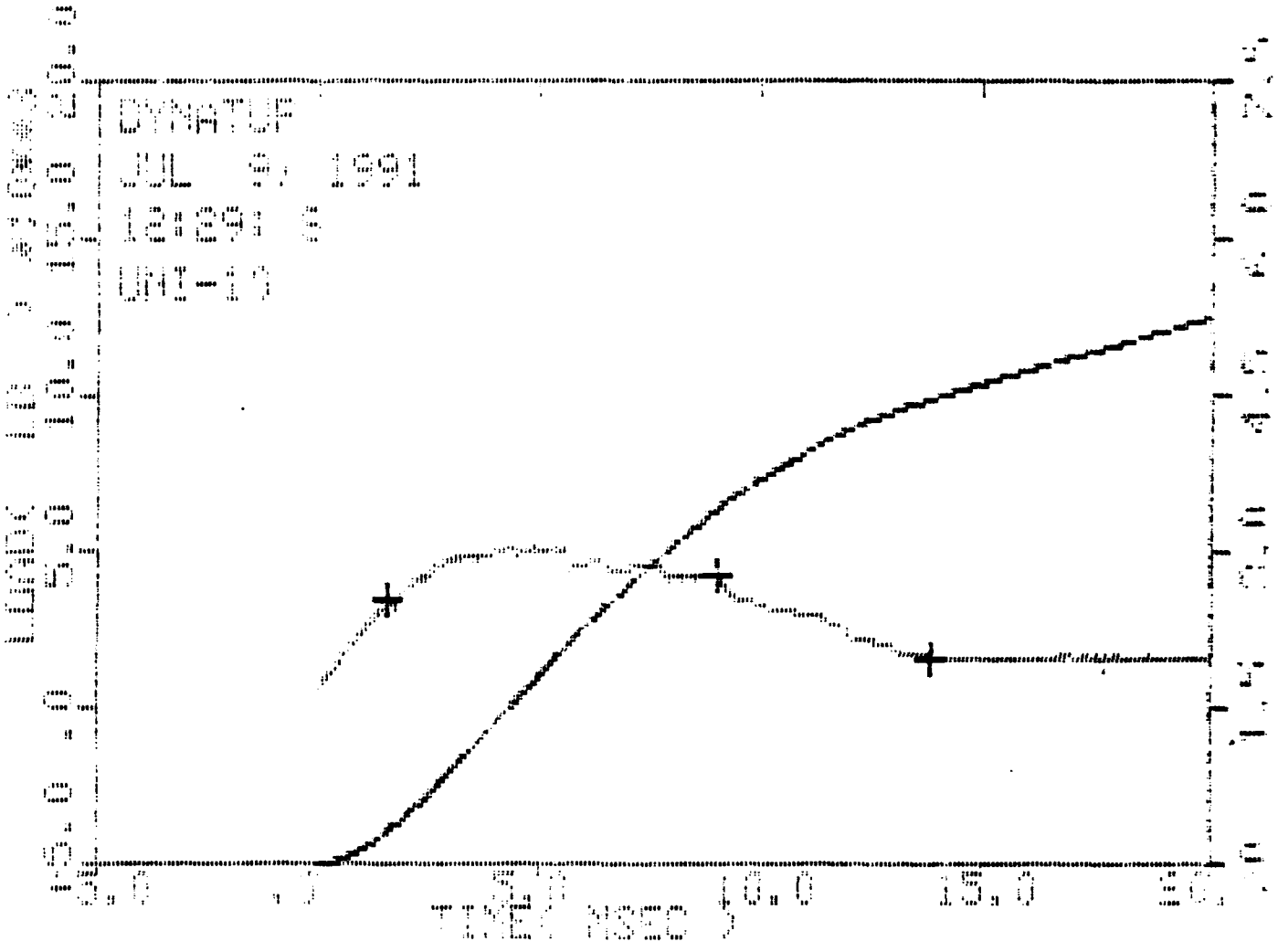

Specimen Id.	Temperature F	Slope lb/in	Velocity ft/sec	Time msec	Load lb	Energy ft-lb	Deflect inch
UNI-10	75.00	.000					
Impact:			10.03			907.58	
Yield:				.00	.00	.00	.00
Maximum Load:				4.33	5195.66	151.99	.51
Failure(.00%):				.00	.00	.00	.00
Energy After Max Load:						434.36	
Total Energy:				25.55		586.34	2.48
pt 1:			9.91	1.55	3438.83	31.95	.19
pt 2:			8.25	8.98	4273.92	341.92	1.00
pt 3:			7.66	13.82	1685.93	448.49	1.46

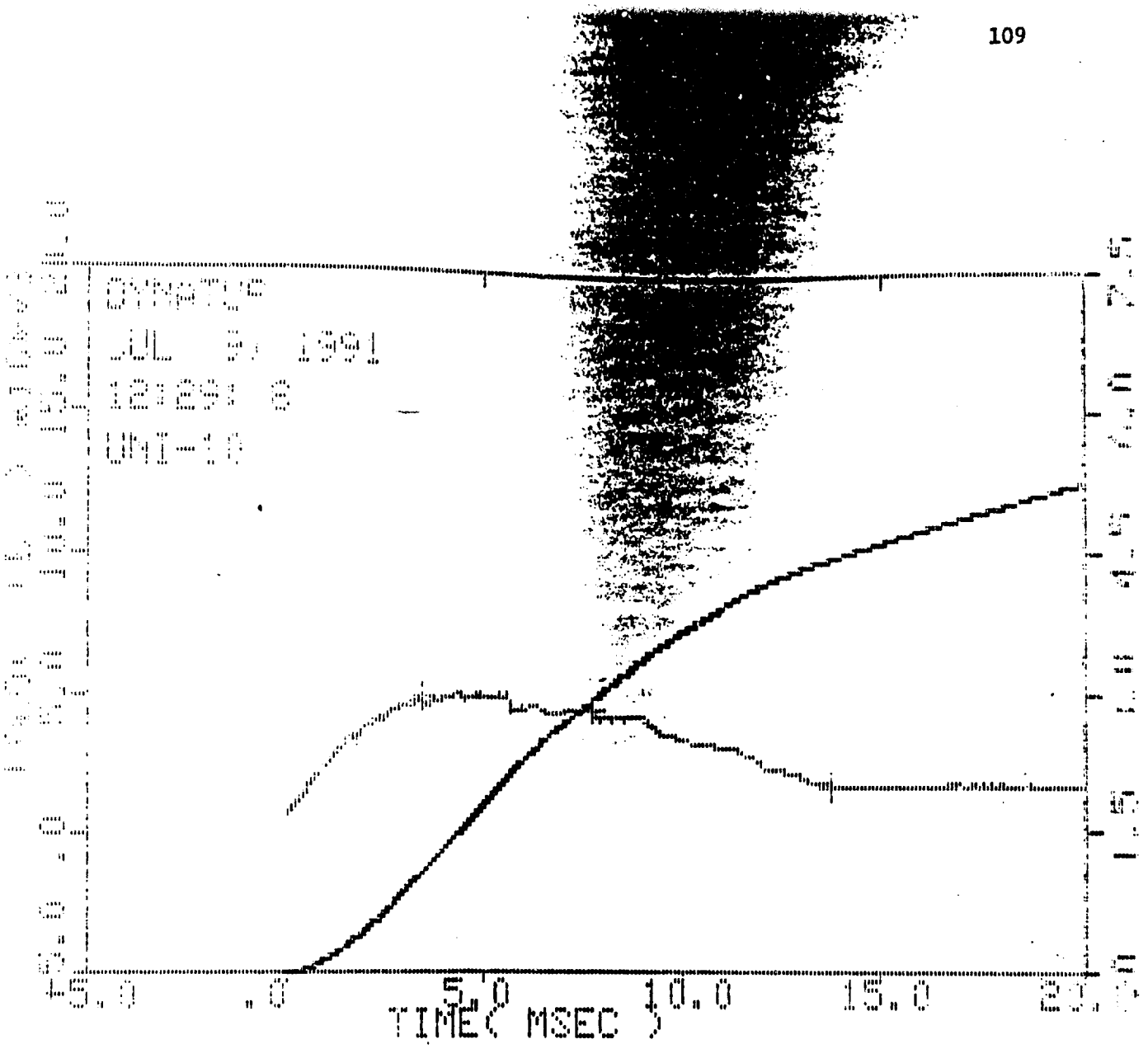

Specimen Id.	Temperature F	Slope lb/in	Velocity ft/sec	Time msec	Load lb	Energy ft-lb	Deflect inch
UNI-10	75.00	.000					
Impact:			10.03			907.58	
Yield:				.00	.00	.00	.00
Maximum Load:				4.33	5195.66	151.99	.51
Failure(.00%):				.00	.00	.00	.00
Energy After Max Load:						434.36	
Total Energy:				25.55		586.34	2.48
Pt. 1:			9.52	3.45	5018.40	110.83	.41
Pt. 2:			8.50	7.75	4549.65	299.10	.97
Pt. 3:			7.67	13.72	1709.57	447.19	1.46